Site-Specific Tyrosine Phosphorylation of the Type III Secretion Chaperone CesT Regulates Effector Hierarchy and Promotes Enteropathogenic *Escherichia coli* Intestinal Disease

by

Cameron S. Runté

Submitted in partial fulfilment of the requirements
for the degree of Master of Science

at

Dalhousie University
Halifax, Nova Scotia
August 2017

TABLE OF CONTENTS

LIST OF TABLES

LIST OF FIGURES

ABSTRACT

Enteropathogenic *E. coli* (EPEC) is a global enteric pathogen that causes serious gastrointestinal disease and inflicts a significant burden on healthcare systems worldwide. Recent phosphoproteomic studies suggest that phosphotyrosine modifications are widespread in bacteria and likely have significant impact on virulence factor regulation. In this study, we provide the first evidence that tyrosine phosphorylation of a multicargo chaperone, CesT, is functionally important for EPEC type III secretion system (T3SS)-mediated pathogenesis. The conserved phosphosites, Y152 and Y153, are located within a unique domain of CesT at the C-terminus. Positional tyrosine to phenylalanine mutations resulted in differential secretion of CesT-dependent type III effectors, and loss of phenotypes associated with disease progression *in vitro.* These observations were validated *in vivo* using the closely related mouse pathogen *Citrobacter rodentium,* which requires CesT, and specifically a CesT phosphosite, for significant intestinal colonization. This study identifies a novel research direction to pursue limitation of EPEC pathogenesis.

LIST OF ABBREVIATIONS USED

aa	amino acid
A/E	Attaching and Effacing
Amp	Ampicillin
blaM	β-lactamase (gene)
BLAST	Basic local alignment search tool
BYK	Bacterial tyrosine kinase
CCF2	FRET-based fluorescent substrate (ThermoFisher Scientific; K1023)
CesT	Chaperone for *E. coli* secreted protein Tir
CID	Collision induced dissociation
DMEM	Dulbecco's Modified Eagle Medium (Invitrogen)
DNA	Deoxyribonucleic acid
DSPK	Dual-specificity protein kinase
EGTA	Ethylene glycol-bis(β-aminoethyl ether)-N,N,N',N'-tetraacetic acid
EHEC	Enterohemorrhagic *E. coli*
EPEC	Enteropathogenic *E. coli*
ESTK	eukaryotic-like serine/threonine kinase
FBS	Fetal bovine serum
HCD	Higher-energy collisional dissociation
H-NS	Histone-like nucleoid structuring protein
IPTG	Isopropyl β-D-1-thiogalactopyranoside
LB	Luria-Bertani broth
LEE	Locus of Enterocyte Effacement

LC-MS/MS	Liquid chromatography tandem mass spectrometry
MH+	Protonated molecule (precursor ion observed in positive ion mode)
mRNA	messenger ribonucleic acid
MS	Mass spectrometry
MS/MS	Tandem mass spectrometry
MW	Molecular weight
OD	Optical density
ORF	Open reading frame
PAI	Pathogenicity island
PBS	Phosphate buffered saline
PCR	Polymerase chain reaction
pTyr	phosphotyrosine (phosphorylated tyrosine amino acid)
SDS-PAGE	Sodium dodecyl sulfate-polyacrylamid gel electrophoresis
STEC	Shiga-toxigenic *E. coli*
STY	Serine, Threonine, Tyrosine
T3S	Type III Secretion
T3SC	Type III Secretion Chaperone
T3SS	Type III Secretion System
TEM-1	β-lactamase (protein)

ACKNOWLEDGEMENTS

I would like to thank my supervisors Dr. Nik Thomas and Dr. Jason Leblanc for taking me on as a graduate student and providing excellent mentorship throughout the program. I have learned many valuable lessons and am extremely grateful for having had the opportunity to direct research at a new and exciting question for the bacterial pathogenesis field. I would also like to thank the members of my advisory committee, Dr. Song Lee and Dr. Jan Rainey, who provided invaluable support for my research.

I am thankful to have had the opportunity to work with and learn from Dr. Alejandro Cohen in the Department of Biochemistry, at the Proteomics Core Facility. The mass spectrometry data required in this project presented a unique challenge to identify and I would not have been successful in doing so without Alex's thoughtful insights. Additionally, significant thanks goes out to the many students and faculty within the department that have positively impacted my time at Dalhousie. Namely, Dr. Cheng, Dr. Stadnyk, Dr. McCormick, Dr. Jain, Aaron Liu, Landon Getz, Sabrina, Jamie, Karla, Peter, and many others. I will always remember the Pro Tips.

Last but not least I would like to thank my family for always providing support and guidance both personally and professionally. I will herein thank Erin, not only for your patience, but for inspiring me to pursue opportunities beyond Dalhousie; somewhere I will always remember fondly.

CHAPTER 1. INTRODUCTION

1.1 Pathogenic *Escherichia coli*

Escherichia coli is a Gram-negative facultative anaerobe belonging to the *Enterobacteriaceae* family of bacteria. As a commensal component of the mammalian gut microbiota, *E. coli* is commonly found living within the mucus layer of the intestinal colon. However, several strains of *E. coli* have acquired specific virulence factors that confer a competitive advantage and promote the establishment of new replicative niches within the host (LeBlanc, 2003). The nature of these virulence traits defines the range of disease possibilities. Pathogenic *E. coli* are divided into intestinal pathogens, causing mild to severe diarrheal disease, and extraintestinal pathogens that cause a variety of infections including urinary tract infections, meningitis, and septicemia (Kaper and Nataro, 2004).

Strains of *E. coli* that cause diarrheal disease in humans have been grouped into at least six distinct pathotypes based on specific virulence factors that enable the bacteria to cause infections with clear epidemiological, clinical, and pathological features. The diarrheagenic *E. coli* pathotypes include: enteroinvasive *E. coli*, diffusely adherent *E. coli,* enterotoxigenic *E. coli*, enteropathogenic *E. coli* (EPEC), enterohemorrhagic *E. coli* (EHEC), and enteroaggregative *E. coli* (EAEC). It is currently reported by the World Health Organization that approximately 600 million people acquire diarrheal disease from contaminated food or water each year. Children less than five years, particularly those within low-income, sub-tropical regions, are particularity susceptible to infection from diarrheagenic *E. coli* pathotypes, which account for roughly 100,000 deaths per year (WHO, 2017).

Traditionally, the most severe form of enteric disease caused by pathogenic *E. coli* involves strains of the EHEC pathotype (also known as Verotoxigenic *E. coli* (VTEC) or Shiga Toxigenic *E. coli* (STEC)) that produce Shiga toxin (Hacker & Kaper, 2000). These infections are generally transmitted by zoonosis through a low infectious dose (1-100 living cells), rendering these bacteria a serious threat to food safety in countries worldwide including the United States, Canada, Scotland, and Japan (LeBlanc, 2003). Encoded by the Shiga Toxin 1 (*stx1*) and 2 (*stx2*) genes, the Shiga toxin enters cells that express the globotriaosylceramide (Gb3) receptor, where it specifically cleaves the 28S rRNA of the 60S ribosomal subunit, which halts eukaryotic protein synthesis and induces cytotoxicity (Obrig & Karpman, 2012). Due to the prevalence of Gb3 on human endothelial cells of the intestine and kidney, as well as on the surfaces of circulating platelets and erythrocytes, dissemination of the Shiga toxin often results in a severe systemic disease called Hemolytic Uremic Syndrome (HUS) that is characterized by acute renal failure, thrombocytopenia, and destruction of red blood cells (Goldwater & Bettelheim, 2012).

In a clinical setting, patients that have contracted diarrheagenic *E. coli* often present in a similar fashion to alternative causes of gastrointestinal disease with diarrhea as the principal symptom. STEC is often suspected when the diarrhea is bloody (roughly 50% of Stx+ patients), however identifying the exact strain is vital for public health authorities to confirm, investigate, and control outbreaks. Differentiation is accomplished by stool culture and serotyping of the lipopolysaccharide O-polysaccharide (O) and flagellar (H) antigens, and alternatively by PCR amplification of specific gene targets (Haugum *et al.,* 2014; Wang, Clark, & Rodgers, 2002). While many serotypes exist, the most notorious EHEC serotype, O157:H7, has been associated with a number of North

American outbreaks linked to contaminated food and water. Notable Canadian incidences include the water-borne outbreak in Walkerton, Ontario in May 2000, or the 2012 XL Foods recall of contaminated beef (Government of Canada, 2012; Salvadori *et al.,* 2009). More recently, General Mills and Ardent Mills in 2016 and 2017, respectively, have had to recall millions of pounds of flour products contaminated with STEC O121 (CFIA, 2017; U.S. FDA, 2016). Such food (beef, spinach, lettuce, flour, and unpasteurized apple juice) and water sourced outbreaks impose a significant burden on healthcare systems, and additionally result in severe economic losses (Frenzen *et al.,* 2005).

The propensity for gain and loss of virulence determinants from the *E. coli* genome is exemplified by the emergence of non-O157 Shiga toxin-positive serotypes associated with recent outbreaks (Bouzari, Jafari, & Aslani, 2012). Perhaps the most detrimental incident to date occurred with the cause of the Germany outbreak in 2011. With this particular outbreak there were 855 cases of HUS, and 18 deaths due to EAEC O104:H4 that had acquired the *stx2a* gene, likely from EHEC O157:H7, by a phage transduction event within an unknown source (Muniesa *et al.,* 2012). The severe disease associated with this particular outbreak was the result of traditional EAEC virulence factors, which mediate enhanced adherence to epithelial surfaces, working in combination with the cytotoxic effects of Stx2. (Muniesa *et al.,* 2012). The widespread HUS associated with this particular outbreak took the medical community by surprise, and provided a stark reminder of the global significance of this versatile pathogen.

1.1.1 Enteropathogenic *E. coli* (EPEC)

The prevalence of EPEC in the industrialized world has declined over the past several decades; however it remains one of the most important diarrheal pathogens infecting young children in developing nations worldwide (Bouzari *et al*., 2012; Contreras & Ochoa, 2011; Hazen *et al*., 2016; Ochoa *et al.,* 2008). Upon colonization of the small intestine, the mild to severe diarrheal disease manifests from deregulated ion transport at the epithelial barrier, which can lead to rapid wasting and death without proper supportive management (Arenas-Hernández, Martínez-Laguna, & Torres, 2012). For most immunocompetent individuals the disease is self-limiting, where in the murine infection model of EPEC and EHEC disease it has been demonstrated that pathogen-restricting inflammation contributes to rapid enterocyte shedding and eventual bacterial clearance (Arenas-Hernández, Martínez-Laguna, & Torres, 2012; Collins *et al.,* 2014; Wiles *et al.,* 2004). The population most susceptible to severe disease are infants less than 2 years of age (mortality rate 10-40%) living in tropical and subtropical endemic regions worldwide (Arenas-Hernández, Martínez-Laguna, & Torres, 2012; Contreras & Ochoa, 2011).

All EPEC strains are negative for Shiga toxin, which defines the pathotype from EHEC (Pearson *et al.,* 2016). Furthermore, EPEC is subdivided into typical or atypical (aEPEC) strains based on the presence of the *E. coli* adherence factor (EAF) plasmid (Trabulsi, Keller, & Gomes, 2002). This virulence plasmid encodes two major operons: *bfp* and *perABC*, with the *bfp* operon encoding the type IV bundle forming pilus (BFP), and the *perABC* operon encoding regulatory genes required for *bfp* transcription and activation of the locus of enterocyte effacement (LEE) pathogenicity island (PAI) (Girón, Ho, & Schoolnik, 1991; McDaniel, Jarvis, Donnenberg, & Kaper, 1995; Tobe *et al.,* 1999).

The LEE PAI is of critical importance to EPEC infection, and to this thesis, and will therefore be discussed in detail in the next section. By definition, all aEPEC strains are LEE+, *bfp–,* and *stx*–, whereas typical EPEC are LEE+, *bfp*+*, stx*– (Contreras & Ochoa, 2011).

Of the diarrheagenic *E. coli* pathotypes, EPEC and EHEC colonization of the intestinal epithelial surface is characterized by a distinct histopathology known as the 'attaching and effacing' (A/E) lesion (Moon *et al.,* 1983). Following initial adherence to the epithelial cells, these bacteria form actin-rich pedestals that mediate intimate attachment to the host, and cause a localized destruction of the microvilli brush border (Jarvis *et al.,* 1995). This mechanism of attachment is shared with rabbit-specific EPEC and the mouse-restricted pathogen *Citrobacter rodentium*, another member of the *Enterobacteriaceae* family (Collins *et al.,* 2014; Deng *et al.,* 2003; Moon *et al.,* 1983). Due to its prevalence in developing nations and its highly analogous mechanism of pathogenesis to EHEC, the prototypical EPEC O127:H6 strain E2348/69, first identified by Levine *et al.,* 1978, is well studied in laboratories worldwide (Pearson *et al.,* 2016).

1.1.2 The EPEC LEE Pathogenicity Island Encodes a T3SS

The ability of all A/E pathogens to form epithelial lesions characteristic of disease is determined by a 35-40 kb pathogenicity island (PAI) called the locus of enterocyte effacement (LEE). (McDaniel *et al.,* 1995). The EPEC LEE contains 41 open reading frames (of > 50 amino acids (aa)), organized into five polycistronic operons (LEE1-LEE5), two bicistronic operons (*espG-rorf1* and *grlRA*), and 4 monocistronic entities (*etgA, cesF, map,* and *escD*) (Burkinshaw *et al.,* 2015; Elliott *et al.,* 1999; Lara-Ochoa, Oropeza, &

Huerta-Saquero, 2010; Mellies *et al.,* 1999). Nearly half of these genes encode structural components of a multimeric type III secretion system (T3SS), which is a common virulence factor for many mammalian and plant pathogens (Deng *et al.,* 2004, 2017; Elliott *et al.,* 2002; Hueck, 1998). T3SSs are structurally conserved biological nanomachines that deliver bacterial effector proteins directly from the bacterial cytoplasm into the host cell without passing through the extracellular space (Galán *et al.,* 2014). EPEC effector proteins may be encoded within the LEE or outside the LEE, where they are designated non-LEE encoded (*nle*) effectors. In addition to T3SS structural components and effectors, the LEE encodes chaperone proteins, an adhesin protein (intimin) and its receptor (Tir), as well as transcriptional regulators responsible for coordination of gene expression (Barba *et al.,* 2005; Elliott *et al.,* 2002; Iyoda *et al.,* 2006; McDaniel *et al.,* 1995).

1.2 Bacterial Type III Secretion Systems

The T3SS is a specialized biological nanomachine, or 'injectisome,' complex evolutionarily related to flagella that delivers multiple bacterial effector proteins into the extracellular space or directly into the cytosol of target eukaryotic cells (Abby & Rocha, 2012). Effector proteins delivered by the T3SS are distinct from bacterial toxins (Galán *et al.,* 2009). While both effectors and toxins exert their effects on living cells or organisms, toxins often exert a single biochemical activity that is meant to permanently disrupt cellular homeostasis. In contrast, effectors specifically manipulate host cell signalling pathways, often working as a collective group. It is additionally possible for a single effector to have more than one functional activity (Dean & Kenny, 2009; Kenny & Valdivia, 2009). In

addition to all EPEC and EHEC serotypes, T3SSs and diverse effector proteins are widely distributed among significant mammalian pathogen species of the following genera: *Yersinia*, *Chlamydia*, *Bordetella*, *Burkholderia*, *Pseudomonas, Salmonella*, *Shigella*, *Vibrio* (Galán & Wolf-Watz, 2006). Several Gram-negative bacterial species involved in commensal or mutualistic relationships also require T3SSs to promote adaptation to their replicative niche (Büttner & He, 2009; Galán *et al.,* 2014; Silver *et al.,* 2007). In recent years, advances in cryo-electron microscopy technology have provided remarkable near-atomic resolution images of the conserved T3SS architecture (Fujii *et al.,* 2012; Nans *et al.,* 2015; Notti & Stebbins, 2016; S. Wagner *et al.,* 2010). Although the structural features of this secretion system are well conserved across bacterial species, the Type III Secretion (T3S) effectors delivered by the bacterium into the eukaryotic cell are often pathogen specific (Galán *et al.,* 2009, 2014). For clarity, in the following section I describe current information on the structure and assembly of the T3SS using *E. coli* nomenclature as it has direct relevance to this thesis. The term effector secretion is herein defined as the export of effectors into the extracellular space, whereas effector translocation (or injection) refers to direct delivery of an effector protein from the bacterial cytoplasm into the eukaryotic cell, mediated by the T3SS.

1.2.1 Structure and Assembly of the T3SS

Upon complete assembly, the T3SS is comprised of at least 20 proteins that combine to span the bacterial inner and outer membranes and the eukaryotic cell plasma membrane (refer to Figure 1.1). There are several substructures within the T3SS apparatus. Notably, a cytoplasmic hexameric ATPase complex (EscN), an inner

membrane export apparatus, a cytoplasmic ring (C-ring; SepQ) that surrounds the ATPase complex and export apparatus, a basal body (which encircles an inner rod and the needle, and spans the bacterial inner and outer membrane), and a translocon, which

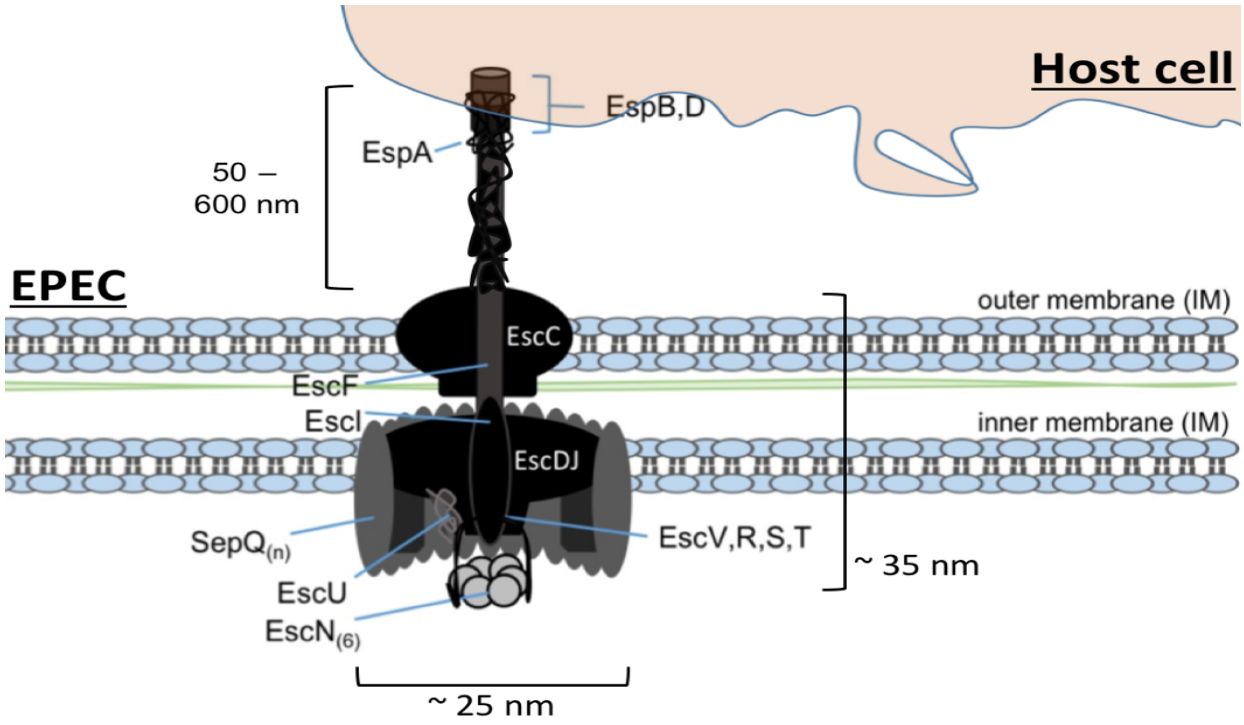

Figure 1.1: Illustration of the *E. coli* T3SS structural architecture in contact with a host cell. The length of EspA, which extends from the EscF needle structure and T3SS basal body (~ 35 nm length) as a helical filament, may vary from 50-600nm up to the translocon pore formed by EspB and EspD (Sekiya *et al.,* 2001).

---

forms a pore in the host membrane (Galán *et al.,* 2014). The precise mechanism of T3SS assembly is still under investigation, with some features potentially varying between species (Burkinshaw & Strynadka, 2014). In general, discrete stages of assembly exist, with the first being assembly of the basal body ring structures of the inner (EscD, EscJ) and outer (EscC) membrane which are formed in a process that requires the general secretion pathway (Sec) (Costa *et al.,* 2015). Second, the inner rod (EscI) and needle

(EscF) components, which function as the conduit for translocator and effector secretion, are secreted by the basal body, which signals completion of the T3SS (Deng *et al.,* 2017).

Located embedded within the inner membrane at the cytoplasmic face of the basal body is the export apparatus (EscR-V), which functions as an entry portal that all substrates must pass through to enter the conduit above the ATPase complex. The architecture of the export apparatus remains poorly characterized due to a lack of structural information for EscR, EscS, EscT, and the transmembrane domains of EscU and EscV (Deng *et al.,* 2017). However, it is well known that EscU is an autoprotease that upon self-cleavage induces a switch from secretion of early substrates (EscI and EscF) to translocators (EspA, EspB, and EspD) and effectors, which coincides with docking of chaperone-effector complexes at the inner membrane (Shaulov *et al.,* 2017; Thomassin, He, & Thomas, 2011; Zarivach *et al.,* 2008).

Surrounding the export apparatus and ATPase complex is the C-ring structure (SepQ). Together with the ATPase complex, the C-ring acts as a central sorting platform for substrate docking and subsequent secretion (Deng *et al.,* 2017). ATP hydrolysis and the proton motive force (PMF) are both required for efficient secretion, which depends upon substrate unfolding to accommodate travel through the conduit that is only 10-25Å in diameter (Akeda & Galán, 2005; Crepin *et al.,* 2005; Radics, Königsmaier, & Marlovits, 2014). Proteins that are transported across the bacterial inner membrane by the Sec or twin-arginine translocation (Tat) pathways possess conserved N-terminal signal peptides that are often cleaved during secretion (Costa *et al.,* 2015). Proteins secreted through the T3SS lack defined cleavable signals, however, less conserved residues (typically enriched for Ser, Thr, Ile, Pro) within the first ~20 amino acids of such proteins function

as targeting signals for the T3SS (Arnold *et al.,* 2009; Hueck, 1998; McDermott *et al.,* 2011). Interestingly, early, middle, and late substrates of the T3SS do not have clear differences in this secretion signal, which highlights the importance for other regulatory factors to tightly coordinate the secretion hierarchy (Deng *et al.,* 2015).

1.2.2 Regulation of the LEE-encoded T3SS

The master regulator of the LEE is the LEE-encoded regulator (Ler), which is a 15 kDa protein encoded as the first gene of the LEE1 operon (Mellies *et al.,* 1999). Expression of *ler* is influenced by several transcriptional regulators that respond to various stimuli (Table 1.1). Ler has been demonstrated to promote transcription of genes encoded in LEE1-LEE5 through antagonizing H-NS-dependent repression, suggesting that it is required for coordinated expression of virulence genes (Bustamante *et al.,* 2001; Mellies *et al.,* 1999). Additionally, Ler forms a feedback loop with the bicistronic GrlRA (Global Regulator Ler Repressor and Activator) operon encoded between LEE1 and LEE2 (Barba *et al.,* 2005). Upon Ler-dependent displacement of H-NS at the GrlRA promoter, transcriptional repression is alleviated, allowing GrlA to bind DNA in close proximity to the *ler* promoter and further activate Ler expression. This feedback mechanism is moderated through GrlR, which can directly bind to GrlA to prevent *ler* activation (Barba *et al.,* 2005). Additionally, expression of GrlA negatively regulates flagellar gene expression, which is indicative of a direct link between activation of genes necessary for host cell attachment in coordination with shutoff of bacterial motility (Iyoda *et al.,* 2006). Controlled expression of the LEE PAI engineered into non-pathogenic *E. coli* K12 has been demonstrated to produce a T3SS injectisome similar to those found in EPEC (Ruano-Gallego *et al.,* 2015).

Despite the multifactorial regulation of the LEE PAI (Table 1.1) and complex T3SS assembly mechanism, generation of non-pathogenic bacterial strains with a modified T3SS could be an efficient mechanism to deliver heterologous proteins directly into mammalian cells for therapeutic purposes (Reeves *et al.,* 2015; Ruano-Gallego *et al*., 2015).

Table 1.1: Transcriptional regulators that influence expression of Ler to promote coordinated activation of T3SS genes within the EPEC LEE PAI.

Regulator	Positive / Negative (+ / -)	Location	Stimuli	Reference
H-NS	-	Chromosome	Thermoregulation, non-secretion environment	(Rosenshine, Umanski, & Friedberg, 2002)
Ler	-	LEE1	autoregulatory	(Berdichevsky *et al.,* 2005)
GrlR	-	LEE PAI	Ler activation	(Barba *et al.,* 2005; Deng *et al.,* 2004)
GrlA	+	LEE PAI	Ler activation	(Barba *et al.,* 2005; Deng *et al.,* 2004)
SspA	+	Chromosome	Nutrient Starvation	(Hansen & Jin, 2012; Williams, Ouyang, & Flickinger, 1994)
QseA	+	Chromosome	Quorom sensing	(Kendall *et al.,* 2010; Sharp & Sperandio, 2007; Sperandio, Li, & Kaper, 2002)
PerC	+	EAF plasmid	Environmental	(Bustamante *et al.,* 2011; Mellies *et al.,* 1999)
Fis	+	Chromosome	Growth phase	(Goldberg *et al.,* 2001)
IHF	+	Chromosome	Environmental	(Friedberg *et al.,* 1999)

1.2.2.1 Coordinated Regulation of Substrate Secretion in the EPEC T3SS

For the T3SS to correctly assemble and function, a strict secretion hierarchy is imposed. An autocleavage event of EscU at a conserved NPTH motif induces the first secretion switch from early (EscI, EscF) to middle (EspA, EspB, EspD) and late (effectors) substrates (Zarivach *et al.,* 2008). EscU interaction with EspI and EscP have been

implicated in the timing of this switching event (Feria *et al.,* 2012; Sal-Man, Deng, & Finlay, 2012). The autocleavage itself promotes a conformational change in a highly conserved surface region of EscU, which potentially facilitates interaction with different components of the T3SS (Zarivach *et al.,* 2008). The EscP protein is a T3SS substrate secreted at low levels that is known to interact with EscI, EscF, EscU, and the multicargo type III secretion chaperone (T3SC) CesT (Feria *et al.,* 2012). EscP was demonstrated to regulate the length of the needle (EscF) as a molecular measuring device similar to the *Yersinia* YscP and flagellar FliK proteins (Feria *et al.,* 2012). In *Yersinia*, the YscP binding to YscU (EscU homolog) significantly decreased YscU autoproteolytic activity (Ho *et al.,* 2017). The timing of the EscU autocleavage event in EPEC may therefore reflect the interaction with EscP, however this has not been directly demonstrated (Deng *et al.,* 2017).

The second major secretion switch, from translocator (middle) to effector (late) proteins, is dependent on specific environmental cues (Deng *et al.,* 2005, 2015). In context of infection, the translocator proteins are secreted to form a pore in the host cell membrane through which the effectors then travel (Shaulov *et al.,* 2017). As an intestinal pathogen, for EPEC to contact the host cell its T3SS must penetrate a thick layer of mucus. This requires polymerization of EspA into a hollow filamentous structure that connects the needle (EscF) to the translocon pore (EspB/EspD) that forms in the host membrane (refer to Figure 1.1). Once complete, the translocation channel is established as a direct connection between the bacterial and host cytosol. *In vitro*, the switching event to effector secretion evidently involves EscP localized at the T3SS sorting platform. Here, EscP interacts with the secretion gatekeeper protein SepL in an intracellular calcium concentration-dependent manner (Shaulov *et al.,* 2017). EscU autocleavage, SepL-EscP

interaction, and SepD are required for translocator secretion (Deng *et al.,* 2004, 2005, 2015; Shaulov *et al.,* 2017; Zarivach *et al.,* 2008). Upon a decrease in calcium concentration upon completion of the T3SS conduit, the SepL-EscP complex dissociates, which promotes the switch to effector secretion (Shaulov *et al.,* 2017).

Spatiotemporal regulation of effector protein secretion is critical for bacterial colonization and subversion of host innate signalling pathways. Owing to the diverse nature of T3SS effectors, the regulation of effector secretion is a complex, multifaceted process that is often dependent on transcriptional, translational, and/or post-translational factors (Bhatt *et al.,* 2016; Katsowich *et al.,* 2017; Ramu *et al.,* 2013; Sittka *et al.,* 2007; Thomas *et al.,* 2007; Westermann *et al.,* 2016). At one level, bacterial chaperone proteins are often required for binding to and stabilizing newly synthesized effectors, which promotes effector trafficking to the type III secretion platform (Cooper *et al.,* 2010; Luo *et al.,* 2001; Page, Sansonetti, & Parsot, 2002; Spaeth, Chen, & Valdivia, 2009; Thomas *et al.,* 2005). Given the relevance of type III secretion chaperones (T3SC) to this thesis, they will be covered in greater detail in Section 1.2.3.

1.2.3 Type III Secretion Chaperone (T3SC) Proteins

Specific molecular chaperone proteins within the bacterial cytoplasm that are required to bind to and promote secretion of T3SS substrates are known as type III secretion chaperones (T3SCs). These T3SCs do not exhibit hallmark features of traditional heat shock protein (Hsp) chaperones, such as nucleotide binding and hydrolyzing, or protein folding activities (Hartl & Hayer-Hartl, 2002; Saibil, 2013). T3SCs are classified on the basis of substrate specificity: Class I chaperones bind to one (IA) or

more (IB) effectors, Class II bind to translocators, and Class III bind to needle proteins (Parsot, Hamiaux, & Page, 2003). Despite sharing low primary sequence identity, all known T3SC are small (~110-161 amino acids) and share an acidic isoelectric point (pI) (Izoré, Job, & Dessen, 2011). Diverse functional roles have been identified for T3SCs in addition to their primary function which is to sequester their cognate virulence protein(s) and prevent its premature interaction with other bacterial proteins in the cytosol (Stebbins & Galán, 2003; Thomas *et al.,* 2012). Multiple lines of evidence also suggest that T3SCs function in recruitment and docking events to cytoplasmic components of the T3SS, such as EscN, and EscP (Feria *et al*., 2012; Thomas *et al*., 2005, 2012). An additional regulatory function of T3SCs was first demonstrated for *Salmonella* SicA (class IA T3SC), which exerted an indirect regulatory effect on expression of the SopE (Darwin & Miller, 2001; Tucker & Galán, 2000). Functional roles for chaperone mediated control of virulence gene expression is currently an expanding research topic in T3SS pathogenesis, and is discussed in greater detail in Section 1.2.6.

1.2.3.1 Structure and Functional Dynamics of T3SCs

Class II and Class III chaperones possess remarkably similar quaternary structures that consist of three tetratricopeptide (TPR) fold motifs, characterized by two antiparallel α-helices that are involved in establishment of protein-protein contacts (Izoré *et al.,* 2011). These motifs are also found in classical Hsp chaperones, which bind to multiple substrates through TPRs (Pallen, Francis, & Fütterer, 2003). Both Class IA and IB chaperones share conserved 3-dimenstional dimeric structures (Izoré *et al.,* 2011). The dimerization interface involves overlapping parallel (IA) or angled (IB) helical domains

from each monomeric subunit (Luo *et al.,* 2001; van Eerde *et al.,* 2004). Extended regions of surface-exposed hydrophobic residues within the N-terminal region of the chaperone facilitate its binding to effectors (Galán & Wolf-Watz, 2006; Luo *et al.,* 2001). Effector proteins possess a chaperone-binding domain located within the first 50-100 amino acids downstream of their type III secretion signal (Galán *et al.,* 2014; Thomas *et al.,* 2007). Cytoplasmic chaperone binding maintains the effector in a stable, elongated state, where the N-terminal secretion signal is recognizable by the T3SS ATPase (Rodgers *et al.,* 2010; Stebbins & Galán, 2001; Thomas *et al.,* 2012). ATP hydrolysis at the T3SS apparatus contributes to dissociation of the chaperone-effector complex, which allows the effector to be secreted in an unfolded state and the chaperone recycled (Akeda & Galán, 2005; Radics *et al.,* 2014). Chaperone interactions with components of the secretion platform have been identified for a number of T3SSs (Deng *et al.,* 2017). Therefore, chaperone affinity for this inner membrane-bound platform is thought to contribute to overall secretion hierarchy.

In EPEC, CesAB is a class II chaperone that undergoes a conformational change upon binding with EspA, which allows CesAB to interact with the ATPase (EscN) (L. Chen *et al.,* 2013). CesAB is required for secretion of EspA and EspB, however, it is not required for EspB stability (Creasey *et al.,* 2003). EspB secretion requires a SepD/SepL-dependent signal ($EspB_{20-70}$) that immediately follows the N-terminal secretion signal ($EspB_{1-20}$) (Deng *et al.,* 2015). Interestingly, CesAB binding to EspB does not require this domain, and CesAB has not been demonstrated to directly interact with SepD or SepL at the secretion platform (Deng *et al.,* 2015). It was recently demonstrated that a decrease in calcium concentration promotes dissociation of a SepL-EscP complex at the T3SS

sorting platform. This dissociation promotes the secretion switch from translocators (EspA, EspB, EspD) to subsequent effectors, which critically involves the class IB chaperone CesT. As CesT is the major focus of this study, it will be discussed in greater detail as we proceed. Multicargo T3SC (class IB) are required by a number of mammalian and plant pathogens to coordinate secretion of virulence effectors. The currently known class IB chaperones and their cognate effectors are listed in Table 1.2.

Table 1.2: Class IB chaperone proteins and their known effector binding partners.

Organism	Chaperone	Effector	Reference
E. coli (EPEC / EHEC)	CesT	Tir*	Abe *et al.,* 1999; Elliott *et al.,* 1999
		Map*	Creasey *et al.,* 2003
		EspG*	Thomas *et al.,* 2007
		EspF	Thomas *et al.,* 2007
		EspH*	Mills *et al.,* 2008; Thomas *et al.,* 2005
		EspZ	Thomas *et al.,* 2005
		NleA	Thomas *et al.,* 2005
		NleF	Thomas *et al.,* 2005
		NleG	Thomas *et al.,* 2007
		NleH1	Thomas *et al.,* 2005
		NleH2	Thomas *et al.,* 2007
Chlamydia trachomatis	Mcsc	Cap1	Spaeth *et al.,* 2009
		Ct618	Spaeth *et al.,* 2009
	Slc1	TARP	Chen *et al*., 2014
		Ct694	Chen *et al*., 2014
		Ct695	Chen *et al*., 2014
		Ct875/TepP*	Chen *et al*., 2014
Shigella flexneri	Spa15	IpaA	Page *et al.,* 2002
		IpgB1*	Page *et al.,* 2002
		IpgB2*	Hachani *et al.,* 2008
		OspC1	Schmitz *et al.,* 2009
		OspC2	Page *et al.,* 2002
		OspC3	Page *et al.,* 2002
		OspB1	Page *et al.,* 2002
		OspD1	Parsot *et al.,* 2005
		OspD2	Schmitz *et al.,* 2009

Salmonella enterica	SrcA	SseL	Cooper *et al*., 2010
		PipB2	Cooper *et al.,* 2010
	InvB	SipA*	Bronstein, Miao, & Miller, 2000
		SopA	Ehrbar *et al.,* 2004
		SopE*	Ehrbar *et al.,* 2003
		SopE2*	Ehrbar *et al.,* 2003

Table 1.2 Continued

Organism	**Chaperone**	**Effector**	**Reference**
Xanthomonas campestris	HpaB	AvrBs1	Büttner *et al.,* 2004
		AvrBs3	Büttner *et al.,* 2004
		XopF1	Büttner *et al.,* 2007

Note: the effector proteins noted by an asterisk (*) are involved in manipulation of host cytoskeletal dynamics.

1.2.3.2 The Functional Importance of Class IB T3SCs is Highlighted by Common Themes in Enteric Bacterial Pathogenesis

The actin cytoskeleton of eukaryotic cells is an active network of helical filaments (F-actin) composed of globular actin (G-actin) subunits that is essential for diverse processes, such as cell communication, polarity, motility, and cell division (Burridge & Wennerberg, 2004; Hall, 1998). The ability to manipulate host cytoskeletal dynamics is a critical aspect of virulence for enteric bacterial pathogens (Bhavsar, Guttman, & Finlay, 2007; Burridge & Wennerberg, 2004). As such, a variety of T3SS effectors required for cytoskeletal disruption must interact with their respective T3SCs for efficient temporal trafficking to the T3SS (refer to Table 1.2) (Caron *et al.,* 2006; Kodama *et al.,* 2007; Ogawa *et al.,* 2008; Ohya *et al.,* 2005; Okada *et al.,* 2014; Tucker & Galán, 2000). The majority of host signalling pathways that regulate assembly and disassembly of actin filaments converge on Rho family GTPases, which make these enzymes a common target for disruption by pathogens. The nature of specific cytoskeletal rearrangements

induced by bacterial effectors is dependent on the lifecycle of the pathogen (Goosney, Knoechel, & Finlay, 1999). For example, intracellular pathogens such as *Shigella* and *Salmonella* deploy T3SS effectors to induce membrane "ruffling" that promotes bacterial invasion. IpgB1 and IpgB2 are two Spa15-dependent *Shigella* T3SS effectors that activate Rho GTPases to dysregulate host cell membrane architecture (Klink *et al.,* 2010; Ohya *et al.,* 2005).

By contrast, A/E pathogens such as EPEC, which do not invade host cells, stimulate cytoskeletal rearrangements to facilitate intimate bacterial contact with the host membrane. For fulminant virulence, this requires CesT-dependent secretion of Tir, EspG, EspH, and Map working in combination with the CesT-independent effectors EspM2 and EspT (Navarro-Garcia, Serapio-Palacios, Ugalde-Silva, Tapia-Pastrana, Chavez-Dueñas, *et al*., 2013). Map, EspT, and EspM2 mimic RhoGEFs (Rho guanine exchange factors) to activate Rho GTPases, while EspH inactivates mammalian RhoGEFs (Wong *et al.,* 2012). EspG imitates a small GTPase itself, which has been demonstrated to to disrupt microtubule networks required for tight junctions maintenance between epithelial cells and vesicle trafficking at the Golgi (Glotfelty & Hecht, 2012; Navarro-Garcia, Serapio-Palacios, Ugalde-Silva, Tapia-Pastrana, Chavez-Dueñas, *et al*., 2013). Tir stability and efficient secretion is strictly dependent on its interaction with CesT (Abe *et al.,* 1999; Elliott *et al.,* 1999). Upon translocation into the target cell plasma membrane, Tir initiates a host-driven regulatory cascade that activates the actin-related protein 2/3 (Arp2/3) complex to induce actin nucleation and polymerization underneath the site of bacterial attachment (Campellone & Leong, 2005; Kenny *et al.,* 1997; Schüller *et al.,* 2007). Collectively, it is evident that cytoskeletal disruption is of paramount importance to

EPEC, with CesT-dependent effector secretion being a major focal point for this virulence program.

A second overarching feature of the enteric bacterial pathogen infection cycle is the modulation of host innate immune sensing pathways. This step is fundamental for both extracellular and intracellular pathogens to establish their own unique replicative niche within the host. To accomplish this, bacterial pathogens have evolved a multitude of highly specific effector proteins to target critical aspects of the innate immune signalling pathways of the host. Specifically, regulation of pro-inflammatory cytokine expression through events such as inflammasome inactivation, disruption of vesicle trafficking, and blockade of pro-inflammatory transcription factor import to the host nucleus are modes by which effector proteins have been demonstrated to dampen the immune response (Cunha & Zamboni, 2013; Gao *et al.,* 2009; Garib *et al.,* 2016; Sellin, Müller, & Hardt, 2017; Yen, Sugimoto, & Tobe, 2015). Without proper coordination of effector translocation into host cells during infection, which explicitly involves multicargo T3SCs, the pathogenicity of the bacterial strain is severely altered. Accordingly, deletion of CesT, Spa15, or SrcA has been experimentally observed to attenuate *C. rodentium*, *S. flexneri,* or *S. enterica,* respectively, in mouse models of infection (Cooper *et al.,* 2010; Deng *et al.,* 2004; Hachani *et al.,* 2008).

1.2.4 Additional Roles for Chaperone Control of Virulence Gene Expression

Examples of chaperone-mediated regulation of virulence gene expression in enteric bacterial pathogens is tied to class IB T3SC in just two instances: Spa15 and CesT (Faherty & Maurelli, 2009; Katsowich *et al.,* 2017; Parsot *et al.,* 2005). However, the class

II chaperone SicA in *S. enterica* and its homolog IpgC from *S. flexneri* interact with AraC-family transcriptional activators InvF and MxiE, respectively, to promote effector gene expression (Darwin & Miller, 2001; Mavris *et al.,* 2002; Pilonieta & Munson, 2008). SicA and IpgC act as partitioning factors to prevent premature association of transclocator proteins under non-secretion conditions (Mavris *et al.,* 2002; Tucker & Galán, 2000). InvF is encoded by the first gene of the *Salmonella* pathogenicity island 1 (SPI-1), which encodes a T3SS required for host cell invasion (Darwin & Miller, 1999).

For *Shigella*, a 30kb region of the 200kb virulence plasmid (VP) encodes a functional T3SS, substrates, chaperones, and four transcriptional regulators (VirF, VirB, MxiE, and orf81). VP expression is repressed by H-NS at 30^{o}C, but not at 37 ^{o}C, where *virF* expression activates *virB*, which is required for transcription of "entry region" genes, including translocators and early effectors (Gall *et al.,* 2005; Schroeder & Hilbi, 2008). Following secretion of IpaB and IpaC translocators, IpgC is free to complex with MxiE to activate gene expression of a second set of effectors *(ospD3, E1, E2, G, ipaH)*. (Mavris *et al.,* 2002). This second wave of effector transcription is repressed by Spa15-OspD1 interaction with MxiE until secretion events upon host cell contact remove OspD1 and Spa15 from the cytoplasm via the T3SS (Faherty & Maurelli, 2009).

In the A/E pathogens EPEC and EHEC, evidence for regulation of effector gene expression by the class IB chaperone CesT also exists. It was demonstrated that the effector NleA is expressed only upon host cell contact, and that expression is repressed by the post-transcriptional regulator CsrA (carbon storage regulator A) binding to the 5' untranslated region (UTR) of *nleA* mRNA (Katsowich *et al.,* 2017). Upon host cell contact, it is evident that Tir is the effector translocated through the T3SS with greatest efficiency

(Mills *et al.,* 2013; Mills *et al.,* 2008; Thomas *et al.,* 2007). It was proposed that Tir secretion generates a pool of 'free' CesT in the cytoplasm to subsequently alleviate CsrA binding to the *nleA* 5'UTR, allowing translation initiation (Katsowich *et al.,* 2017). CsrA has been demonstrated to interact with mRNA for a number of bacterial genes to repress translation by binding to specific motifs at ribosome binding sites (Tony Romeo, Vakulskas, & Babitzke, 2013). In contrast, CsrA has been occasionally observed to behave as a positive regulator by protecting mRNA from RNase degradation, or remodelling of mRNA translation initiation regions to promote ribosome binding (Patterson-Fortin *et al.,* 2013; Yakhnin *et al.,* 2013). Specifically for the LEE PAI, positive regulation of SepL, EspA, EspB, EspD, EscF, and EscD transcript levels has been attributed to CsrA binding upstream of the *LEE4* transcript (Bhatt *et al*., 2009). Based on experimental evidence presented in this thesis, further insight on the role of CesT for *nleA* regulation will be highlighted in the Results and Discussion.

1.3 CesT: A Critical Factor for A/E Pathogenesis

The chaperone for *E. coli* secreted protein Tir (CesT; 156aa) was originally identified by two research groups simultaneously. Both demonstrated that CesT interacts with Tir, and that intracellular stability of Tir was significantly reduced in a *cesT* mutant, despite no change in *tir* transcription levels (Abe *et al.,* 1999; Elliott *et al.,* 1999). The *cesT* gene is located immediately downstream of *tir* and upstream of intimin (*eae*) within the LEE5 operon. Upon its translocation, Tir is inserted into the host membrane where it acts as the receptor for intimin on the bacterial surface, and initiates the host-driven signalling cascade required for actin pedestal formation (Campellone *et al.,* 2002; de Grado *et al.,*

1999; Hartland *et al.,* 1999; Hicks *et al.,* 1998). Deletion of *tir, cesT,* or *eae* prevents pedestal formation during *in vitro* EPEC infection of human cells and causes significant attenuation of *C. rodentium* in a mouse model of A/E pathogenesis (Abe *et al.,* 1999; Allen-Vercoe *et al.,* 2006; Deng *et al.,* 2004, 2003; Frankel *et al.,* 1996).

CesT is currently known to interact with at least 11 different T3S effector proteins, five of which are located outside the LEE PAI (Table 1.2). Interaction of CesT with the effector Map (Mitochondrial associated protein) was demonstrated by a yeast two-hybrid screen, which classified CesT as a bivalent T3SC (Creasey *et al.,* 2003). It was subsequently demonstrated that CesT is a multivalent chaperone after CesT-affinity binding column assays with total secreted protein from a Δ*sepD* genetic background, which hypersecretes effectors, identified EspZ, EspH, NleA, NleF, NleG, NleH1, NleH2, EspF, and EspG as new CesT-interacting partners (Thomas *et al.,* 2005, 2007).

CesT monomers possess three α-helical and six β-strand secondary structures (N'--α-β-β-β-α-β-β-α-β--C'), with the dimerization interface centered around the second α-helical secondary structure encoded from aa S63-E78 (Luo *et al.,* 2001). CesT is larger than other class IB T3SC, with position H128 and N129 being at the exact C-termini of Spa15 and InvB, respectively (Ramu *et al.,* 2013). The additional C-terminal region of CesT provides one extra β-strand relative to other class I chaperones, which is encoded from M139-S145 (Luo *et al.,* 2001). Surface-exposed hydrophobic residues of CesT have been implicated in chaperone-effector binding. Specifically, non-conservative substitution of valine-116 to arginine prevents CesT interaction with Tir (Delahay *et al.,* 2002). Val_{116} is predicted to contribute to formation of an amphipathic α-helix (α3; P107-G131)

structure that is conserved in other class I T3SCs, however this notion should be subject to further investigation (Delahay *et al.,* 2002; Luo *et al.,* 2001).

It is well established that Tir and CesT contribute to formation of an effector secretion hierarchy, although the exact mechanism behind this has yet to be elucidated (Mills *et al.,* 2008, 2013; Ramu *et al.,* 2013; Thomas *et al.,* 2007). Tir translocation into host cells is more efficient than all other LEE- and non-LEE-encoded EPEC effectors (Mills *et al.,* 2013, 2008). Due to the requirement of CesT for Tir secretion and the requirement of Tir for efficient secretion of other CesT-interacting effectors, it is very likely that CesT and Tir are required to establish the secretion hierarchy of T3S effectors (Thomas *et al.,* 2007). At the inner membrane, CesT and Tir both interact with the T3SS ATPase EscN, and the CesT-EscN interaction can occur without CesT bound to Tir (Gauthier & Finlay, 2003; Thomas *et al.,* 2005). Additionally, CesT and Tir have been demonstrated to interact with EscP and SepL, respectively, under conditions that promote translocator protein secretion (Feria *et al.,* 2012; Wang *et al.,* 2008). Under low calcium conditions, EscP dissociates from a complex with SepL, which promotes the switch from translocator to effector secretion (Shaulov *et al.,* 2017). Taken together, this evidence suggests that CesT-Tir and EscP-SepL form a complex at the secretion platform that prevents CesT-Tir access to EscN until the EscP-SepL complex dissociates .

1.3.1 The Unstructured CesT C-terminal Domain is Required for Effector Secretion

The C-terminal region of CesT (156 aa) from S146 to R156 did not resolve in the crystal structure and is predicted to encompass an unstructured region of the protein (Delahay *et al.,* 2002; Luo *et al.,* 2001; Ramu *et al.,* 2013). In a detailed study of the C-

terminus, it was noted that deletion of CesT S146-R156 ($CesT_{1-145}$) prevented secretion of NleA but not Tir; despite this domain lacking a functional role for CesT binding to effectors (Ramu *et al.,* 2013). In this study, the Δ*sepD* genetic background was used to quantitatively screen a CesT variant library generated by error-prone PCR to identify amino acids critical to CesT function with respect to effector secretion (Ramu *et al.,* 2013). Substitution mutation of serine 145, 146, or 147 with Ala, Thr, or Glu was quantitatively demonstrated to reduce overall protein secretion, with mutation of S147 completely abrogating NleA secretion (Ramu *et al.,* 2013). Collectively, this study revealed that a unique T3SC C-terminal domain was required for overall effector secretion, and that it may contribute to establishing the effector hierarchy between Tir and other CesT-interacting effectors (Ramu *et al.,* 2013).

1.3.2 The C-terminal Region of CesT is Tyrosine Phosphorylated

A mass spectrometry (MS) based analysis of EHEC O157:H7 and *E. coli* K12 identified the second largest phosphotyrosine (pTyr) proteome in bacteria to date, behind *Shigella* (Hansen *et al.,* 2013; Standish *et al.,* 2016). The pTyr modification is a well-studied post-translational regulatory mechanism in eukaryotic cell biology, however it remains less well characterized in bacteria (Deutscher & Saier Jr., 2006; Grangeasse, Nessler, & Mijakovic, 2012). Based on the increasing number of publications in the field, mass spectrometry technology has now reached a point where comprehensive identification of prokaryotic phosphoproteomes is achievable to a high degree of saturation (Dephoure *et al.,* 2013). The next major challenge for the field has become the

integration of newly identified kinases, phosphatases, and the phosphoprotein substrates into regulatory networks within the cell (Macek & Mijakovic, 2011).

CesT was one of eight LEE-encoded proteins identified by Dr. Anne-Marie Hansen and colleagues that is tyrosine phosphorylated by EHEC O157:H7 (Hansen *et al.,* 2013). Two neighbouring tyrosine residues, Y152 and Y153, within the unstructured C-terminal domain of CesT were identified as phosphorylation sites. Phosphorylation of both Y152 and Y153 within the same tryptic peptide was not observed (Hansen *et al.,* 2013). Etk and Wzc are the only characterized *E. coli* tyrosine kinases to date, and both are structurally different from traditional eukaryotic tyrosine kinases (Cozzone *et al.,* 2004; Hansen *et al.,* 2013). Site-specific phosphorylation of Y152 or Y153 was observed in an EHEC *etk wzc* double mutant, indicating that a currently unknown kinase can serve to phosphorylate CesT (Hansen *et al.,* 2013). However, functional analysis of the CesT phosphosites was not reported in this study.

The combination of datasets presented by Hansen and colleagues greatly expanded the known repertoire of tyrosine phosphorylated *E. coli* proteins involved in core physiological signalling pathways and virulence. Overall, 512 unique phosphotyrosine sites were identified on 342 proteins of *E. coli* K12 and EHEC O157:H7, which strongly suggests that this post-translational modification is of paramount importance. However, it was not logistically possible to provide a comprehensive functional analysis of each site identified within the study. Phosphorylation sites mapped by highly sensitive LC-MS/MS must therefore be assessed by independent methods to determine whether or not functional relevance exists (Dephoure *et al.,* 2013).

1.4 Phosphorylation in Bacterial Pathogenesis is an Expanding Research Area

Bacterial pathogens live under a range of host conditions and therefore must employ intricate signalling pathways to coordinate virulence gene regulation in response to environmental stimuli such as toxins, metabolites, host-cell contact, and quorum sensing. At one level this involves control of gene expression, however at the post-translational level there are a diverse range of reversible modifications that often produce significant changes to the structural properties of proteins to regulate function or expression level (Dell *et al.,* 2010; Deutscher & Saier Jr., 2006; Grangeasse, Stülke, & Mijakovic, 2015; Katsowich *et al.,* 2017; Soufi *et al.,* 2015). Generally, the range of post-translational modifications include addition of i) chemical functional groups (alkyl, phosphoryl, glucosyl, and acyl), ii) small proteins (ubiquitin, and small ubiquitin-like modifiers (SUMO)), or iii) modification of amino acid chemical properties (deamidation, deimidation, and oxidation) (Bah & Forman-Kay, 2016). A single protein may be post-translationally modified on a number of specific amino acids, which contributes to the multiple levels at which the protein might function. Given the relevance of protein phosphorylation to this thesis and how it is applicable to prokaryotic examples in the literature, this type of modification is subsequently introduced in greater detail.

Phosphorylation of serine, threonine, and tyrosine (STY phosphorylation) residues replaces a neutral phosphate-acceptor hydroxyl (OH) group with a 3-dimensional (3D) tetrahedral phosphate (PO_4^{2-}) structure capable of forming novel intramolecular or intermolecular electrostatic interactions. In context of serine, threonine, and tyrosine phosphorylation, the modification is acid-stable, and thus can be studied by conventional phosphoprotein enrichment approaches that typically involve acidic treatment steps (Fíla

& Honys, 2012). Basic amino acid residues such as histidine, lysine, and arginine may also be phosphorylated, forming what is known as a phosphoramidate residue, which is susceptible to acid hydrolysis and is therefore often missed in standard phosphoproteomic studies (Cieśla, Frączyk, & Rode, 2011). In general, the added phosphate group locally imposes two negatively charged oxygen atoms at physiological pH, altering steric and electrostatic properties of the amino acid sequence to generate secondary structural changes; often to confer protein:protein interactions critical to regulatory networks within a cell (Bah & Forman-Kay, 2016). In this thesis the specific tyrosine phosphorylation sites of the T3SC CesT are of principal focus due to the requirement of CesT for A/E pathogenesis. It is currently unknown what kinase(s) and phosphatase(s) regulate the CesT phosphorylation status, however an incredibly diverse range of pTyr-binding domains (including Src homology 2 (SH2), Hakai pTyr-binding (HYB), and C2 domains) exist among eukaryotic proteins for recognition of pTyr sites to confer protein:protein interactions (Jin & Pawson, 2012; Kaneko *et al.,* 2012; Wagner *et al.,* 2013). While such PTB domains have not been identified for prokaryotic proteins to date, we sought to address the question of whether pTyr-mediated regulation of CesT function exists; presumably through unidentified CesT:protein interaction(s) conferred by the reversible phosphorylation modification.

A number of prokaryotic cellular processes regulated by phosphorylation have been identified, including cell growth, capsular polysaccharide or lipopolysaccharide biosynthesis, septum formation, sporulation, metabolite consumption, biofilm formation, and response to oxidative stress or heat-shock (reviewed by Cozzone, 2006; Grangeasse, Stülke, & Mijakovic, 2012). However, characterization of prokaryotic

signalling processes influenced by phosphorylation has often proved challenging by kinase or substrate mutation; either due to functional redundancies or minimally observable phenotypes. It is well established that roughly one third of all eukaryotic proteins are phosphorylated, with most modified amino acids localized to specific intrinsically disordered protein (IDP) domains (Bah & Forman-Kay, 2016; Chen *et al.,* 2006; Xie *et al.,* 2007). In recent years the development of highly sensitive mass spectrometry-based detection techniques has expanded the understood diversity of prokaryotic phosphoproteomes and revealed that a significant portion of the phosphosites identified relate to core metabolic pathways (> 30%) and essential genes; including many involved in biosynthesis of nucleotides, amino acids, and exopolysaccharide capsule (Grangeasse, 2016; Hansen *et al.,* 2013; Lin *et al.,* 2015; Macek *et al.,* 2007, 2008; Standish *et al.,* 2016). Specific examples are infrequently established in the literature that relate to bacterial virulence factor regulation (introduced in section 1.4.1), however the expanding study of site-specific phosphorylation is recognized as a major functional tool in bacterial signal transduction.

1.4.1 Prokaryotic STY Phosphorylation

One of the most difficult challenges in bacterial physiology is to understand how environmental stimuli are integrated and transmitted by vast intracellular protein networks to influence the overall pathogenesis mechanism. Throughout an infection cycle, multiple phosphorylation and de-phosphorylation reactions involving bacterial virulence factors are catalyzed by endogenous or host kinase and phosphatase enzymes to contribute to pathogenesis (Cozzone, 2006; Whitmore & Lamont, 2012). Traditional bacterial tyrosine

kinases (BYKs) and eukaryotic-like serine/threonine kinases (ESTKs) catalyze phosphate group additions, while diverse protein phosphatases such as eukaryotic-like tyrosine phosphatases (PTPs), dual-specificity phosphatases (DSPs), and low molecular weight PTPs (LMW-PTPs) catalyze phosphate removal reactions (Canova & Molle, 2014; Grangeasse, Nessler, & Mijakovic, 2012; Whitmore & Lamont, 2012). These enzymes are widely distributed among infectious bacterial species (Grangeasse, 2016; Sajid *et al.,* 2015; Whitmore & Lamont, 2012). BYKs are structurally distinct from eukaryotic tyrosine kinases, with transmembrane domains and the characteristic Walker A and B ATP-binding motifs of BYKs in their cytoplasmic catalytic domain (Deutscher & Saier Jr., 2006). In contrast, traditional ESTKs are found in each domain of life with several conserved amino acid regions known as Hanks-signatures and catalytic domains that are structurally conserved (Grangeasse, 2016). Interestingly, dual-specificity protein kinases (DSPKs), which are widespread among Eukaryota have also been reported in *Bacillus spp*., *S.* Typhimurium, *Chlamydophila pneumoniae,* and *Mycobacterium tuberculosis* (Arora *et al.,* 2012; Johnson & Mahony, 2007; Kusebauch *et al.,* 2014; Ostrovsky & Maloy, 1995). DSPKs autophosphorylate on tyrosine, serine, or threonine residues and phosphorylate substrates on tyrosine, serine and threonine (Deutscher & Saier Jr., 2006; Grangeasse, 2016; Kusebauch *et al.,* 2014).

Several DSPK enzymes have been identified in *M. tuberculosis* that play a functional role in cell growth and virulence. *M. tuberculosis* claims an estimated 1.4 million lives per year, and possess at least 11 two-component regulatory systems and 11 ESTK enzymes of the Pkn family (PknA-K) (Prisic *et al.,* 2010). These Pkn enzymes likely organize into a network for activation of one another, and protein phosphorylation status

has been demonstrated to correspond to various growth conditions (Prisic *et al.,* 2010). PknA and PknB are both essential for *M. tuberculosis* replication, with PknB implicated as a key factor in latency regulation, while PknG phosphorylation is critical for virulence in mice (Ortega *et al.,* 2014; Sherman & Grundner, 2014). Members of the Pkn family have been identified as phosphorylated on tyrosine despite *M. tuberculosis* lacking traditional BYKs (Kusebauch *et al.,* 2014). Specific members of the Pkn family (PknB, -D, -E, -F, -G) are additionally capable of catalyzing Tyr phosphorylation of protein substrates (Kusebauch *et al.,* 2014). Several observations of *M. tuberculosis* Tyr phosphorylation were extended to conserved proteins of the soil-dwelling bacterium *Mycobacterium smegmatis*, indicating that the pTyr modification exists to support regulation of bacterial physiology, and is not an exclusive pathogenesis mechanism (Kusebauch *et al.,* 2014; Sherman & Grundner, 2014). Topics introduced in this section will be revisted in Chapter 4.3 (Discussion) as the nature of DSPKs is suspected to be of importance for CesT phosphorylation.

1.4.2 Reviewing the Recently Expanded *E. coli* and *Shigella flexneri* Phosphotyrosine Proteome

Shigella spp. are the most closely related members of the *Enterobacteriaceae* family to *E. coli* (Beld & Reubsaet, 2012). It was therefore not surprising that an identical phosphopeptide enrichment approach to that of Hansen and colleagues for EHEC O157:H7 and *E. coli* K12 analysis yielded a tremendous amount of pTyr proteins in *S. flexneri* (12.1% of all ORFs) (Standish *et al.,* 2016). Both *E. coli* and *S. flexneri* datasets demonstrated that proteins involved in core metabolic pathways are enriched for pTyr modifications (33-35%), while virulence proteins account for <5% of the pTyr proteome

(Hansen *et al.,* 2013; Standish *et al.,* 2016). Of particular relevance to T3SS biology, phosphopeptides corresponding to the class IB T3SC in both *Shigella* (Spa15; 128 aa) and EHEC (CesT; 156 aa) were identified in high confidence through mass spectrometry data for two specific tyrosine residues (Hansen *et al.,* 2013; Standish *et al.,* 2016). However, the position of the two pTyr sites of Spa15 (Y71, Y108) are not conserved in CesT; and as noted previously, CesT phosphorylation was observed in a unique unstructured C-terminal domain at Y152 or Y153 (Hansen *et al.,* 2013). Distinct phosphorylation sites on neighbouring amino acids are very rare for prokaryotes, with the only two reported examples other than CesT being the Ser-431 and/or Thr-432 phosphorylation of the cyanobacterial protein KaiC (Kim *et al.,* 2015), or Y717 or Y718 phosphorylation of EHEC Etk (Hansen *et al.,* 2013). Functional analysis of the Spa15 phosphosites was not conducted in the proteomic study by Standish *et al.*, 2016.

Additional *Shigella* T3SS-associated proteins phosphorylated on tyrosine that were not functionally characterized by Standish and colleagues include the needle length regulator Spa32, the ATPase Spa47, and the IpaC component of the translocon pore (Standish *et al.,* 2016). Tyrosine phosphorylation of the EHEC T3SS translocon proteins EspA, EspB, and EspD was observed, however functional significance was not reported (Hansen *et al.,* 2013). The phosphotyrosine modification may therefore be of significance for formation of the *E. coli* or *S. flexneri* T3SS translocon pore (based on its conservation across functionally related proteins of two distinct genera) yet future studies will be required to address this question experimentally. The remainder of this thesis will focus on functional characterization of the CesT phosphotyrosine sites in context of A/E pathogenesis.

1.5 Research Objectives

The major objective of this research is to functionally assess the impact of each CesT phosphosite in context of effector secretion and enteric disease. An important secondary objective is to extend and validate the previous observations of EHEC CesT phosphorylation in the closely related A/E pathogen EPEC. This study is the first to assign a regulatory impact for tyrosine phosphorylation to a type III secretion chaperone, and therefore presents a new research direction in bacterial pathogenesis.

CHAPTER 2. MATERIALS AND METHODS

2.1 Bioinformatic Analysis of CesT

Computational analysis of CesT from EPEC O127:H6 (str. E2348/69) was performed with the protein Basic Local Alignment Search Tool (BLASTP) from the National Centre for Biotechnological Information (NCBI). The CesT amino acid sequence (GenBank: AAK26723.1) in FASTA format was used as a query to probe the non-redundant NCBI database with default search parameters. The sequence identity (%) for matches to full-length CesT (156 aa) from A/E pathogen isolates were recorded. A representative multiple alignment of CesT from five A/E pathogen isolates was generated with the Constraint-Based Multiple Alignment Tool (COBALT) from NCBI using default settings to highlight positional amino acid substitutions across the primary sequence. The standard pairwise constraint settings were unmodified for the COBALT analysis.

2.2 Growth of Bacterial Cultures

Bacterial strains generated and used in this study are listed in Table 2.1. Bacteria were routinely cultured overnight in Luria-Bertani (LB) broth (1% [w/v] tryptone, 0.5% [w/v] yeast extract, 1% [w/v] NaCl) at 37 ^{o}C. Antibiotics (Sigma) were added when appropriate, to a final concentration of 100 µg/ml ampicillin (Amp), 50 µg/ml kanamycin (Kan), 50 µg/ml streptomycin (St), 30 µg/ml chloramphenicol (Cm), and 10 µg/ml tetracycline (Tet). For experiments that required activation of T3SS gene expression, bacteria were cultured without antibiotics, under static conditions in serum-free Dulbecco's Modified Eagle Medium (DMEM) (Invitrogen; #11995) in a humidified, 5% CO_2 incubator at 37 ^{o}C.

Table 2.1: Strains and plasmids used in the study.

Strains	Description	Source/comment
EPEC O126:H7	EPEC strain E2348/69, streptomycin-resistant	Levine *et al.,* 1978
EHEC O157:H7	EHEC, Shiga toxin positive	Griffin *et al.,* 1988
EPEC Δ*cesT*	Non-polar *cesT* deletion mutant	Abe *et al.,* 1999
EPEC Δ*sepD*	Non-polar *sepD* deletion mutant	Deng *et al.,* 2005
EPEC Δ*sepD*Δ*cesT*	Double mutant derived from Δ*sepD*	Thomas *et al.,* 2005
EPEC *cesT*(S147A)	Expresses CesT(S147A) from the EPEC chromosomal *cesT* locus	Ramu *et al.,* 2013
EPEC *cesT*(Y152F)	Expresses CesT(Y152F) from the EPEC chromosomal *cesT* locus	This study
EPEC *cesT*(Y153F)	Expresses CesT(Y153F) from the EPEC chromosomal *cesT* locus	This study
EPEC *cesT*(Y152F, Y153F)	Expresses CesT(Y152F,Y153F) from the EPEC chromosomal *cesT* locus	This study
EPEC *tir::tir-blaM*	Merodiploid chromosomal construct for expression of Tir-TEM-1 built into EPEC	This study
EPEC *espF::espF-blaM*	Merodiploid chromosomal construct for expression of EspF-TEM-1 built into EPEC	This study
EPEC *nleA::nleA-blaM*	Merodiploid chromosomal construct for expression of NleA-TEM-1 built into EPEC	This study
EPEC *nleH1::nleH1-blaM*	Merodiploid chromosomal construct for expression of NleH1-TEM-1 built into EPEC	This study
EPEC *nleH2::nleH2-blaM*	Merodiploid chromosomal construct for expression of NleH2-TEM-1 built into EPEC	This study
Δ*cesT tir::tir-blaM*	Merodiploid chromosomal construct for expression of Tir-TEM-1 built into EPEC Δ*cesT*	This study
Δ*cesT espF::espF-blaM*	Merodiploid chromosomal construct for expression of EspF-TEM-1 built into EPEC Δ*cesT*	This study
Δ*cesT nleA::nleA-blaM*	Merodiploid chromosomal construct for expression of NleA-TEM-1 built into EPEC Δ*cesT*	This study
Δ*cesT nleH1::nleH1-blaM*	Merodiploid chromosomal construct for expression of NleH1-TEM-1 built into EPEC Δ*cesT*	This study
Δ*cesT nleH2::nleH2-blaM*	Merodiploid chromosomal construct for expression of NleH2-TEM-1 built into EPEC Δ*cesT*	This study
cesT(S147A) *tir::tir-blaM*	Merodiploid chromosomal construct for expression of Tir-TEM-1 built into EPEC *cesT* (S147A)	This study
cesT(S147A) *espF::espF-blaM*	Merodiploid chromosomal construct for expression of EspF-TEM-1 built into EPEC *cesT* (S147A)	This study
cesT(S147A) *nleA::nleA-blaM*	Merodiploid chromosomal construct for expression of NleA-TEM-1 built into EPEC *cesT* (S147A)	This study
cesT(S147A) *nleH1::nleH1-blaM*	Merodiploid chromosomal construct for expression of NleH1-TEM-1 built into EPEC *cesT* (S147A)	This study
cesT(S147A) *nleH2::nleH2-blaM*	Merodiploid chromosomal construct for expression of NleH2-TEM-1 built into EPEC *cesT* (S147A)	This study
cesT(Y152F) *tir::tir-blaM*	Merodiploid chromosomal construct for expression of Tir-TEM-1 built into EPEC *cesT* (Y152F)	This study
cesT(Y152F) *espF::espF-blaM*	Merodiploid chromosomal construct for expression of EspF-TEM-1 built into EPEC *cesT* (Y152F)	This study
cesT(Y152F) *nleA::nleA-blaM*	Merodiploid chromosomal construct for expression of NleA-TEM-1 built into EPEC *cesT* (Y152F)	This study

Table 2.1 Continued		
Strains	**Description**	**Source/comment**
cesT(Y152F) *nleH1::nleH1-blaM*	Merodiploid chromosomal construct for expression of NleH1-TEM-1 built into EPEC *cesT* (Y152F)	This study
cesT(Y152F) *nleH2::nleH2-blaM*	Merodiploid chromosomal construct for expression of NleH2-TEM-1 built into EPEC *cesT* (Y152F)	This study
cesT(Y153F) *tir::tir-blaM*	Merodiploid chromosomal construct for expression of Tir-TEM-1 built into EPEC *cesT* (Y153F)	This study
cesT(Y153F) *espF::espF-blaM*	Merodiploid chromosomal construct for expression of EspF-TEM-1 built into EPEC *cesT* (Y153F)	This study
cesT(Y153F) *nleA::nleA-blaM*	Merodiploid chromosomal construct for expression of NleA-TEM-1 built into EPEC *cesT* (Y153F)	This study
cesT(Y153F) *nleH1::nleH1-blaM*	Merodiploid chromosomal construct for expression of NleH1-TEM-1 built into EPEC *cesT* (Y153F)	This study
cesT(Y153F) *nleH2::nleH2-blaM*	Merodiploid chromosomal construct for expression of NleH2-TEM-1 built into EPEC *cesT* (Y153F)	This study
cesT(Y152F, Y153F) *tir::tir-blaM*	Merodiploid chromosomal construct for expression of Tir-TEM-1 built into EPEC *cesT* (Y152F, Y153F)	This study
cesT(Y152F, Y153F) *espF::espF-blaM*	Merodiploid chromosomal construct for expression of EspF-TEM-1 built into EPEC *cesT* (Y152F, Y153F)	This study
cesT(Y152F, Y153F) *nleA::nleA-blaM*	Merodiploid chromosomal construct for expression of NleA-TEM-1 built into EPEC *cesT* (Y152F, Y153F)	This study
cesT(Y152F, Y153F) *nleH1::nleH1-blaM*	Merodiploid chromosomal construct for expression of NleH1-TEM-1 built into EPEC *cesT* (Y152F, Y153F)	This study
cesT(Y152F, Y153F) *nleH2::nleH2-blaM*	Merodiploid chromosomal construct for expression of NleH2-TEM-1 built into EPEC *cesT* (Y152F, Y153F)	This study
DH5α	*E. coli* strain used for cloning	Invitrogen
DH5α λ*pir*	*E. coli* strain used for cloning; permissive for pRE112 or pCX391 replication	Invitrogen
BL21	*E. coli* host for protein overexpression	Novagen
pEVS104/C118λpir	Conjugation helper strain with plasmid based on pRK2013; Does not replicate in hosts without λpir.	Stabb & Ruby, 2002
NH4	EPEC Δ*hsdR*; contains a mutation in the type-I restriction modification system. Used as a helper strain for cloning.	Hobson *et al.,* 2008
Citrobacter rodentium	*C. rodentium* DBS100	ATCC 51459
*C. rodentium Δ*cesT	*cesT* deletion mutant	Deng *et al.,* 2004
C. rodentium ΔnleA	*nleA* deletion mutant	Deng *et al.,* 2004
C. rodentium cesTY152F	Expresses CesT(Y152F) from the *C. rodentium* chromosomal *cesT* locus	This study
C. rodentium cesTY153F	Expresses CesT(Y153F) from the *C. rodentium* chromosomal *cesT* locus	This study
C. rodentium cesTY152F, Y153F	Expresses CesT(Y152F,Y153F) from the *C. rodentium* chromosomal *cesT* locus	This study
Plasmids	**Description**	**Source/comment**
pAMH275	Expression of EHEC *cesT* from the LEE5 promoter in low copy vector pSec10	Received from Anne-Marie Hansen

Table 2.1 Continued		
Plasmids	**Description**	**Source/comment**
pAMH276	Expression of EHEC *cesT* Y152F from the LEE5 promoter in low copy vector pSec10	Received from Anne-Marie Hansen
pAMH277	Expression of EHEC *cesT* Y153F from the LEE5 promoter in low copy vector pSec10	Received from Anne-Marie Hansen
pAMH278	Expression of EHEC *cesT* Y152F,Y153F from the LEE5 promoter in low copy vector pSec10	Received from Anne-Marie Hansen
pAMH279	Expression of EHEC *cesT* Y152D from the LEE5 promoter in low copy vector pSec10	Received from Anne-Marie Hansen
pAMH280	Expression of EHEC *cesT* Y153D from the LEE5 promoter in low copy vector pSec10	Received from Anne-Marie Hansen
pAMH281	Expression of EHEC *cesT* Y152D/Y153D from the LEE5 promoter in low copy vector pSec10	Received from Anne-Marie Hansen
pAMH282	Expression of EHEC *cesT* Y152E/Y153E from the LEE5 promoter in low copy vector pSec10	Received from Anne-Marie Hansen
pFLAG-CTC	Vector for expression of ORF-FLAG fusion constructs from the *tac* promoter	Sigma
pCesT-FLAG	EPEC *cesT* cloned as a HindIII/KpnI fragment into the pFLAG-CTC expression vector, expresses CesT-FLAG from the *tac* promoter	Thomas *et al.,* 2005
pCesT(Y152F/Y153F)-FLAG	EPEC *cesT(Y152F/Y153F)* cloned as a HindIII/KpnI fragment into the pFLAG-CTC expression vector, expresses CesT(Y152F/Y153F)-FLAG from the *tac* promoter	This study
pCesT(Y152F)-FLAG	EPEC *cesT(Y152F)* cloned as a HindIII/KpnI fragment into the pFLAG-CTC expression vector, expresses CesT(Y152F)-FLAG from the *tac* promoter	This study
pCesT(Y153F)-FLAG	EPEC *cesT(Y153F)* cloned as a HindIII/KpnI fragment into the pFLAG-CTC expression vector, expresses CesT(Y153F)-FLAG from the *tac* promoter	This study
pAT113	Monocopy expression vector for GFP; used to transform chromosomal EPEC *cesT* variant strains for fluorescence microscopy	This study
pNleA-FLAG	pACYC184 with cloned *nleA* allele, expresses NleA-FLAG from the *nleA* promoter	Ramu *et al.,* 2013
p(Tir)-NleH2-FLAG	Promoter region for *tir* regulating NleH2-FLAG expression	Thomas *et al.,* 2007
pCX341	Vector for formation of fusions with the *blaM* gene (encoding TEM-1 β-lactamase); derivative of pCX340 with the pBR322 ori for lower copy number and P_{trc} promoter. Used experimentally as a translocation control for unfused TEM-1.	Mills *et al.,* 2008; Charpentier *et al.,* 2004
pCX442	pCX391 derivative; conjugative suicide plasmid that encodes *tir-blaM,* received from Ilan Rosenshine	Mills *et al.,* 2008
pCX446	pCX391 derivative; conjugative suicide plasmid that encodes *espF-blaM*, received from Ilan Rosenshine	Mills *et al.,* 2008
pCsrA (ASKA)	High-copy plasmid from the ASKA library; expresses *csrA* by the IPTG-inducible *lac* promoter	Kitagawa *et al.,* 2010

2.3 DNA Isolation

Genomic DNA was isolated from bacterial strains using the Wizard genomic DNA isolation kit (Promega) as recommended by the manufacturer. Plasmids were isolated from bacterial strains using the Monarch spin miniprep kit (NEB) as recommended by the manufacturer. Oligonucleotides used for cloning and sequencing are listed in Table 2.2, and were routinely ordered from Integrated DNA Technologies (IDT). Synthetic gene block (IDT) sequences used for generation of *cesT* phosphosite variant EPEC and *C. rodentium* strains are listed in Appendix A.

Table 2.2: List of oligonucleotides used in this study.

Name	Oligonucleotide Sequence (5' → 3')	Restriction Site
CesT/For/FLAG	CCCAAGCTTTCATCAAGATCTGAACTTTTA	HindIII
CR003 – 152/153	CCGGTACCTCTTCCGGCGAAAAAATGTTTATTATCGC	KpnI
CR004 – 152	CCGGTACCTCTTCCGGCGTAAAAATGTTTATTATC	KpnI
CR005 – 153	CCGGTACCTCTTCCGGCAAAATAATGTTTATTATC	KpnI
CR-NleA-fwd	GCGGTACCATGAACATTCAACCGATCGTAAC	KpnI
CR-NleA-rev	GCGAATTCCCGACTCTTGTTTCTTGGATTATATC	EcoRI
CR-NleH1-fwd	GCGGTACCATGCTATCACCATCTTCTGTAAA	KpnI
CR-NleH1-rev	GCACAATTGCCAATTTTACTTAATACCACACTAATAAG	MfeI
CR-NleH2-fwd	GCGGTACCATGTTATCGCCCTCTTCTATAA	KpnI
CR-NleH2-rev	GCACAATTGCCTATCTTACTTAATACTACACTAATAAG	MfeI
CR-NleA-Bla-seqF	GCATGCAAGAGAAGGTGCCATTTTCC	None
CR-NleH1-Bla-seqF	CGATACAACAGAGACAAATGTCTTATATGATCGCACG	None
CR-NleH2-Bla-seqF	CCATCATTACCAGCACAAGCTGAACAGGC	None
CR-Tir-Bla-seqF	GGCAAGGTATCCAAAGTACTTATGCGC	None
CR-EspF-Bla-seqF	CGAAAAGTCTTGATACTTCAGGTCTTAAGCCAAGCC	None
NT379	AAGAGCTCCTCGGAATAGTCTATCGGCTCA	SacI
NT380	TATCGCTTGAGCTAATTTCCTC	None
NT381	AAGAGCTCTCCTAACTATAGCGTTATACAG	SacI
NT382	TTTTCATATGTTCATTTTCTAATGTTATTCC	NdeI
NT383	ACGAATATATGATGATCTATGG	None
NT384	AAGCTGAGCAACGCTTTCACCCGT	None

Note: Restriction enzyme cleavage sites are underlined.

2.4 Construction of EPEC and *C. rodentium cesT* variants

Single-copy chromosomal EPEC and *C. rodentium* strains that express phosphodeficient CesT variants were generated by mutation of the *cesT* locus by allelic exchange. EPEC genomic DNA was used in a PCR with primers NT379 and NT380 to generate an 857 base pair amplicon that was cloned into pBluescript SacI and EcoRV sites, to generate pEPcesT. This plasmid was digested with NdeI and KpnI to create the vector backbone for synthesized *cesT* sequence gene blocks (Integrated DNA Technologies) that code for site-specific tyrosine to phenylalanine substitutions within CesT (Appendix A). The gene blocks were directionally cloned as NdeI/KpnI fragments. The respective recombinant clones, which encompass the *tir-cesT-eae* locus (each containing specific *cesT* mutations) were then subcloned as SacI/KpnI DNA fragments into the pRE112 suicide plasmid using DH5$\alpha\lambda$*pir* as a cloning host. A similar approach was used for *C. rodentium* using primers NT381 and NT382 for PCR with *C. rodentium* DNA to generate pCRcesT, followed by ligation cloning to gene blocks coding for specific *C. rodentium cesT* alleles in pRE112. All *cesT* mutations within their respective suicide plasmid constructs were verified by DNA sequencing. Suicide plasmid constructs were mobilized into recipient strains via triparental conjugation with recipient single crossover merodiploid clones (EPEC or *C. rodentium*) selected on solid growth media containing streptomycin and chloramphenicol (for EPEC) or ampicillin and chloramphenicol (for *C. rodentium*). After streak purification of merodiploid clones on selective antibiotic media, sucrose selection was performed to isolate mutants with a second crossover event as previously described (Ramu *et al.,* 2013). Bacterial isolates that exhibited growth on sucrose but not chloramphenicol were then streak purified. Several isolates were subjected to PCR analysis for the *cesT* allele, followed by Sanger DNA sequencing at

Genome Quebec, McGill University (Applied Biosystems 3730xl DNA Analyzer), to identify the appropriate *cesT* sequence mutation.

2.4.1 Construction of FLAG tagged EPEC CesT variants

To create plasmids expressing CesT(Y152F)-FLAG, CesT(Y153F)-FLAG, and CesT(Y152F, Y153F)-FLAG, genomic DNA from EPEC was amplified by PCR using forward primer CesT/For/FLAG paired with either CR004-152, CR005-153, or CR003-152/153 respectively. Purified PCR products were cloned into HindIII/KpnI digested pFLAG-CTC to create C-terminal FLAG fusions to the indicated CesT sequence variants. Plasmid constructs were used to transform *E. coli* DH5α via heat-shock. In each case, transcription was regulated by the recombinant *tac* promoter on the plasmid. All constructs were confirmed by sequencing, then moved into EPEC NH4 (type I restriction system deficient strain) and subsequently EPEC Δ*cesT* by electroporation.

2.4.2 Generation of Effector-β-lactamase Fusions

The coding regions of CesT-interacting T3SS effectors NleA, NleH1, and NleH2 were amplified by PCR and cloned into pCX341 to generate C-terminal translational fusions to TEM-1 beta lactamase (encoded by the *blaM* gene). This cloning step was carried out in DH5$\alpha\lambda$pir *E. coli*. The effector-*blaM* fusion constructs in pCX341-based plasmids were digested with KpnI and XbaI, and run on a 1% agarose gel to identify insert sequence. Each insert band was extracted from the gel (Qiagen kit gel extraction) and subcloned into the pCX391 suicide plasmid digested with KpnI and XbaI. DH5$\alpha\lambda$pir cells transformed via heat-shock were selected on LB tetracycline (10μg/mL) plates. The

pCX442 (Tir-TEM-1) and pCX446 (EspF-TEM-1) suicide plasmids derived from pCX391 were previously received from Ilan Rosenshine. These plasmids were transformed into DH5αλpir to finalize a total of five donor strains to be used in a conjugation experiment. Each donor contained a single pCX391-based effector-*blaM* fusion that was to be targeted for chromosomal integration within six different EPEC recipient strains: *wild type, ΔcesT, cesT(S147A), cesT(Y152F), cesT(Y153F), and cesT(Y152F,Y153F)*. Single crossover integration of the plasmid via homologous recombination conferred resistance to tetracycline for the EPEC recipients. Streptomycin (50 μg/ml) was included in the selection media to prevent growth of DH5αλpir donors. Suicide plasmid-encoded effector-*blaM* constructs were verified by sequencing prior to conjugation.

2.5 Enrichment of CesT-FLAG for Analysis by Liquid Chromatography Tandem-Mass Spectrometry (LC-MS/MS)

For enrichment of CesT-FLAG proteins by immunoprecipitation (Figure 2.1), bacterial cultures were initially grown in 5 mL of LB medium for 18 h, then subcultured 1:50 into 50 mL of DMEM and grown for an additional 5.5 h at 37 ^{o}C, 5% CO_2. Cells were harvested by centrifugation and washed twice with PBS before resuspension in 1 mL of urea-containing lysis buffer (20 mM 4-(2-hydroxyethyl)-1-piperazineethanesulfonic acid (HEPES), pH 8.0; 9M urea; 1 mM β-glycerophosphate; 1 mM sodium orthovanadate; 2.5 mM sodium pyrophosphate). Cell lysates were sonicated at amplitude control setting 4 (20% output) with a Misonix XL-2000 ultrasonic liquid processor (Qsonica). Insoluble debris was cleared by centrifugation at 20,000x g for 15 min at 15^{o}C, and soluble lysates were reduced using 5 mM dithiotheitol at 56 ^{o}C for 20 min, then cooled to room

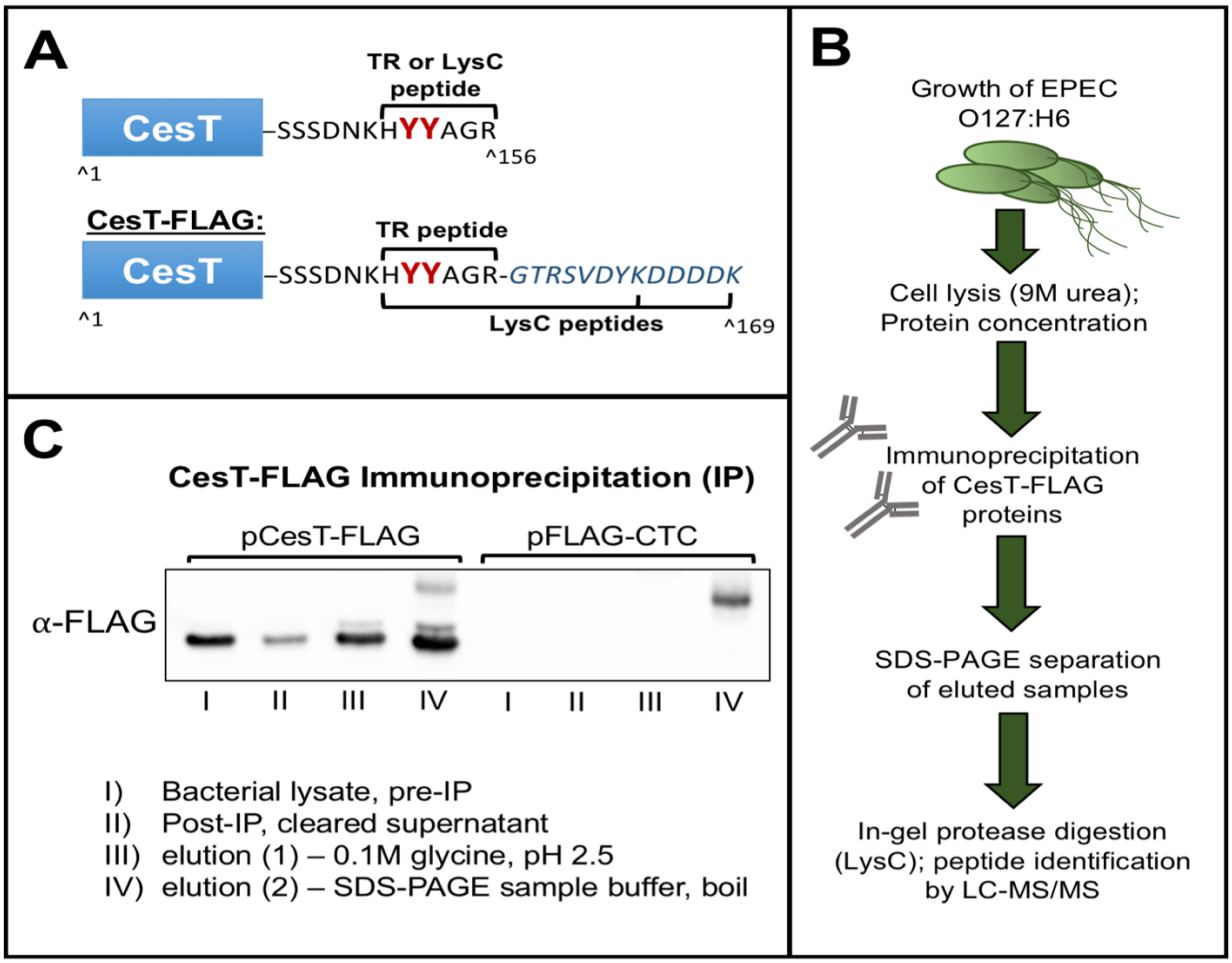

Figure 2.1: Approach to assess the CesT C-terminus by LC-MS/MS without phosphopeptide enrichment. (A) CesT was C-terminally fused to the FLAG epitope (DYKDDDDK) by a quintameric linker (GTRSV) in the pFLAG-CTC vector to create CesT-FLAG. LysC digestion was conducted to avoid production of small positively charged C-terminal peptides commonly encountered with a trypsin (TR) digest. (B) Five-step schematic of the enrichment approach with (C) immunoblot analysis of the sample before and after immunoprecipitation. Bacterial strains were cultured under conditions to promote T3SS gene expression. LC-MS/MS analysis revealed both phosphorylated and non-phosphorylated CesT-FLAG C-terminal peptides.

---

temperature and treated with 20 mM iodoacetamide for 15 min in the dark. The soluble lysates were diluted to a final concentration of 0.5 M urea and 20 mM HEPES buffer (pH 8.0) and subsequently concentrated with an Amicon® 10K centrifugal filter (Millipore) to a final volume of 1 mL in PBS-Tween (PBS-T) (0.05% Tween-20, Sigma). Post-concentration, 1 mg of the soluble protein was added to 50 μL of Anti-FLAG M2 Affinity

Gel (Sigma), prepared per the manufacturer's instructions. Following overnight immunoprecipitation at room temperature, antibody-bound proteins were eluted by addition of SDS-PAGE sample buffer and boiling for 5 min. Samples were separated by SDS-PAGE and stained by Coomassie blue G-250, as previously described (Neuhoff *et al*., 1985). Bands corresponding to CesT-FLAG samples at the appropriate migration distance (MW ~ 19.2 kDa) were excised from the gel and stored at -20^{o}C until further use.

2.5.1 Phos-Tag Phosphoprotein Gel Stain

Eluted protein samples from immunoprecipitation were separated by SDS-PAGE. The Phos-Tag gel stain procedure was carried out as per the manufacturer's instructions, with minor modifications (GeneCopoeia, P005A). Briefly, imaging of phosphorylated protein species within the Phos-tag stained gels was conducted with a VersaDoc MP5000 using fluorescence excitation at 550nm to detect phosphoproteins and at 649 nm for total proteins. Ovalbumin from the Low-Range MW Standard (Bio-Rad; 161-0304) was used as positive control for phosphoprotein detection, and lambda phosphatase (New England BioLabs) was used to enzymatically dephosphorylate samples as needed.

2.5.2 Sample Processing for LC-MS/MS

Excised gel slices stained with Coomassie blue G-250 were processed for LC-MS/MS as previously described (Shevchenko *et al.,* 2007), with minor modifications. Briefly, gel slices were de-stained with 50% acetonitrile (ACN) for 2 h, then cut into ~1 mm cubes and rinsed twice with 200μL of dH_2O. Gel cubes were reduced with 10 mM dithiotheitol at 56^{o}C for 30 min, alkylated with 55 mM iodoacetamide for 30 min at room

temperature in the dark, and dehydrated with 200 μL ACN. Dried gel cubes were saturated with 100 ng/μL of Endoproteinase LysC (New England BioLabs) for 2 h, then 20 μL of 50 mM ammonium bicarbonate was added and the samples were incubated overnight at 37 ^{o}C. Digested peptides were extracted from the gel cubes by treatment with a solution of 50% ACN, 5% formic acid. The peptide-containing solution was dried to a pellet in a vacuum centrifuge and subsequently resuspended in 15-30μL of a 3% ACN, 0.5% formic acid solution. This solution containing the concentrated peptides was transferred to a 300 μL HPLC vial and subject to analysis by LC-MS/MS on an LTQ Orbitrap VelosPRO mass spectrometer (ThermoFisher Scientific).

2.5.3 Mass-spectrometry based identification of CesT phosphopeptides

CesT-FLAG or CesT(Y153F)-FLAG peptide samples, digested with LysC, were analyzed on a LTQ Orbitrap VelosPRO mass spectrometer equipped with an UltiMate 3000 Nano-LC system (ThermoFisher Scientific). Chromatographic separation of the digests was performed on PicoFRIT C18 self-packed 75 μm x 60 cm capillary column (New Objective, Woburn, MA) at a flow rate of 300 nL/min. MS and MS/MS data was acquired using a data-dependent acquisition method in which a full scan was obtained at a resolution of 30,000, followed by ten consecutive MS/MS spectra in both higher-energy collisional dissociation (HCD) and collision-induced dissociation (CID) mode (normalized collision energy 36%). Internal calibration was performed using the ion signal of polysiloxane at m/z 445.120025 as a lock mass.

Raw MS data was evaluated in Proteome Discoverer 2.1 (ThermoFisher Scientific). Peak lists were searched against NCBI protein database for EPEC O127:H6

(strain E2348/69) as well as the cRAP database of common contaminants (Global Proteome Machine Organization) and custom FASTA sequences for the CesT-FLAG proteins. Search criteria included LysC protease with two missed cleavages permitted. Cysteine carbamidomethylation was set as a fixed modification, while methionine (Met) oxidation, N-terminal Met loss, and phosphorylation on serine, threonine, and tyrosine were included as variable modifications. A mass accuracy tolerance of 5 ppm was used for precursor ions, while 0.02 Da for HCD fragmentation or 0.6 Da for CID fragmentation was used for product ions. Percolator was used to determine confident peptide identifications using the standard 0.1% false discovery rate (FDR). Site-specific determination of phosphorylated amino acids was confirmed using PhosphoRS (ThermoFisher Scientific). Product b and y ion series corresponding to the fragmented CesT-FLAG or CesT(Y153F)-FLAG parent ions were visually assessed for confirmation of the specific phosphorylation site assigned by the PhosphoRS algorithm.

2.6 *In vitro* Protein Secretion Assays

Assays for total secreted proteins derived from EPEC strains were performed as previously described (Thomas *et al.,* 2005). Ethylene glycol-bis(β-aminoethyl ether)-N,N,N',N'-tetraacetic acid (EGTA) to a final concentration of 2mM was added to DMEM when required to chelate calcium, promoting effector secretion. All secretion assay experiments were repeated three times, with representative data shown. Bradford protein quantification assays were carried out using Pierce Coomassie reagent as directed by the manufacturer. OD_{600} readings were obtained to normalize sample volume to cell number (1:1 volume of culture supernatant and Coomassie reagent). Absorbance values at 595nm were detected on an Eppendorf Biophotometer. A bovine serum albumin (BSA)

standard curve was generated to determine the linear range of the Bradford assay (y = 2915.2*x* – 428.66; R^2 = 0.947; where x = A_{595} and y = protein concentration (μg/mL)).

2.6.1 TEM-1 Inactivation of Ampicillin

A single 5 mL liquid suspension of ampicillin susceptible *E. coli* ATCC 25922 overnight culture was used to spread plate a uniform culture covering the approximate entirety of the Müeller-Hinton agar plate. Two sterile 10 μg ampicillin (Amp10) disks (BD; 231264) were subsequently added to each plate (separated from each other by >5 cm). A 1 mL fraction of wild type or *cesT* (Y153F) *nleA::nleA-blaM* cultures grown for 24 h in DMEM supplemented with 2 mM EGTA were centrifuged for 1 min at 15,000 x g in an Eppendorf benchtop centrifuge to pellet whole cells. The culture supernatant, containing secreted protein, was subjected to two additional centrifugation steps at 15,000 x g followed by filter-sterilization to remove any remaining bacterial cells. 30 μL of this secreted protein fraction was applied to each sterile ampicillin 10 μg (Amp10) disk. The labelled plates were placed in a 37 ^{o}C incubator for 18 h, then imaged and measured the next day.

2.6.2 Protein Electrophoresis and Immunoblotting

Sodium Dodecyl Sulfate-Polyacrylamide Gel Electrophoresis (SDS-PAGE) was carried out with the method of Laemmli (Laemmli, 1970), with minor modifications made to accommodate use of a Bio-Rad mini-Protean system under constant voltage (100 V). The polyacrylamide concentrations routinely used include 10% (effector secretion or translocation analysis), 12% (CesT migration analysis from a whole cell lysate), and 15%

(immunoprecipitation elution sample separation). All Blue Pre-stained Protein Standards (Bio-Rad) were used as molecular weight markers unless otherwise indicated. Coomassie G-250 staining for total protein visualization was routinely conducted as previously described (Neuhoff, Stamm, & Eibl, 1985).

Transfer of proteins separated by SDS-PAGE to a polyvinylidene difluoride (PVDF) membrane support (Millipore) was performed using the Trans-Blot™ Turbo® Transfer System (Bio-Rad) operating at 15 V. For immunoblotting, antibodies were used at the following dilutions; anti-FLAG (mouse), 1:10,000 (Sigma); anti-TEM-1 (mouse), 1:10,000 (Santa Cruz Biotechnology); anti-calnexin (mouse), 1:1000 (Cell Signaling); anti-RNA polymerase (mouse), 1:2000 (Santa Cruz Biotechnology); anti-Tir (mouse), 1:1000 (Thomas *et al.,* 2007); anti-EspB (mouse), 1:1000 (Gauthier *et al.,* 2005); goat anti-mouse conjugated to horseradish peroxidase (HRP), 1:5,000 (Rockland Immunochemicals); goat anti-rabbit conjugated to HRP, 1:5,000 (Rockland Immunochemicals). Anti-CesT (mouse) monospecific antibodies raised against a synthetic peptide (LENEHMKIEEISSSDNK) corresponding to a portion of the CesT C-terminal region were affinity purified against the peptide by the supplier and used in immunoblots at a 1:10000 dilution (Ramu *et al.,* 2013). Immunoblots were developed using Clarity™ Western Blotting Substrates (Bio-Rad) to induce chemiluminescent signal emission. Chemiluminescence was detected using a Bio-Rad VersaDoc MP5000. For comparative analyses, experimental and control measurements from the same membrane were processed for densitometry using ImageLab software.

2.7 *In vitro* HeLa cell Infections

HeLa cells are a widely used epithelial cell line for *in vitro* study of EPEC infection (Mills *et al.,* 2008, 2013; Thomassin, He, & Thomas, 2011). HeLa cells were routinely passaged (every 4-5 days) into fresh DMEM +10% Fetal Bovine Serum (FBS) growth media following a 2 min enzymatic treatment with 0.25% trypsin/EDTA. A hemocytometer (Hausser Scientific) was used to enumerate cell density per mL prior to HeLa cell seeding for infection assays. Experimental conditions for a number of *in vitro* infection assays are detailed in the following sections.

2.7.1 Fluorescence Microscopy

HeLa cells were seeded onto glass coverslips within a 24-well tissue culture plate at a density of 10,000 cells/mL, grown for 24 h, then infected with EPEC strains at an MOI of 50 for 3 h. Infected cells were fixed for 15 min in 2.5% paraformaldehyde (PFA) and permeabilized with PBS/0.1% Triton X-100. The HeLa cell F-actin cytoskeleton was stained with Alexa Fluor 568 phalloidin (1:300; Molecular Probes). Coverslips were mounted onto microscope slides in ProLong Gold anti-fade reagent (Molecular Probes) and imaged using a Zeiss Axiovert 200M Inverted Microscope outfitted with a Hamamatsu ORCA-R2 digital camera. Quantification of intimate bacterial attachment (binding index) was conducted as previously described (Thomassin *et al*., 2011; Vingadassalom *et al*., 2010). Briefly, the percentage of HeLa cells harboring at least five bacteria (identified by GFP fluorescence) that were associated with F-actin pedestal foci were counted (63X oil immersion objective). Three independent experiments were performed, with at least 50 cells examined per infection condition.

2.7.2 Host Cell Fractionation by Ultracentrifugation

HeLa cells were seeded into 10 cm tissue culture dishes at a density of 10,000 cells/mL, grown for 24 h, then infected with the indicated EPEC strains at an MOI of 50 for 3 h. Cells were washed three times with ice-cold phosphate-buffered saline (PBS) and subjected to fractionation as previously described (Gauthier, De Grado, & Finlay, 2000; Gruenheid *et al.,* 2004). Briefly, cells were resuspended in 300 μL of homogenization buffer (3 mM imidazole, 250 mM sucrose, 0.5 mM ethylenediaminetetraacetic acid (EDTA), pH 7.4) supplemented with cOmplete ^{TM} protease inhibitor cocktail (Roche) and mechanically disrupted by vigorous passage through a 22-gauge needle. The resultant suspension was centrifuged at low speed (3000 x g) for 15 min at 4^{o}C to pellet unbroken cells, bacteria, nuclei, and cytoskeletal components. The supernatant was subjected to high-speed ultracentrifugation (100,000 x g) for 30 min at 4^{o}C (Beckman Coulter Optima^{TM}) to separate host cell membranes (pellet) from cytoplasm (supernatant).

2.7.3 Real-Time Effector Translocation Analysis

A high-throughput, population based kinetic assay that makes use of the *blaM* reporter gene has been well established to study the hierarchical nature of effector translocation in EPEC pathogenesis (Charpentier & Oswald, 2004; Mills *et al.,* 2013). The *blaM* gene encodes TEM-1 beta-lactamase, which has previously been utilized as a stable translational fusion to study chromosomal- or plasmid-encoded ORFs of EPEC and *S.* Typhimurium by a fluorescence reporter assay (Mills *et al.,* 2013). In context of EPEC pathogenesis, chimeric effector-TEM-1 fusion proteins expressed natively from single copy genes provided sensitive detection of translocation efficiency differences for both

LEE and non-LEE encoded effectors (Mills *et al.,* 2013). The real-time translocation assay measurements report on the accumulation rate of the CCF2 (ThermoFisher Scientific; K1023) hydrolysis product (blue fluorescence), which reflects the concentration of effector-TEM-1 in the infected HeLa cells (Mills *et al.,* 2008). Without translocation of the effector-TEM-1 fusion, the cephalosporin core of the CCF2 substrate remains uncleaved, permitting fluorescence resonance energy transfer (FRET) required for green fluorescent emission (Charpentier & Oswald, 2004).

On day 1 of the protocol, HeLa cells were seeded in 96-well plates (black with clear bottom, ThermoFisher Scientific) at a density of $2x10^4$ cells/well in DMEM (Invitrogen) supplemented with 10% FBS. In parallel, bacterial strains encoding chromosomal *effector-blaM* fusions were grown overnight in LB at 37 ^oC, shaking at 200 rpm. On day 2, bacterial cultures were diluted 1/200 into DMEM and grown statically in conditions known to stimulate T3SS expression (37 ^oC, 5% CO_2 for 4 h to $OD_{600\ nm}$ of 0.2-0.35) to create a 'pre-activated' culture. At the 3 h mark of the culture pre-activation, HeLa cells were washed twice with DMEM +10% FBS +2.5 mM probenecid (herein referred to as DFP media), and treated with 20 μL of 6X CCF2-AM (Invitrogen; K1023) substrate loading solution dissolved in 100μL DFP media. The cells were incubated for 40 min at room temperature in the dark, then washed an additional three times with 100 μL DFP to titer out extracellular CCF2-AM substrate from the growth media. $OD_{600\ nm}$ measurements were recorded for each bacterial culture at the 4 hr mark of pre-activation to normalize infection inoculum to an MOI of 50, 100, or 200. Immediately upon bacterial inoculation, the plates were placed in a plate reader (Victor X5; PerkinElmer) set to 37 ^oC, which was where the infection took place for 100 min. Infected cells were excited at 405 nm, and

emission was recorded at 460 nm and 535 nm at 10 min intervals over the course of infection. Experimental data was collected with PerkinElmer 2030 software and adjusted for background blue and green fluorescence with the following formula in Microsoft Excel:

$R = [BS_{RAW} – BS_{UNI}] / [GS_{RAW} – GS_{BK}]$

BS_{RAW}, measured product fluorescence at 460 nm; BS_{UNI}, average background 460 nm fluorescence from uninfected HeLa cells loaded with CCF2-AM substrate at each measured time-point; GS_{RAW}, measured product fluorescence at 535 nm; GS_{BK}, average background 535 nm fluorescence from uninfected HeLa cells without CCF2-AM substrate. To normalize well-to-well variation in number of HeLa cells and/or efficiency of CCF2-AM substrate uptake, all samples were run in duplicates, and R values for each condition at each time-point were averaged. Real-time translocation data is representative of average R values for at least three independent experiments. Wild type EPEC expressing β-lactamase (unfused) was used as an experimental negative control.

2.8 Mice infections with *C. rodentium*

All animals were handled under the approval of the University Committee on Laboratory Animals under protocol #16-001, Dalhousie University, which applies the guidelines of the Canadian Council on Animal Care. Healthy female C57BL/6 mice ordered from Charles River Laboratories were acclimatized for 14 days in cages within the IWK Health Centre animal care facility. The mice were randomized into 7 groups (n=5 per group) for separate treatments. Bacterial inocula for the respective groups were prepared by growing 25 mL cultures in LB broth (16 h, 37 ^{o}C, 200 rpm), started from a

freshly grown single colony. The overnight cultures were pelleted by centrifugation, resuspended in 2.5 mL of sterile PBS, then normalized to cell number. Mice were infected by oral gavage (2.0 $x10^{10}$ bacterial cells per mouse). The remaining culture was used to enumerate the live inocula by plating dilutions onto LB agar. Mice weights were monitored, and stool samples were collected at day 3, 5, 7, and 9 to monitor bacterial shedding. After 9 days, mice were sacrificed to harvest colon tissue samples. Stool or colon material was weighed, homogenized in PBS, then subjected to serial dilution and plating onto MacConkey agar. *Citrobacter* appeared as small colonies with pink centres surrounded by a clear haze after 24 h of growth at 37 ^{o}C. *C. rodentium* colony identification was confirmed by PCR of the *cesT* allele.

2.9 Statistical Analyses

All statistical analyses, where indicated in Chapter 3 (Results) were conducted with GraphPad Prism 6.0 software using the recommended default parameters. Independent sample group means were analysed by the unpaired t-test method without the assumption of the same standard deviation for each group. For the TEM-1 translocation assay detailed by Chapter 2.7.3, group means (two samples per test) were analysed for each time point measured during the infection assay and the results of statistical significance ($P< 0.01$ or $P< 0.05$) were summarized in table format throughout Chapter 3.6 and 3.7.

CHAPTER 3. RESULTS

3.1 Tyrosine Phosphorylation Sites of CesT are Conserved by all A/E Pathogens

It was previously reported that CesT possesses an extra β-strand secondary structure (β6) relative to other T3SC that is encoded by the M139-S145 region near the C-terminus (Luo *et al.,* 2001). Three-dimensional (3D) structural characterization of EHEC CesT by X-ray crystallography revealed that the C-terminal domain downstream of β6 was unresolved (Luo *et al.,* 2001). The functional significance of this C-terminal region for type III effector secretion was recently established, and two neighbouring tyrosine residues within were subsequently identified as sites of phosphorylation (Hansen *et al.,* 2013; Ramu *et al.,* 2013). To begin investigation on the potential functional importance of CesT phosphorylation at the C-terminus, a bioinformatics analysis was conducted to identify phosphosite conservation using software provided by the NCBI. The non-redundant BLASTP revealed 1183 NCBI database entries of full-length CesT with 95-100% amino acid sequence identity to the CesT query sequence from EPEC E2348/69 (GenBank: AAK26723.1). Sequence analysis was conducted with the COBALT software through NCBI for representative strains of the A/E pathogens EPEC, EHEC, Rabbit EPEC (REPEC), *C. rodentium,* and *Escherichia alberti* (Figure 3.1). Conservative amino acid substitutions are observed throughout the CesT sequence, however the tyrosine phosphosites Y152 and Y153 are invariant for all 1183 A/E pathogen isolates identified by BLASTP. Structurally disordered regions are conserved within protein families across all domains of life and are frequently essential for cell signalling and regulatory functions (Bah *et al.,* 2016; Chen *et al.,* 2006; Uversky, Oldfield, & Dunker, 2005).

Figure 3.1: Multiple sequence alignment of CesT from representative A/E pathogens. The COBALT software from NCBI was used with default alignment parameters and the identity setting. Identical amino acids are coloured in red. The region of the sequence encoding the additional β-strand secondary structure (β6) and the unstructured C-terminal domain (X) unique to CesT are depicted below the alignment. Asterisks(*) indicate previously observed sites of CesT phosphorylation (Y152 and Y153).

3.2 LC-MS/MS Identification of Site-Specific Tyrosine Phosphorylation at the CesT C-terminus

The remainder of this study focused on identification of regulatory function for the C-terminal CesT phosphotyrosine (pTyr) sites. However, to establish the pTyr modification as a conserved *E. coli* regulatory mechanism, it was important to extend the phosphorylation observation from EHEC to the closely related A/E pathogen EPEC. The unstructured C-terminal region of CesT (-SSDNKHYYAGR) contains many polar and positively charged amino acids. This imposed a significant challenge for generation of suitable tryptic peptides for LC-MS/MS analysis of Y152 and Y153. The pTyr peptide enrichment approach performed by Hansen *et al*. 2013 identified phosphotyrosine residues of CesT from peptides with at least one missed trypsin cleavage site at K150.

For this reason, the mass spectrometry approach to assess CesT Y152 and Y153 was intentionally biased away from identification of small C-terminal peptides ([K]HYYAGR) that were frequently observed following digestion with trypsin (data not shown). To accomplish this, EPEC Δ*cesT* strains were complemented with recombinant CesT C-terminally fused to the FLAG epitope (DYKDDDDK) by a quintameric linker peptide (GTRSV) in pFLAG-CTC (Sigma).

Addition of the FLAG sequence (-GTRSVDYKDDDDK) does not impact CesT stability (Figure 3.2), nor does it abolish the ability of CesT to interact with EscN or secrete Tir and NleA (Thomas *et al.,* 2005). Plasmid-encoded CesT-FLAG fusions for CesT(Y152F), CesT(Y153F), and CesT(Y152F, Y153F) were constructed to evaluate aspects of contextual amino acid sequence on site-specific phosphorylation. Interestingly, in the Δ*sepD*Δ*cesT* genetic background, complementation with pCesT-FLAG did not restore total secretion to the level of Δ*sepD* ($P < 0.0001$) or Δ*sepD*Δ*cesT* complemented with pCesT ($P < 0.01$). However, complementation with pCesT(Y153F)-FLAG restored total secretion levels to that of pCesT (Figure 3.2B). Consistent with the impact of the FLAG tag on CesT-dependent secretion, complementation of Δ*cesT tir::tir-blaM* or Δ*cesT nleA::nleA-blaM* with pCesT-FLAG failed to restore the level of effector translocation into HeLa cells to that of the wild type CesT effector-TEM-1 fusion (Figure 3.2C). Nonetheless, the advantages of a reliable high affinity FLAG-antibody immunoprecipitation and downstream proteolytic LysC digestion method for LC-MS/MS analysis outweighed the negative functional impact of this chimeric protein.

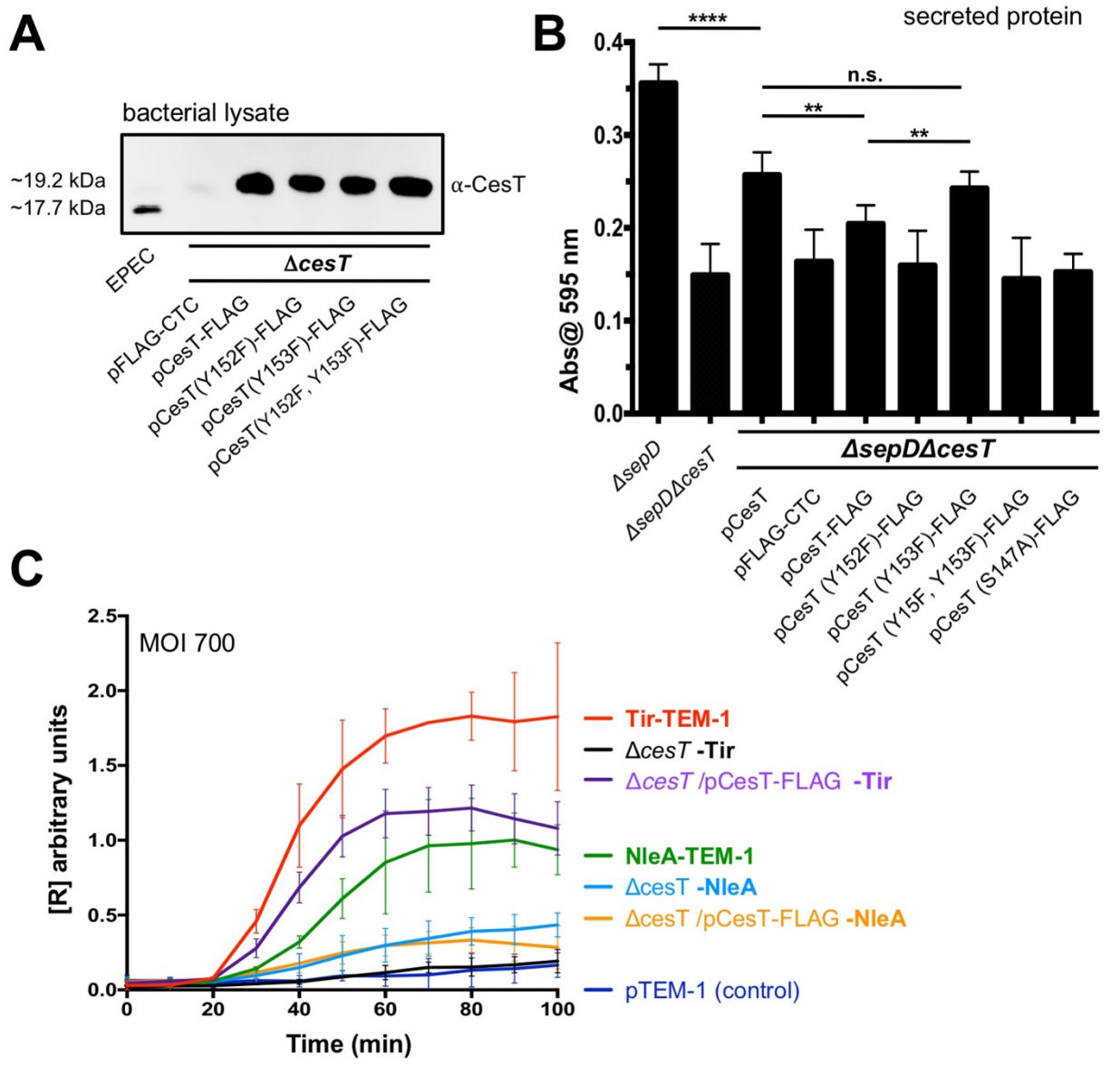

Figure 3.2: The C-terminal FLAG tag does not decrease protein stability but has a negative functional impact on CesT-dependent effector secretion. (A) Immunoblot analysis of EPEC CesT and sequence variants of CesT-FLAG expressed in EPEC Δ*cesT.* This FLAG tag imposes a 1.5 kDa increase in protein size and adds a net -2 charge (at pH 7), resulting in migration retardation during SDS-PAGE. (B) Secreted protein quantitation from the indicated bacterial cultures grown in DMEM by a simple Bradford Assay. Unpaired t-tests were used to compare the data (** $P < 0.01$; **** $P < 0.0001$). (C) HeLa cells pre-loaded with CCF2/AM were infected at MOI = 700 with bacterial strains 'pre-activated' in DMEM for 4 h. The [R] value (y-axis) is a quantitative ratio representative of effector-TEM-1 accumulation within infected HeLa cells. Wild type EPEC carrying pTEM-1 (unfused beta-lactamase) was used as a negative control for non-T3SS-specific beta-lactamase translocation. Each data point represents the average from three independent experiments.

Immunoblotting with phospho-motif specific antibodies is a common method to monitor protein phosphorylation, however not all sites can be detected by this approach (Dephoure *et al.,* 2013). Over the past decade, phosphate-binding molecules (termed 'phos-tag') have been developed to sensitively detect multiple forms of protein phosphorylation through non-covalent binding to dianionic phosphorylated residues (Kinoshita, Kinoshita-Kikuta, & Koike, 2009, 2012). This commercially available technology, when coupled to a fluorophore, can be applied as a stain for conventional SDS-PAGE gels that are subsequently visualized by fluorescent imaging. As a quality control checkpoint for the LC-MS/MS sample isolation procedure, the GeneCopoeia Phos-Tag system was used to stain immunoprecipitated CesT-FLAG protein separated by SDS-PAGE (Figure 3.3).

To initially validate the specificity of the GeneCopoeia system, 500 ng of the dually-phosphorylated protein, ovalbumin (45 kDa), was treated with lambda (λ) phosphatase (25 kDa) and compared to an untreated sample following SDS-PAGE and Phos-Tag staining (Figure 3.3A). Dual serine phosphorylation of the ovalbumin control at S68 and S344 was confirmed by LC-MS/MS (data not shown). Fluorescent emission was captured at 549 nm to detect phosphoprotein, which revealed ovalbumin only in the non-phosphatase treatment sample. When emission was captured at 649 nm to detect total protein, ovalbumin was detected in both phosphatase-treated and untreated lanes. A slight increase in band migration was noted for the phosphatase treated ovalbumin (Figure 3.3A). It was therefore clear that the Phos-Tag stain was capable of detecting as little as 5 ng of phosphorylated ovalbumin (Figure 3.3B). When the stain was applied to immunoprecipitated CesT-FLAG samples, faint but observable phosphoprotein bands

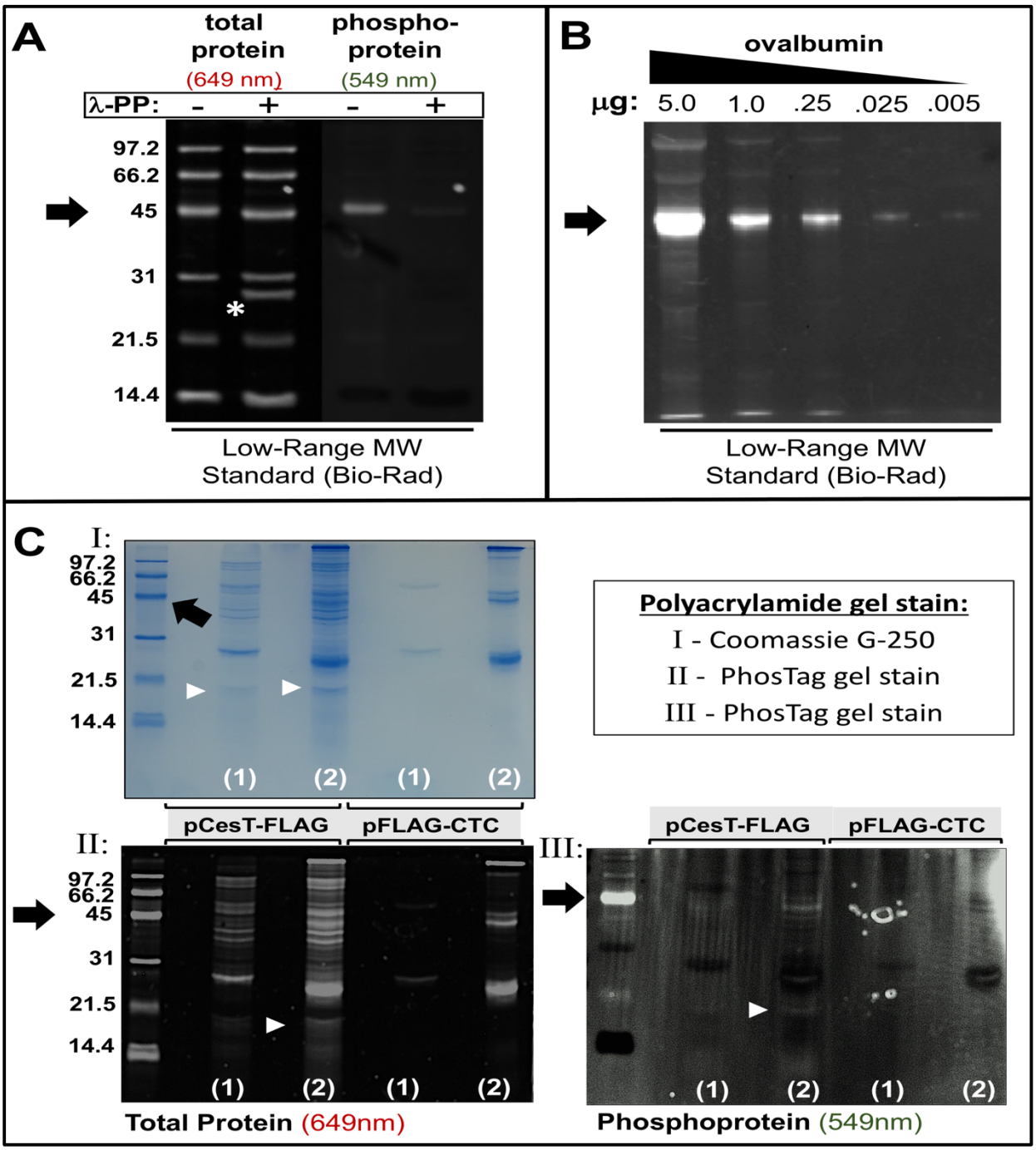

Figure 3.3: Phos-tag™ Phosphoprotein Gel Stain. (A-C) Samples separated by SDS-PAGE were subject to Phos-Tag Phosphoprotein Gel Stain (GeneCopoeia™). Excitation of the fluorescent stain at 549nm (green) detects phosphorylated serine, threonine, or tyrosine residues; whereas excitation at 649nm (red) identified total protein levels. Black arrows indicate ovalbumin from the Low-Range MW Standard (Bio-Rad), which is a 45 kDa protein phosphorylated at two serine residues. Vertical numbering (bold, black) indicates MW (kDa) of the Low-Range MW Standard Ladder constituent proteins. (A)

Lambda (λ) phosphatase (λ-PP) treatment depleted detectable ovalbumin phosphoprotein and induced a slight increase in band migration during SDS-PAGE. The white asterisk (*) indicates the position of λ-phosphatase. (B) The phosphoprotein detection sensitivity for the Phos-Tag stain was established by dilution of ovalbumin. (C) EPEC *ΔcesT* complemented with pCesT-FLAG or empty pFLAG-CTC (negative control) were subject to FLAG antibody immunoprecipitation. Samples were eluted from the FLAG antibody by (1) 0.1M glycine, pH 2.5 or subsequent (2) SDS-PAGE sample buffer treatment. Purified samples were separated by SDS-PAGE and stained with Coomassie G-250 (panel I) or Phos-Tag Gel Stain (panel II and III). White arrowheads indicate the presence of a band consistent with the MW of CesT-FLAG that is absent from the negative control lanes.

---

were detected that were absent in the vector control (pFLAG-CTC). Relative to total protein detected by Phos-Tag and subsequent Coomassie G-250 staining, the phosphoprotein signals were faint, indicating that the major species of CesT-FLAG immunoprecipitated from EPEC Δ*cesT* lysates was the non-phosphorylated form (Figure 3.3C). Remaining elution volumes were queued for analysis by LC-MS/MS.

The analysis of CesT-FLAG from Coomassie-stained gel slices involved proteolytic digest with LysC, separation of the resultant peptides by high performance liquid chromatography (HPLC) and peptide identification by tandem mass spectrometry (MS/MS). A collection of notable CesT C-terminal peptide spectrum match (PSMs) observations is listed in Table 3.1. From the first stage of the LC-MS/MS analysis, we observed a precursor ion for a 19 amino acid phosphorylated peptide with a protonated molecular mass (MH+) of 2340.98 Da (Figure 3.4A). This peptide (HYYAGRGTRSVDYKDDDDK) matched the C-terminal region of CesT and encompassed the entirety of the FLAG fusion sequence. Critically, the mass shift was observed to be 79.96 Da greater than the non-phosphorylated precursor ion, which was

Table 3.1: Summary of LC-MS/MS observations for CesT-FLAG and CesT(Y153F)-FLAG samples digested with endoproteinase LysC.

Sample (# of PSMs)	Growth Condition	CesT PSM (LysC digest)	Monoisotopic mass (Da)	Best-Site Probability	Best XCorr	Charge
CesT-FLAG (2)	DMEM	HYY[P]AGR-*GTRSVDYKDDDDK*	2340.98 *	Y3 - 97.90%	2.60	+4
CesT-FLAG (3)	DMEM	HYY[P]AGR-*GTRSVDYKDDDDK*	2340.98 *	Y3 - 97.61%	6.51	+4
CesT-FLAG (3)	DMEM	HYY[P]AGR-*GTRSVDYKDDDDK*	2340.98 *	Y3 - 96.01%	2.89	+4
CesT-FLAG (2)	DMEM	HYYAGR-*GTRS[P]VDYKDDDDK*	2340.98 *	S10 – 99.99%	5.35	+4
CesT-FLAG (10)	DMEM +2mM EGTA	HYYAGR-*GTRS[P]VDYKDDDDK*	2340.98 *	S10 – 99.8%	3.35	+4
CesT-FLAG	DMEM	HYYAGR-*GTRSVDYKDDDDK*	2261.02	/	1.93	+4
CesT(Y153F)-FLAG (2)	DMEM	HY[P]FAGR-*GTRSVDYKDDDDK*	2324.99 *	Y2 - 80.51%	2.15	+4
CesT(Y153F)-FLAG (3)	DMEM	HY[P]FAGR-*GTRSVDYKDDDDK*	2324.99 *	Y2 - 84.82%	1.59	+4
CesT(Y153F)-FLAG	DMEM	HYFAGR-*GTRSVDYKDDDDK*	2245.03	/	1.90	+4

Note: The peptide masses noted with an asterisk (*) correspond to a mass shift equivalent to the addition of a single phosphate moiety (79.966; ± 0.02 Da) to the unmodified CesT-FLAG (2261.33 Da) or CesT(Y153F)-FLAG peptide. For a peptide *z = +4* activated by HCD an XCorr value of > 2.6 is defined as the high confidence threshold, and 1.2 is defined as the medium confidence threshold (ThermoFisher Proteome Discoverer 2.1).

identified with a MH+ of 2261.02 Da (Figure 3.4B). The most frequently observed ions had a charge (z) value of +4 and were matched to peptides with one missed cleavage site. Upon selection for MS2 analysis, the precursor ions were fragmented in higher-energy collisional dissociation (HCD) mode to generate a spectra of the product b and y ions (Figure 3.4C). The PhosphoRS algorithm was applied to assign a site-specific probability value for the phosphorylation modification. This revealed a high-confidence probability score of 97.61% that Y3 of the precursor ion was the phosphorylated residue, which corresponds to CesT position Y153 (Figure 3.4C). For comparative purposes, a non-phosphorylated MS/MS spectra for the 19 amino acid CesT-FLAG peptide is shown in Figure 3.5A**.** We did not observe phosphorylation at Y152 for any CesT-FLAG peptides obtained from EPEC lysates.

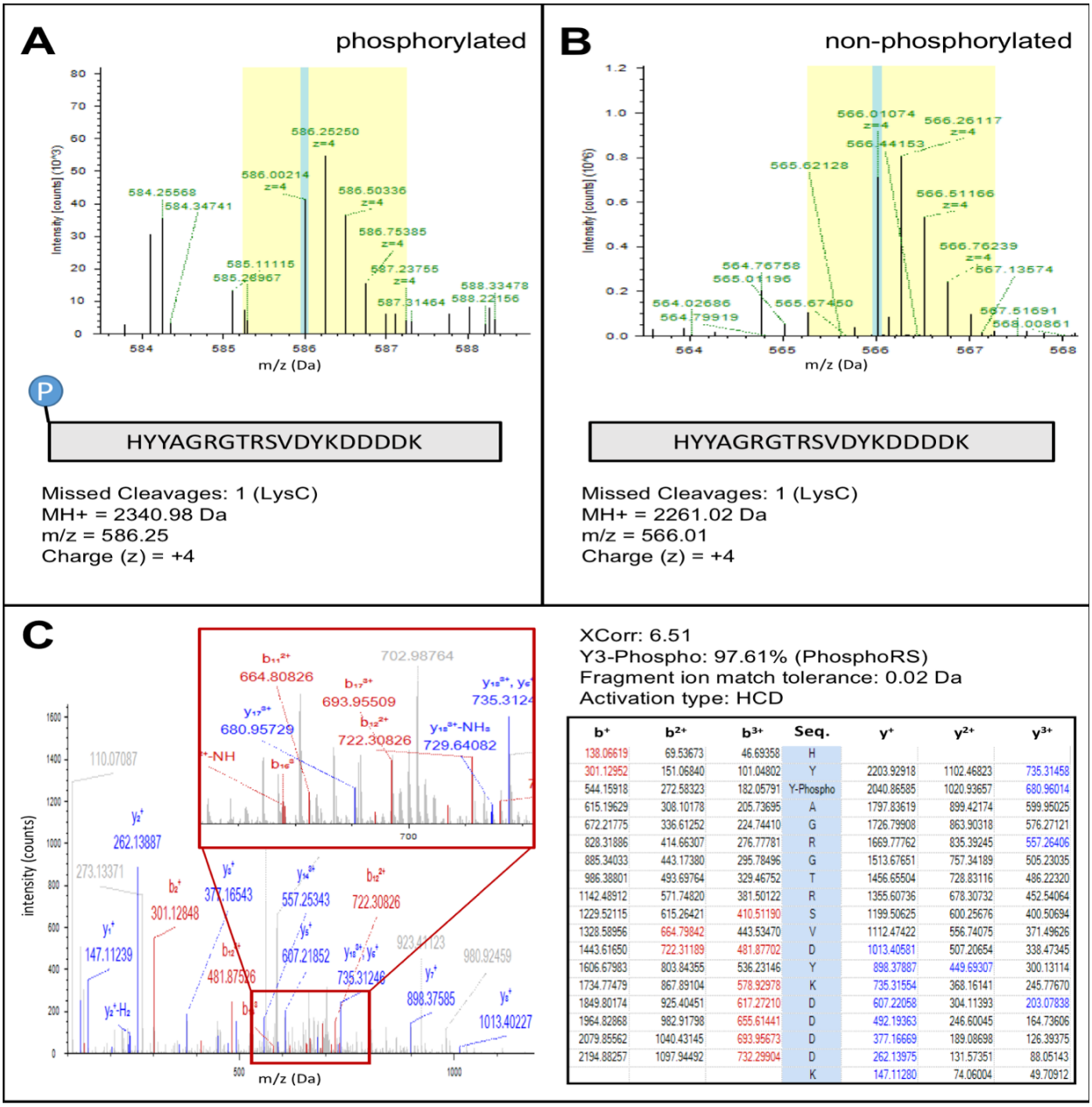

b+	b2+	b3+	Seq.	y+	y2+	y3+
138.06619	69.53673	46.69358	H			
301.12952	151.06840	101.04802	Y	2203.92918	1102.46823	735.31458
544.15918	272.58323	182.05791	Y-Phospho	2040.86585	1020.93657	680.96014
615.19629	308.10178	205.73695	A	1797.83619	899.42174	599.95025
672.21775	336.61252	224.74410	G	1726.79908	863.90318	576.27121
828.31886	414.66307	276.77781	R	1669.77762	835.39245	557.26406
885.34033	443.17380	295.78496	G	1513.67651	757.34189	505.23035
986.38801	493.69764	329.46752	T	1456.65504	728.83116	486.22320
1142.48912	571.74820	381.50122	R	1355.60736	678.30732	452.54064
1229.52115	615.26421	410.51190	S	1199.50625	600.25676	400.50694
1328.58956	664.79842	443.53470	V	1112.47422	556.74075	371.49626
1443.61650	722.31189	481.87702	D	1013.40581	507.20654	338.47345
1606.67983	803.84355	536.23146	Y	898.37887	449.69307	300.13114
1734.77479	867.89104	578.92978	K	735.31554	368.16141	245.77670
1849.80174	925.40451	617.27210	D	607.22058	304.11393	203.07838
1964.82868	982.91798	655.61441	D	492.19363	246.60045	164.73606
2079.85562	1040.43145	693.95673	D	377.16669	189.08698	126.39375
2194.88257	1097.94492	732.29904	D	262.13975	131.57351	88.05143
			K	147.11280	74.06004	49.70912

Figure 3.4: Site-specific identification of tyrosine phosphorylation at Y153 of CesT-FLAG by LC-MS/MS. The precursor ion masses of the phosphorylated (A) and non-phosphorylated (B) endogenous CesT-FLAG peptides were measured in the Orbitrap VelosPRO mass analyzer. The protonated molecular mass (MH+) difference between the phosphorylated and non-phosphorylated peptides is 79.96 Da, which accounts for the phosphorylation modification. The MS/MS spectra and corresponding fragment ion series for the phosphorylated CesT-FLAG precursor ion was analyzed by HCD fragmentation at a match tolerance of 0.02 Da (C). The mass shift caused by phosphorylation is shown by the different b ion masses observed upstream and y ion masses observed downstream of Y3. The red box is an enlargement of a specific window of the spectra in which the y_{17}^{3+} ion peak at 680.96 Da (Y3-phospho) can be visualized.

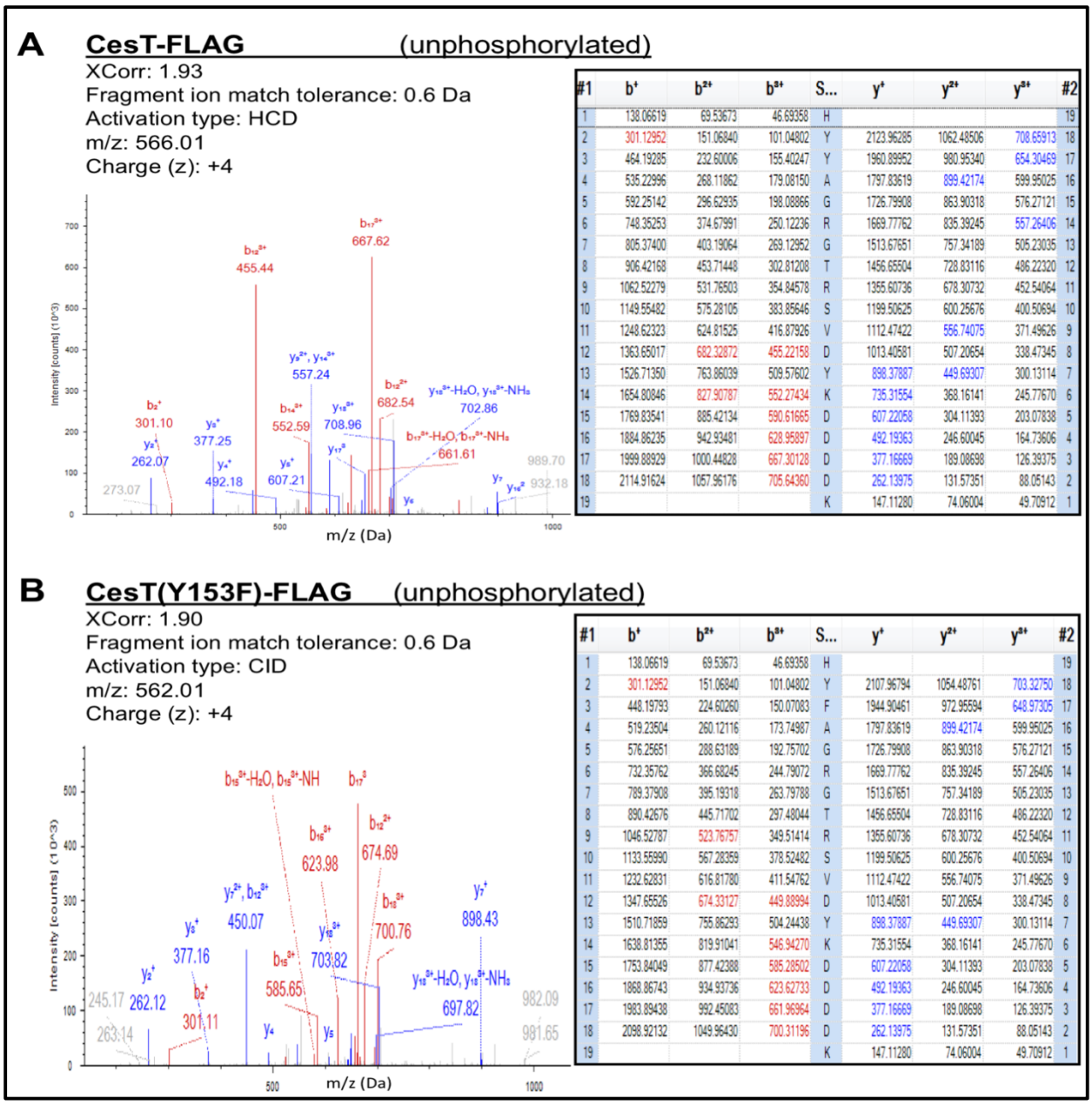

#1	b+	b2+	b3+	S...	y+	y2+	y3+	#2
1	138.06619	69.53673	46.69358	H				19
2	301.12952	151.06840	101.04802	Y	2123.96285	1062.48506	708.65913	18
3	464.19285	232.60006	155.40247	Y	1960.89952	980.95340	654.30469	17
4	535.22996	268.11862	179.08150	A	1797.83619	899.42174	599.95025	16
5	592.25142	296.62935	198.08866	G	1726.79908	863.90318	576.27121	15
6	748.35253	374.67991	250.12236	R	1669.77762	835.39245	557.26406	14
7	805.37400	403.19064	269.12952	G	1513.67651	757.34189	505.23035	13
8	906.42168	453.71448	302.81208	T	1456.65504	728.83116	486.22320	12
9	1062.52279	531.76503	354.84578	R	1355.60736	678.30732	452.54064	11
10	1149.55482	575.28105	383.85646	S	1199.50625	600.25676	400.50694	10
11	1248.62323	624.81525	416.87926	V	1112.47422	556.74075	371.49626	9
12	1363.65017	682.32872	455.22158	D	1013.40581	507.20654	338.47345	8
13	1526.71350	763.86039	509.57602	Y	898.37887	449.69307	300.13114	7
14	1654.80846	827.90787	552.27434	K	735.31554	368.16141	245.77670	6
15	1769.83541	885.42134	590.61665	D	607.22058	304.11393	203.07838	5
16	1884.86235	942.93481	628.95897	D	492.19363	246.60045	164.73606	4
17	1999.88929	1000.44828	667.30128	D	377.16669	189.08698	126.39375	3
18	2114.91624	1057.96176	705.64360	D	262.13975	131.57351	88.05143	2
19				K	147.11280	74.06004	49.70912	1

#1	b+	b2+	b3+	S...	y+	y2+	y3+	#2
1	138.06619	69.53673	46.69358	H				19
2	301.12952	151.06840	101.04802	Y	2107.96794	1054.48761	703.32750	18
3	448.19793	224.60260	150.07083	F	1944.90461	972.95594	648.97305	17
4	519.23504	260.12116	173.74987	A	1797.83619	899.42174	599.95025	16
5	576.25651	288.63189	192.75702	G	1726.79908	863.90318	576.27121	15
6	732.35762	366.68245	244.79072	R	1669.77762	835.39245	557.26406	14
7	789.37908	395.19318	263.79788	G	1513.67651	757.34189	505.23035	13
8	890.42676	445.71702	297.48044	T	1456.65504	728.83116	486.22320	12
9	1046.52787	523.76757	349.51414	R	1355.60736	678.30732	452.54064	11
10	1133.55990	567.28359	378.52482	S	1199.50625	600.25676	400.50694	10
11	1232.62831	616.81780	411.54762	V	1112.47422	556.74075	371.49626	9
12	1347.65526	674.33127	449.88994	D	1013.40581	507.20654	338.47345	8
13	1510.71859	755.86293	504.24438	Y	898.37887	449.69307	300.13114	7
14	1638.81355	819.91041	546.94270	K	735.31554	368.16141	245.77670	6
15	1753.84049	877.42388	585.28502	D	607.22058	304.11393	203.07838	5
16	1868.86743	934.93736	623.62733	D	492.19363	246.60045	164.73606	4
17	1983.89438	992.45083	661.96964	D	377.16669	189.08698	126.39375	3
18	2098.92132	1049.96430	700.31196	D	262.13975	131.57351	88.05143	2
19				K	147.11280	74.06004	49.70912	1

Figure 3.5: MS/MS spectra from un-phosphorylated CesT-FLAG and CesT(Y153F)-FLAG peptides. (A) The MS/MS spectra and corresponding fragment ion series in table format for the unphosphorylated CesT-FLAG precursor ion was analyzed by HCD fragmentation at a match tolerance of 0.6 Da. (B) The MS/MS spectra and corresponding fragment ion series for the unphosphorylated CesT(Y153F)-FLAG precursor ion was analyzed by CID fragmentation at a match tolerance of 0.6 Da. Note the +4 charge (z) of both precursor ions, which had a m/z difference of 4, indicating the loss of the oxygen atom (16 Da) for the Tyr (Y) to Phe (F) sequence mutation of CesT(Y153F)-FLAG.

The next stage of the analysis was directed toward identification of phosphorylation at position Y152 of CesT. To accomplish this, we immunoprecipitated CesT(Y153F)-FLAG from cell lysates and subjected the samples to LC-MS/MS. In this case, we observed 19 amino acid peptides (HYFAGRGTRSVDYKDDDDK) with a small decrease in molecular masses that is accounted for by the loss of an oxygen atom with the Tyr to Phe substitution. The phosphorylated precursor ions had a MH+ of 2324.99 Da whereas the non-phosphorylated precursor was observed at 2245.03 Da; a difference of 79.96 Da (Figure 3.6A & B). Again, the most frequently observed ions had a charge (z) of +4, and were matched to peptides with one missed cleavage site. Our MS/MS data acquisition algorithm achieved medium confidence site-specific probability values (< 80%) for a phosphorylation modification at position Y2 with HCD fragmentation. In collision induced dissociation (CID) mode, the site-specific localization score improved to 84.8% (PhosphoRS) (Figure 3.6C). For comparative purposes, a non-phosphorylated MS/MS spectra for the 19 amino acid CesT(Y153F)-FLAG peptide is shown in Figure 3.5B. Collectively, these data indicate that EPEC mediates phosphorylation of CesT at Y152 and Y153. Furthermore, in the case of Y152 phosphorylation, there is no requirement for the adjacent amino acid at position 153 to be modified. Collectively, the data presented in this chapter substantiate the previous experimental observations of EHEC CesT Y152 and Y153 phosphorylation (Hansen *et al.,* 2013) and extend this site specific protein modification to EPEC.

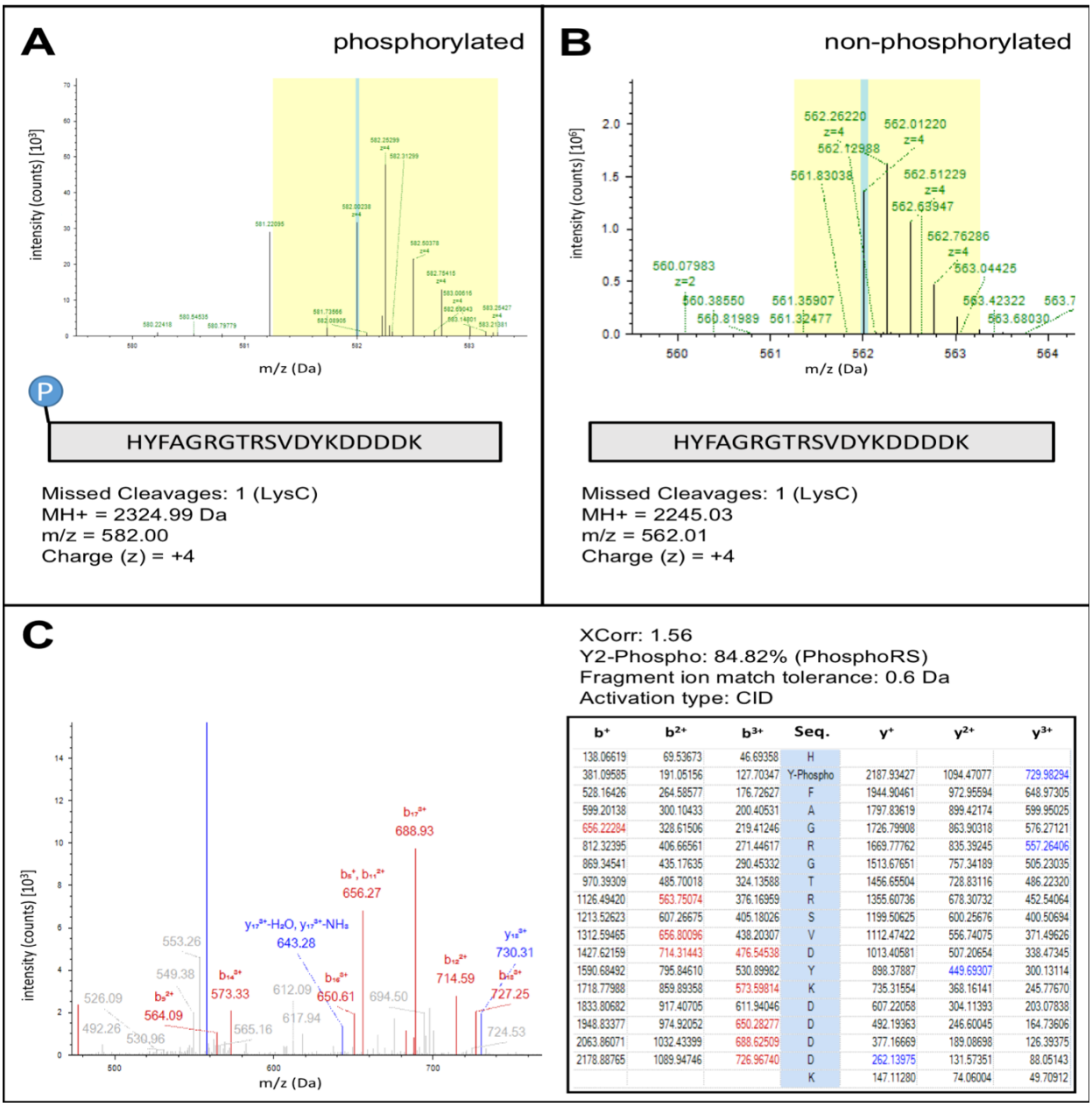

b⁺	b²⁺	b³⁺	Seq.	y⁺	y²⁺	y³⁺
138.06619	69.53673	46.69358	H			
381.09585	191.05156	127.70347	Y-Phospho	2187.93427	1094.47077	729.98294
528.16426	264.58577	176.72627	F	1944.90461	972.95594	648.97305
599.20138	300.10433	200.40531	A	1797.83619	899.42174	599.95025
656.22284	328.61506	219.41246	G	1726.79908	863.90318	576.27121
812.32395	406.66561	271.44617	R	1669.77762	835.39245	557.26406
869.34541	435.17635	290.45332	G	1513.67651	757.34189	505.23035
970.39309	485.70018	324.13588	T	1456.65504	728.83116	486.22320
1126.49420	563.75074	376.16959	R	1355.60736	678.30732	452.54064
1213.52623	607.26675	405.18026	S	1199.50625	600.25676	400.50694
1312.59465	656.80096	438.20307	V	1112.47422	556.74075	371.49626
1427.62159	714.31443	476.54538	D	1013.40581	507.20654	338.47345
1590.68492	795.84610	530.89982	Y	898.37887	449.69307	300.13114
1718.77988	859.89358	573.59814	K	735.31554	368.16141	245.77670
1833.80682	917.40705	611.94046	D	607.22058	304.11393	203.07838
1948.83377	974.92052	650.28277	D	492.19363	246.60045	164.73606
2063.86071	1032.43399	688.62509	D	377.16669	189.08698	126.39375
2178.88765	1089.94746	726.96740	D	262.13975	131.57351	88.05143
			K	147.11280	74.06004	49.70912

Figure 3.6: Site-specific identification of tyrosine phosphorylation at Y152 of CesT(Y153F)-FLAG by LC-MS/MS. The precursor ion masses of the phosphorylated (A) and non-phosphorylated (B) endogenous CesT-FLAG peptides were measured in the Orbitrap VelosPRO mass analyzer. The protonated molecular mass (MH+) difference between the phosphorylated and non-phosphorylated peptides is 79.96 Da, which accounts for the phosphorylation modification. (C) The MS/MS spectra and corresponding fragment ion series for the phosphorylated CesT(Y153F)-FLAG precursor ion was analyzed by CID fragmentation at a match tolerance of 0.6 Da. The Y2-phospho modification is determined by identification of the y_{18}^{3+} ion at 730.31 Da and the corresponding b and y ion series downstream of Y2.

3.3 Phosphosite Mutations Impact CesT-dependent Effector Secretion *in vitro*

To investigate the role of the C-terminal CesT tyrosine residues in context of EPEC T3SS functionality, we constructed chromosomal *cesT* variants that encode site-specific tyrosine (Y) to phenylalanine (F) substitutions. We generated EPEC strains that express i) CesT Y152F, ii) CesT Y153F, and iii) CesT Y152F, Y153F. Importantly, these strains maintain the natural, single-copy chromosomal operon organization that is involved in transcriptional regulation of *cesT* mRNA expression.

EPEC strains encoding *cesT* (Y152F), *cesT* (Y153F), or *cesT* (Y152F, Y153F) all produced the respective CesT substitution variants at a level relatively equivalent to wild type CesT (Figure 3.7A). Therefore, CesT tyrosine residues Y152 and Y153 are not essential for maintaining CesT levels in EPEC. Coomassie G-250 staining of culture supernatants revealed that mutation of these C-terminal tyrosine residues did not impact the secretion of T3SS structural proteins EspA, EspB, and EspD (Appendix C). To promote secretion of the CesT-dependent effectors Tir and NleA, the same bacterial strains were cultured under low calcium conditions by addition of 2mM EGTA to the media. Under this condition, the secretion of EspA, EspB, and EspD was noticeably reduced (Figure 3.7B). Relative to wild type, secretion of Tir was marginally reduced for the *cesT* (Y152F) and *cesT* (Y152F, Y153F) variants. NleA secretion was most abundant in the *cesT* (Y153F) mutant, however this band on the gel was difficult to identify by Coomassie staining due to the presence of a CesT-independent species at an identical molecular weight (Figure 3.7B).

CesT contributes to efficient secretion and translocation of at least 11 effector proteins in EPEC, including Tir and NleA. To investigate the specific role of tyrosine

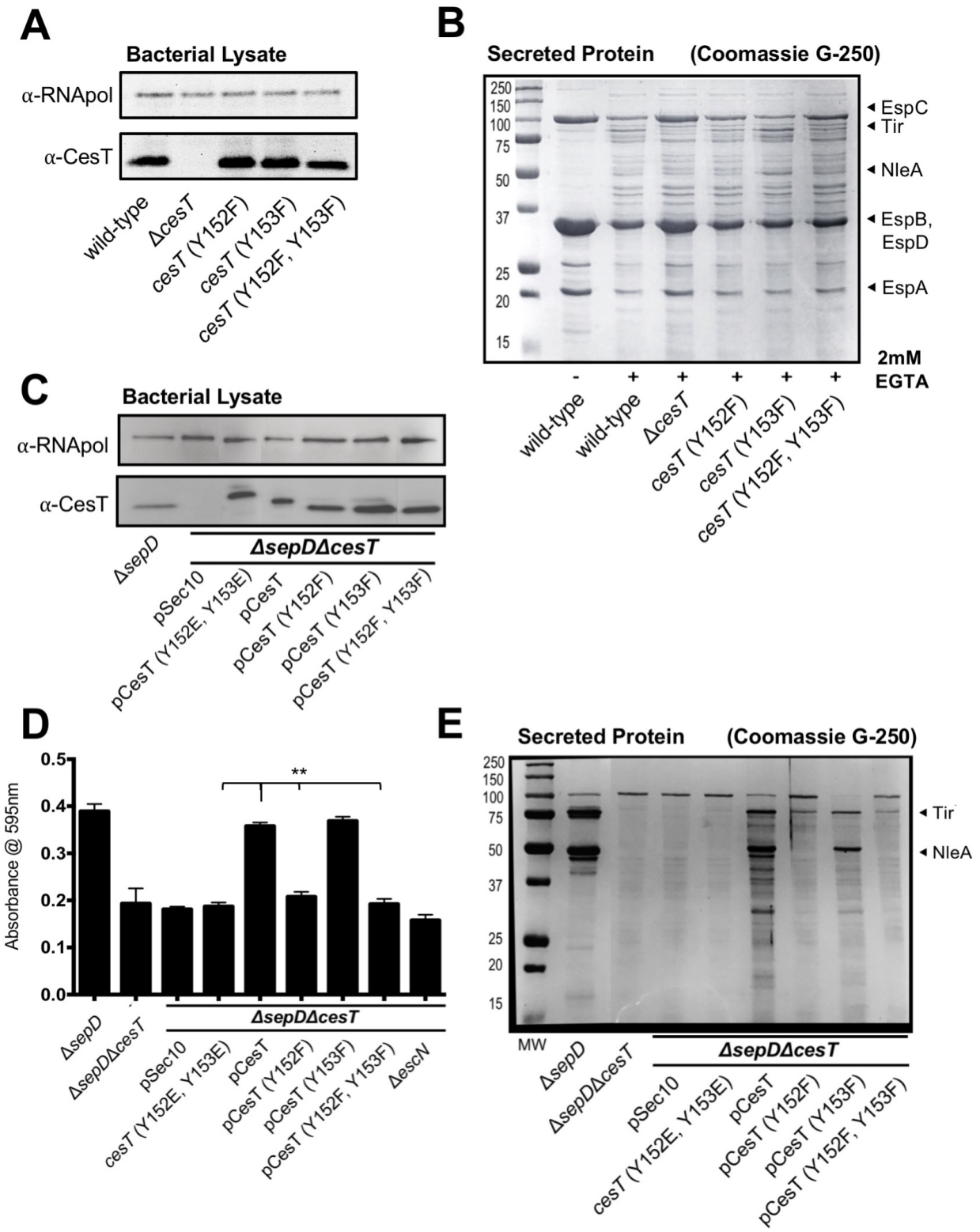

Figure 3.7: *In vitro* protein expression and secretion analysis of EPEC and EPEC CesT phosphosite variants. (A) Whole cell lysates derived from bacteria cultured in DMEM +2mM EGTA were immunoblotted with the indicated antibodies. (B) Total secreted protein preparation, normalized to OD_{600}, from bacteria cultured in DMEM +2mM

EGTA. The secreted protein profile of EPEC has been well characterized and the proteins indicated by arrowheads have been previously identified by mass spectrometry (C) Immunoblot detection of EHEC CesT or CesT variant expression from EPEC lysates cultured in DMEM. The relative abundance of secreted protein (D) and the secretion profile (E) for each strain were derived from the same cultures as the lysates shown in (C). A representative image from 2 independent experiments is shown. Unpaired t-tests were used to compare the data for positional amino acid substitution variants of pCesT (** $P < 0.01$).

---

phosphosites on overall CesT-dependent effector secretion, we utilized the EPEC Δ*sepD* strain, which exhibits undetectable secretion of EspA, EspB, and EspD by Coomassie staining. In EPEC, SepD and SepL are collectively involved as gatekeeper proteins in a temporal switch from secretion of translocator to effector proteins (Deng *et al.,* 2005; Wang *et al.,* 2008). This requires the multifunctional EscP protein, which interacts with SepL in a calcium dependent manner to promote the switch to effector secretion (Shaulov *et al.,* 2017). Deletion of SepD (Δ*sepD*) promotes hypersecretion of effector proteins into culture media in a CesT-dependent manner (Deng *et al.,* 2005).

Genetic complementation of *ΔsepDΔcesT* with EHEC or EPEC CesT restores hypersecretion to near the Δ*sepD* levels. In our hands, a low-copy number plasmid for EHEC CesT expression used to complement *ΔsepDΔcesT* restored ~ 91% of overall hypersecretion relative to EPEC Δ*sepD* in an *in vitro* secretion assay (Figure 3.7D). This demonstrated that EHEC CesT is functional in EPEC with respect to restoring overall secretion. We therefore established low-copy plasmids for EHEC CesT phosphosite variants, received from our collaborators Dr. Anne-Marie Hansen and Dr. Jim Kaper, in the Δ*sepDΔcesT* EPEC background (Figure 3.7C). Complementation with pCesT (Y152F), or pCesT (Y152F, Y153F), showed significantly reduced overall effector secretion, reduced Tir secretion, and undetectable NleA secretion (Figure 3.7D & E). In

stark contrast to these observations, pCesT (Y153F) completely restored overall secretion to the level of pCesT, including no observable difference in the Tir and NleA secretion profile (Figure 3.7D & E). From this data it was clear that there is a critical role for CesT Y152 in supporting total effector secretion in EPEC.

It has become common in protein phosphorylation studies to mutate phosphorylation sites to “phosphomimetic” residues, such as glutamic acid (E) or aspartic acid (D) to imitate a permanent local negative charge that a phosphorylation modification resembles (Dephoure *et al.,* 2013). However, one must consider that phosphomimetics are not a true representation of the local protein biochemical properties imposed by a reversible phosphorylation modification (Bah & Forman-Kay, 2016). Nonetheless, in this study a CesT Y152E, Y153E double substitution phosphomimetic variant was analyzed. Complementation of *ΔsepDΔcesT* with pCesT (Y152E, Y153E) failed to restore overall effector secretion, and rendered secretion of Tir and NleA undetectable (Figure 3.7D & E). This negative functional impact was identical for three aspartic acid phosphomimetic substitution variants: pCesT (Y152D), pCesT (Y153D), and pCesT (Y152D, Y153D); which were assessed by Dr. Thomas (Appendix C). It was therefore clear that the tyrosine phosphosites, in particular Y152, are required to support a reversible protein phosphorylation modification to maintain post-translational regulation of CesT function.

It was intriguing to note the stark changes in migration speed during SDS-PAGE for the various CesT proteins. In particular, the CesT Y152E, Y153E variant migrates markedly slower than wild type CesT, despite having a predicted molecular weight that is 68 Da less than the wild type protein. Amino acid substitutions that introduce local negative charge have been previously observed to alter CesT migration in polyacrylamide

gels (Ramu *et al.,* 2013). When tyrosine to phenylalanine substitutions were made, a difference of only 16 Da (single Phe mutation) or 32 Da (both Tyr sites mutated to Phe), we repeatedly observed increased band migration (Figure 3.7C). It is tempting to hypothesize that a lack of local C-terminal negative charge due to phosphate absence alters CesT migration, however the effects of phosphorylation on electrophoretic mobility are unpredictable (Dephoure *et al.,* 2013).

3.4 The CesT Y152 or Y153 Phosphosite is Required for Efficient Pedestal Formation

Adherence of EPEC to the epithelium is critical for host colonization during the infection process and requires the bundle-forming pilus encoded by an 11.5 kb cluster of genes within the EAF plasmid (Girón *et al.,* 1991; Tobe *et al.,* 1999). Beyond BFP activity, intimate attachment of the bacterial cell to the host membrane is critical for A/E lesion formation *in* vivo and requires T3SS-mediated effector translocation to induce disruption of the host cell actin cytoskeleton (Deng *et al.,* 2004; Navarro-Garcia *et al.,* 2013). CesT interacts with multiple EPEC effectors involved in modulating host actin dynamics, including Tir, EspF, Map, EspH, and EspG/G2 (refer to Introduction (1.2.4)). Tir is an essential colonization factor for all A/E pathogens that is embedded within the host cell membrane, following the CesT- and T3SS-dependent translocation mechanism, where it interacts with the bacterial outer membrane surface protein intimin to tightly anchor the bacterium to the host surface (Gruenheid *et al.,* 2001; Hartland *et al.,* 1999). The two cytoplasmic domains of Tir initiate a host-cell signalling cascade that results in F-actin polymerization directly beneath the site of bacterial attachment, forming what is known as a ‘pedestal’ structure (Gruenheid *et al.,* 2001). To investigate the ability of

phosphodeficient CesT variants to coordinate pedestal formation, an *in vitro* HeLa cell infection was carried out to assess bacterial intimate attachment to human epithelial cells by fluorescence microscopy and an established binding index (Figure 3.8) (Campellone *et al.,* 2004; Thomassin, He, & Thomas, 2011; Vingadassalom *et al.,* 2010). As expected, the Δ*cesT* infection formed significantly fewer pedestals on HeLa cells (5.0 ± 2.4%) compared to the wild type infection (97.8 ± 2.0%) (Figure 3.8B). Both the *cesT* Y152F and *cesT* Y153F variant strains were able to form pedestals on HeLa cells at a comparable level (95.0 ± 2.3% and 98.5 ± 2.1%, respectively) to wild type EPEC (Figure 3.8). However, the *cesT* Y152F, Y153F double mutant was significantly impaired, with pedestal formation on only 24.4 ± 6.3% of HeLa cells (Figure 3.8).

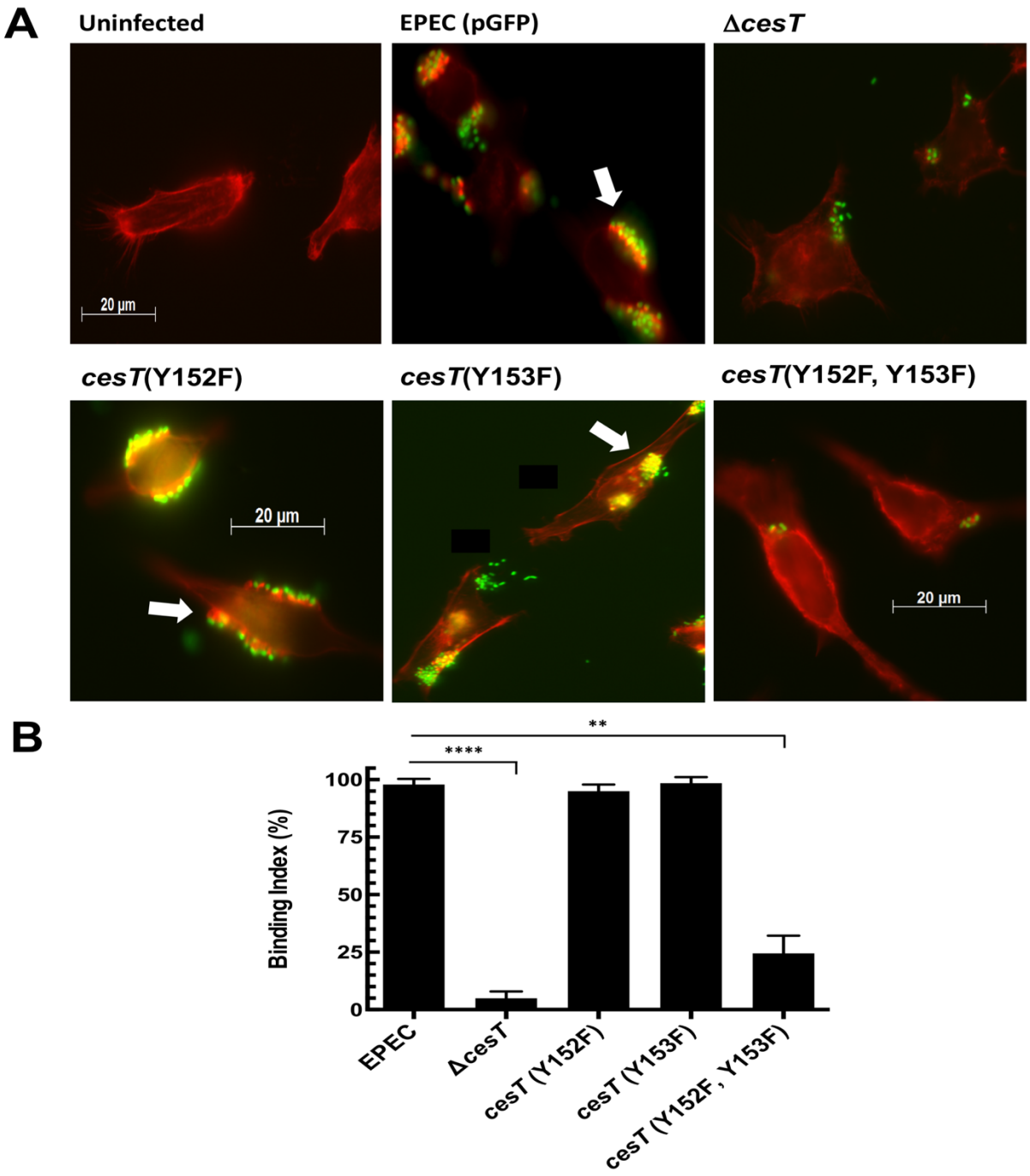

Figure 3.8: C-terminal residue Y152 or Y153 of CesT is required for formation of F-actin pedestals and intimate EPEC attachment. (A) Fluorescence microscopy images of HeLa cells following a 3 h infection with the indicated EPEC strains. EPEC strains contain a plasmid that encodes GFP (green). Alexa-568 Phalloidin (red) was used to detect HeLa cell F-actin. Co-localization of red and green signals appear yellow. Arrows indicate an enrichment of F-actin (red foci) underneath a site of intimate bacterial attachment. Images shown are representative of three independent experiments. (B) Quantification of bacteria intimately attached to HeLa cells using a binding index. The binding index was defined as the percentage of HeLa cells with greater than 5 bound

bacteria that co-localized to an actin pedestal. Data presented are average values for each experimental condition; error bars represent standard deviation (SD). The results are representative of three independent experiments, where at least 50 HeLa cells were counted per sample. An unpaired t-test was used for data comparison, with a two-tailed P value reported (**P = 0.0018; ****P < 0.001).

3.5 Effector Translocation is Affected by CesT Phosphosite Mutation

Similar to other gastrointestinal pathogens such as *Salmonella* and *Shigella* species, EPEC uses an array of effector proteins to evade the mucosal innate immune response and thereby persist within the host (Pearson *et al.,* 2016). NleA and NleH1/H2 are CesT-interacting effectors involved in limiting host inflammatory signalling (Gao *et al.,* 2009; Wan *et al.,* 2011; Yen *et al.,* 2015). Both effectors have been previously demonstrated to localize to HeLa cell membrane fractions upon translocation during *in vitro* infection (Gao *et al.,* 2009; Thanabalasuriar *et al.,* 2010, 2012). A previously described subcellular fractionation procedure was followed to assess the impact of CesT C-terminal pTyr sites on NleA and NleH2 translocation (Gauthier *et al.,* 2000). Briefly, EPEC *cesT* variant strains that expressed either NleA-FLAG or NleH2-FLAG from pACYC184 were used for a 3 h HeLa cell infection and cellular compartments were subsequently isolated by differential centrifugation (Figure 3.9). NleA was only detected in the HeLa membrane fraction when CesT phosphosite Y152 was intact. However, the CesT Y153F substitution variant had no observable effect on NleA translocation relative to wild type (Figure 3.9). NleH2 translocation was evidently CesT-dependent, however NleH2 was detected in the HeLa membrane despite CesT phosphosite mutations. A marginal reduction in NleH2 translocation was observed when both CesT phosphosites Y152 and Y153 were mutated to Phe (Figure 3.9). Collectively, these data indicate that

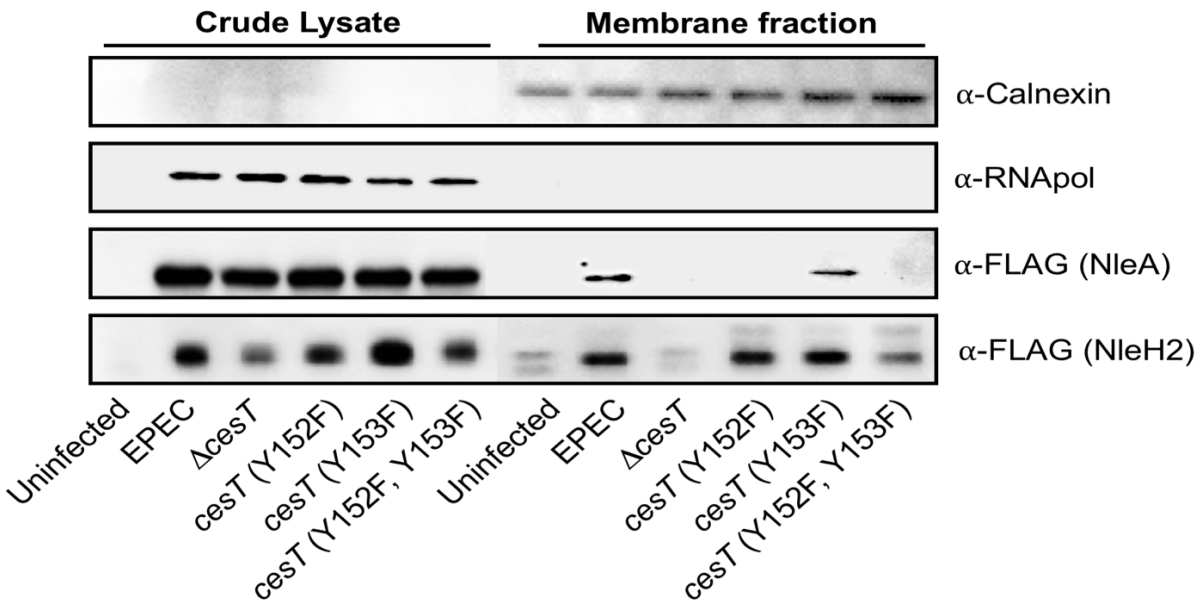

Figure 3.9: HeLa cell fractionation to assess CesT-dependent effector translocation during infection by immunoblot. HeLa cells mock treated or infected with indicated bacterial strains were subjected to a mechanical fractionation procedure. Crude lysate (bacteria, intact HeLa, nuclei) and the total HeLa membrane fractions were separated by SDS-PAGE and subjected to immunoblot analysis with the indicated antibodies. Wild type EPEC or *cesT* variant strains expressed either NleA or NleH2 from pACYC184. Anti-RNA polymerase (RNApol) served to detect bacterial cells or contamination of the membrane fraction. The anti-calnexin blot was a control for HeLa membrane protein to assess subcellular fractionation. This experiment was performed three times, with representative data shown.

C-terminal tyrosine phosphorylation of CesT may be required for efficient NleH2 translocation and that the CesT Y152 phosphosite is important for NleA translocation. A quantitative real-time analysis of effector translocation was subsequently employed to further characterize these observations (Chapter 3.6).

3.6 Real-Time Analysis of Effector Translocation Dynamics in the Context of CesT Phosphosite Mutations

To quantitatively investigate the impact of CesT phosphosite mutations with regard to effector translocation efficiency, five CesT-interacting effectors were selected for

generation of C-terminal TEM-1 translational fusions. Suicide plasmid constructs for *tir-blaM* and *espF-blaM* within SM10*λpir E. coli* were previously received from Dr. Ilan Rosenshine and noted in our strain archive. The protein coding genomic regions of three additional effectors: NleA, NleH1, and NleH2, were amplified by PCR and directionally cloned into the pCX341 vector to create in-frame sequence fusion to the *blaM* gene. It was rationalized that single copy, chromosomal integration of *effector-blaM* genes would provide the most sensitive representation of any CesT phosphosite-dependent differences in translocation efficiency. Upon fusion to the *blaM* gene, the chimeric sequences of *nleA-blaM, nleH1-blaM,* and *nleH2-blaM* were sub-cloned into the pCX391-based suicide vector, sequence verified, and subsequently integrated into their respective chromosomal loci in EPEC *cesT* variants.

To assess the chromosomal effector-*blaM* EPEC strains for TEM-1 beta-lactamase activity, liquid overnight cultures were plated on Müller-Hinton agar plates, and sterile Amp10 disks were added. As an ampicillin sensitive control, the parent EPEC and *cesT* variant strains that did not receive effector-*blaM* constructs were included. As shown in Table 3.2, the zone of clearing around these control Amp10 disks had a mean diameter of 20mm. For all effector-*blaM* fusion strains, increased resistance to Amp10 was noted by a zone of clearing diameter decrease of at least 2 mm (Table 3.2). Within each of the five groups of effector-*blaM* fusions, identical zone of clearing diameters were observed. The only exception to this trend was the Δ*cesT tir::tir-blaM* strain, which was more susceptible to Amp10 than others within the *tir-blaM* group (1-2 mm increase in zone size). Note that Tir stability is negatively impacted by a deletion of CesT, which could account for this increased susceptibility (Abe *et al.,* 1999).

Table 3.2: TEM-1 β-lactamase inactivation of ampicillin (Amp) was observed for each EPEC derived strain containing chromosomal effector-*blaM* fusions.

Controls (-)	Clearing Zone (mm)	*tir::tir*-blaM	Clearing Zone (mm)
Wild type EPEC	20 ± 0	Wild type EPEC	15 ± 0
EPEC ΔcesT	21 ± 1	EPEC ΔcesT	17 ± 0
cesT::cesT(S147A)	20 ± 0	*cesT::cesT*(S147A)	16 ± 1
cesT::cesT(Y152F)	20 ± 0	*cesT::cesT*(Y152F)	16 ± 1
cesT::cesT(Y153F)	20 ± 1	*cesT::cesT*(Y153F)	15 ± 0
cesT::cesT(Y152F/Y153F)	20 ± 0	*cesT::cesT*(Y152F/Y153F)	15 ± 1
nleA::nleA-blaM	**Clearing Zone (mm)**	***espF-espF-blaM***	**Clearing Zone (mm)**
Wild type EPEC	18 ± 1	Wild type EPEC	16 ± 0
EPEC ΔcesT	18 ± 0	EPEC ΔcesT	16 ± 1
cesT::cesT(S147A)	18 ± 1	*cesT::cesT*(S147A)	16 ± 0
cesT::cesT(Y152F)	18 ± 0	*cesT::cesT*(Y152F)	16 ± 0
cesT::cesT(Y153F)	18 ± 1	*cesT::cesT*(Y153F)	16 ± 0
cesT::cesT(Y152F/Y153F)	18 ± 1	*cesT::cesT*(Y152F/Y153F)	16 ± 0
nleH1::nleH1-blaM	**Clearing Zone (mm)**	***nleH2::nleH2-blaM***	**Clearing Zone (mm)**
Wild type EPEC	18 ± 0	Wild type EPEC	18 ± 1
EPEC ΔcesT	18 ± 0	EPEC ΔcesT	18 ± 1
cesT::cesT(S147A)	18 ± 0	*cesT::cesT*(S147A)	18 ± 0
cesT::cesT(Y152F)	18 ± 1	*cesT::cesT*(Y152F)	19 ± 0
cesT::cesT(Y153F)	18 ± 1	*cesT::cesT*(Y153F)	18 ± 0
cesT::cesT(Y152F/Y153F)	18 ± 0	*cesT::cesT*(Y152F/Y153F)	18 ± 1

Note: Liquid culture suspension of the indicated strain was normalized for plating on Müller-Hinton agar with 10 μg Amp disks (BD; 231264). The diameter of the clearing zone around three disks per plate was measured manually. Two independent experiments were conducted; values represent the mean ± measurement uncertainty.

Expression and secretion of the chromosomally-encoded effector-TEM-1 strains was assessed from cultures grown under low calcium conditions. As shown previously, inclusion of 2mM EGTA in DMEM growth media induces effector protein secretion but does not completely abolish translocator (EspA, EspB, EspD) secretion, which occurs independent of CesT. EspB (33 kDa) served as a useful loading control for each immunoblot, and permitted quantitative comparison of differences in effector-TEM-1 secretion for each *cesT* sequence variant (Figure 3.10). A representative image of an EspB blot is shown in Figure 3.10A; for comparative purposes EspB was always blotted on the same membrane as the effector-TEM-1 protein being analyzed (Figure 3.10B-F).

For clarity, the -TEM-1 designation will be dropped for the remainder of this section and the fusion constructs will be described by the name of the effector.

Secretion was undetectable in the Δ*cesT* background for all effectors except EspF, which is unique to CesT-interacting effectors in that it also possesses its own dedicated chaperone, CesF (Class IA T3SC). EspF secretion was noticeably increased for Δ*cesT* relative to wild type, however quantitation of this difference was not statistically significant (Figure 3.10A & F). Notably, the CesT Y153F variant promoted effector secretion at levels better than or relatively equal to wild type CesT in all cases (Figure 3.10).

For NleA, secretion was abolished with mutation of the Y152 phosphosite (Y152F, or Y152F, Y153F) or mutation of Serine-147 (S147A) (Figure 3.10A & D). A previous screen of an EPEC *cesT* variant expression library identified S147 as a critical residue within the CesT C-terminal domain that is required for NleA secretion (Ramu *et al.,* 2013). In the case of *cesT* Y153F, where only Y152 is phosphorylatable, NleA secretion was significantly better than wild type (Figure 3.10D; P=0.036). From these data, we conclude that CesT Y152 is required for NleA secretion, and the removal of phosphosite Y153 increases the level of NleA secretion.

Observed differences in total Tir, NleH1, and NleH2 secretion in context of the *cesT* variants were less striking than for NleA. While secretion of these three effectors was indeed CesT-dependent, and most efficient with phosphosite Y152 intact, it was noted that mutation of both Y152 and Y153 did not abolish detectable secretion by immunoblot (Figure 3.10A). It is therefore clear that tyrosine phosphorylation of CesT is not required for secretion of Tir, NleH1, and NleH2; however CesT phosphosite Y152 promotes more efficient secretion of these effectors.

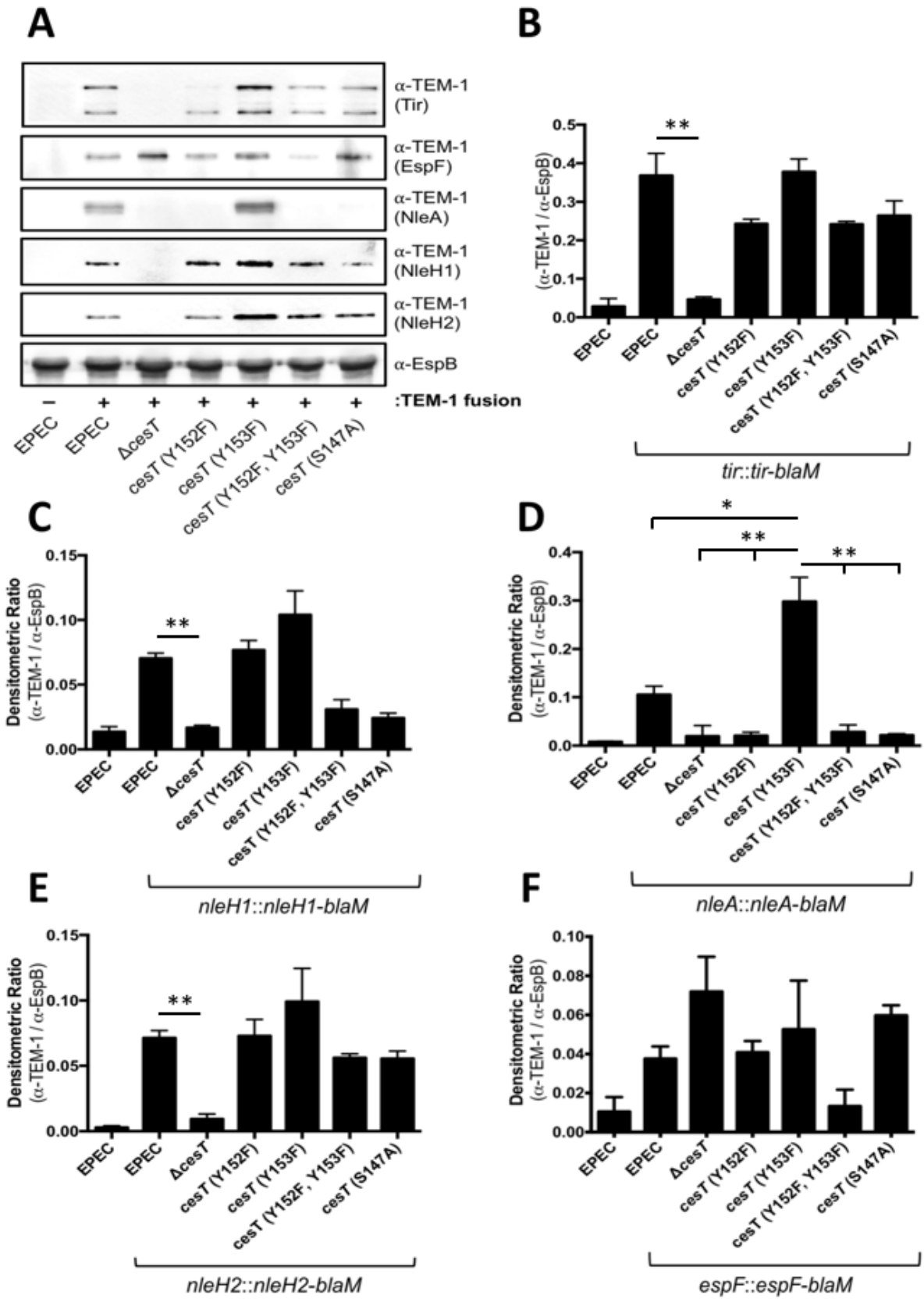
A
α-TEM-1 (Tir)
α-TEM-1 (EspF)
α-TEM-1 (NleA)
α-TEM-1 (NleH1)
α-TEM-1 (NleH2)
α-EspB
:TEM-1 fusion
EPEC
EPEC
ΔcesT
cesT (Y152F)
cesT (Y153F)
cesT (Y152F, Y153F)
cesT (S147A)
B
(α-TEM-1 / α-EspB)
tir::tir-blaM
C
Densitometric Ratio (α-TEM-1 / α-EspB)
nleH1::nleH1-blaM
D
nleA::nleA-blaM
E
nleH2::nleH2-blaM
F
espF::espF-blaM

Figure 3.10: Characterization of effector-TEM-1 secretion in the context of chromosomal *cesT* variants. (A-F) Each chromosomal *cesT* variant expresses a single monocopy effector-*blaM* fusion construct from its native promoter region. To build a total of five individual constructs per *cesT* variant, 30 independent conjugation experiments were performed. (A) The secreted protein fraction of each fusion construct and the parent EPEC strain, cultured in DMEM +2mM EGTA, normalized to OD_{600}, was analyzed by immunoblotting. EspB (T3SS translocon protein) served as a loading control within each individual sample. Representative immunoblots from two independent experiments are shown. (B-F) Densitometry analysis of each immunoblot was normalized to EspB, and is quantitated as the ratio of effector-TEM-1 signal / EspB signal. (B) Quantitation of the Tir-TEM-1 signal included both upper and lower (Tir breakdown) bands. Error bars represent standard deviation; data was compared by multiple unpaired t-test (*$P < 0.05$, **$P < 0.02$).

Previous analyses of the type III effector secretion hierarchy in EPEC have established Tir as the effector that is first translocated into host cells during infection (Mills *et al.,* 2013; Thomas *et al.,* 2007). A significant portion of this work has involved the use of effector-*blaM* fusions expressed from chromosomal loci and high MOI infection conditions to allow representation of all T3S effectors, including those translocated at a low level, in a single experiment (Mills *et al.,* 2013). The purpose of this system in this study was to identify alterations to translocation efficiency for CesT-interacting effectors using chromosomally encoded *cesT* phosphosite variants and single copy effector-*blaM* fusions. To validate the established hierarchy data with a real-time infection assay, the translocation kinetics for each of the five effectors was compared using wild type and Δ*cesT* strains. It was noted that Tir translocation begins first, and accumulates within the HeLa cell population at a significantly higher rate than EspF, NleA, NleH1, or NleH2 (Figure 3.11A). Tir translocation was significantly impaired by 30 min post-infection in a Δ*cesT* strain (Table 3.3). The difference between wild type and Δ*cesT* in context of EspF translocation was not statistically significant. NleA translocation was significantly reduced from 90-100 min in Δ*cesT* relative to wild type; while the differences for NleH1 and NleH2

reached statistical significance from wild type by 50 and 60 min post-infection, respectively. Taken together, these data indicate that rapid Tir translocation begins by 30 min post-infection in a CesT-dependent manner. The rate of Tir accumulation within HeLa cells reached a maximum at approximately 60 min post-infection, which was a time-point consistent with the beginning of statistically significant differences between wild type and Δ*cesT* strains for translocation of the 'second group' of effectors (other than EspF). These observations were not attributed to growth differences between strains (Figure 3.11B).

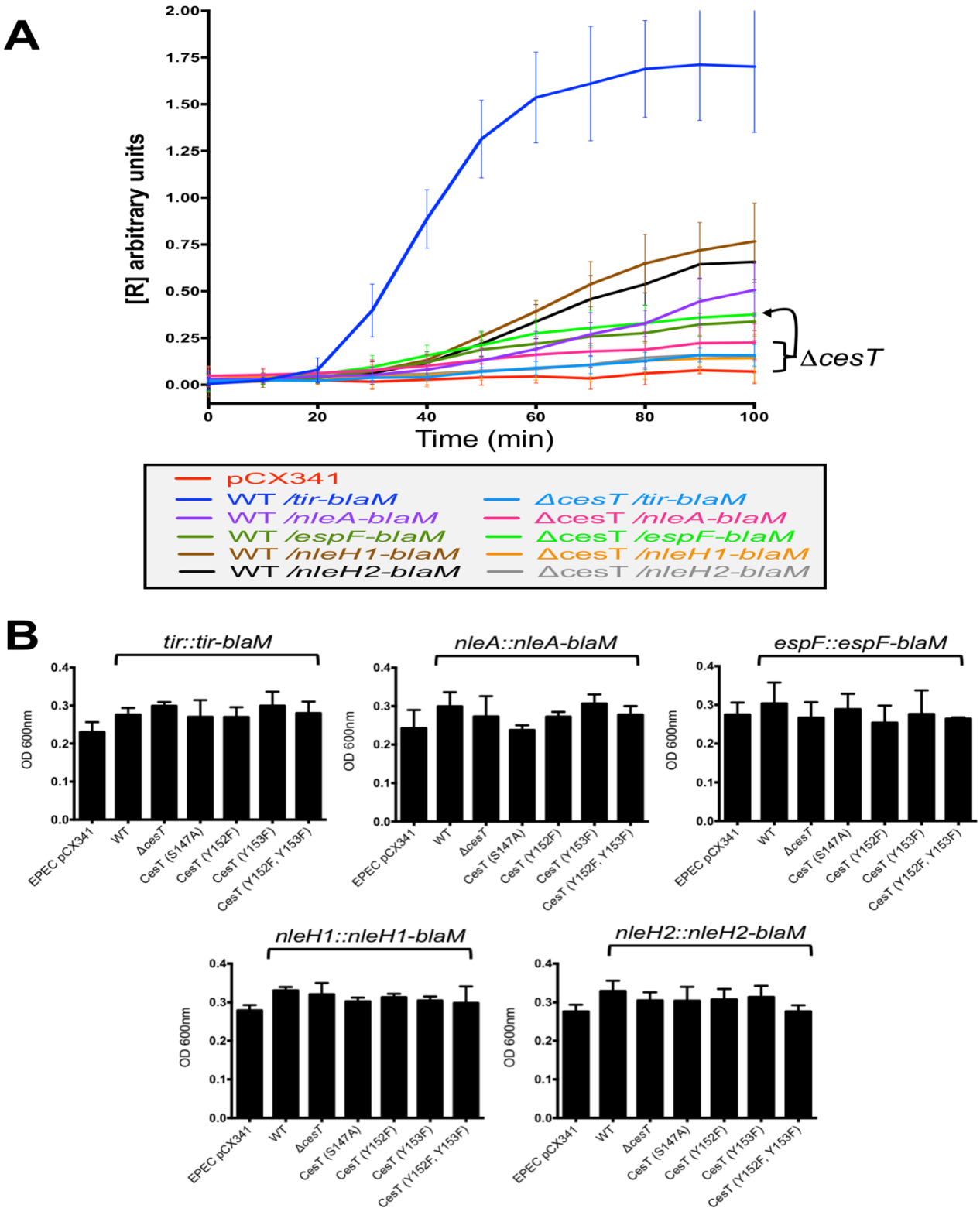

Figure 3.11: Translocation dynamics for EPEC effectors that interact with CesT. (A) EPEC strains, each containing a different chromosomally encoded effector-*blaM* gene, were subjected to kinetic translocation analysis. HeLa cells were pre-loaded with

CCF2/AM and infected at an MOI of 200 with bacterial strains 'pre-activated' in DMEM for 4 h. The [R] value (y-axis) is a quantitative ratio representative of the effector-TEM-1 accumulation within infected HeLa cells. Wild type EPEC carrying pCX341 (expresses native, unfused TEM-1) was used as a negative control for non-T3SS-specific beta-lactamase activity in a translocation competent bacterial population. Each data point represents the average from three independent experiments. (B) EPEC effector-*blaM* strains used in real-time translocation assays do not have significant growth differences after 4 h in DMEM. Liquid overnight cultures grown in 5 mL LB + tetracycline (10 μg/μL) were subcultured 1/200 into DMEM and incubated statically for 4 h at 37 °C, 5% CO_2 to induce T3SS gene expression. $OD_{600\ nm}$ measurements were made with the Biophotometer Plus (Eppendorf) instrument. For MOI calculations based on OD_{600} (x), cell number (y) was determined with the formula y = 746.4337(x) established from viable cell plating based on OD_{600}. For data presentation clarity, statistically significant differences are noted in Table R3.

Table 3.3: Statistically significant infection kinetic differences for wild type compared to *ΔcesT* during real-time analysis of effector-TEM-1 translocation.

Effector-TEM-1 construct	** (P < 0.01)
Tir	t = 30-100 min
EspF	n.s.
NleA	t = 90-100 min
NleH1	t = 50-100 min
NleH2	t = 60-100 min

Note: Statistical analyses were conducted with GraphPad Prism (6.0) using the unpaired t-test method to compare mean and standard deviation at individual time points. The range of time (min) over which the comparison was statistically significant (P < 0.01) is listed below.

Translocation of the five effector-TEM-1 constructs were subsequently analyzed in context of chromosomal *cesT* variants (Figure 3.12). At a low MOI of 50, insignificant translocation efficiency differences were observed for NleA among all *cesT* variant strains despite accumulation of Tir within infected HeLa cells under identical conditions (Figure 3.12A & B). It was recently discovered that NleA expression is induced upon EPEC attachment to the host cell by a post-transcriptional process (Katsowich *et al.,* 2017). Based on an earlier report, it was suspected that increasing the MOI might reduce the amount of time for host cell attachment to occur (Mills *et al*., 2008). In theory, this would

translate to increased NleA expression, and potentially greater observable translocation differences between *cesT* variant strains.

Indeed, when the MOI was raised to 100, NleA translocation for *cesT* (Y153F) increased relative to wild type and the other *cesT* variant strains (Figure 3.12B). Note that Tir translocation was maximal by 70-80 min post-infection at MOI 100 (Figure 3.12A). Furthermore, with MOI at 200 the overall translocation of Tir was markedly increased, and the amount of time to reach its maximal level was reduced to 60-70 min post-infection (Figure 3.12A). Under this infection condition, NleA translocation was significantly increased in a CesT Y152-dependent manner (Figure 3.12B; Table 3.4). Both CesT S147A or Y152F (or Y152F, Y153F) substitution variants decreased NleA translocation to Δ*cesT* levels. Remarkably, the CesT Y153F variant, where the phosphorylation site is locked to Y152 was significantly better at NleA translocation than wild type by 80 min post infection (Table 3.4), thereby suggesting that CesT phosphorylation at Y152 increases the rate of NleA translocation.

It was interesting to note that mutation of CesT Y152, or both Y152 and Y153, to phenylalanine reduced the level of translocation for EspF, NleH1, and NleH2 (Figure 3.12C-E). However the efficiency of translocation for these effectors was not reduced to Δ*cesT* levels by Y152F mutation as was noted for NleA. For NleH1 and NleH2, the CesT Y153F variant supported effector translocation equally to wild type. Taken together, these data suggest that the CesT Y152 phosphosite supports improved translocation efficiency for EspF, NleH1, and NleH2; and that the Y152 phosphosite is critically required for NleA.

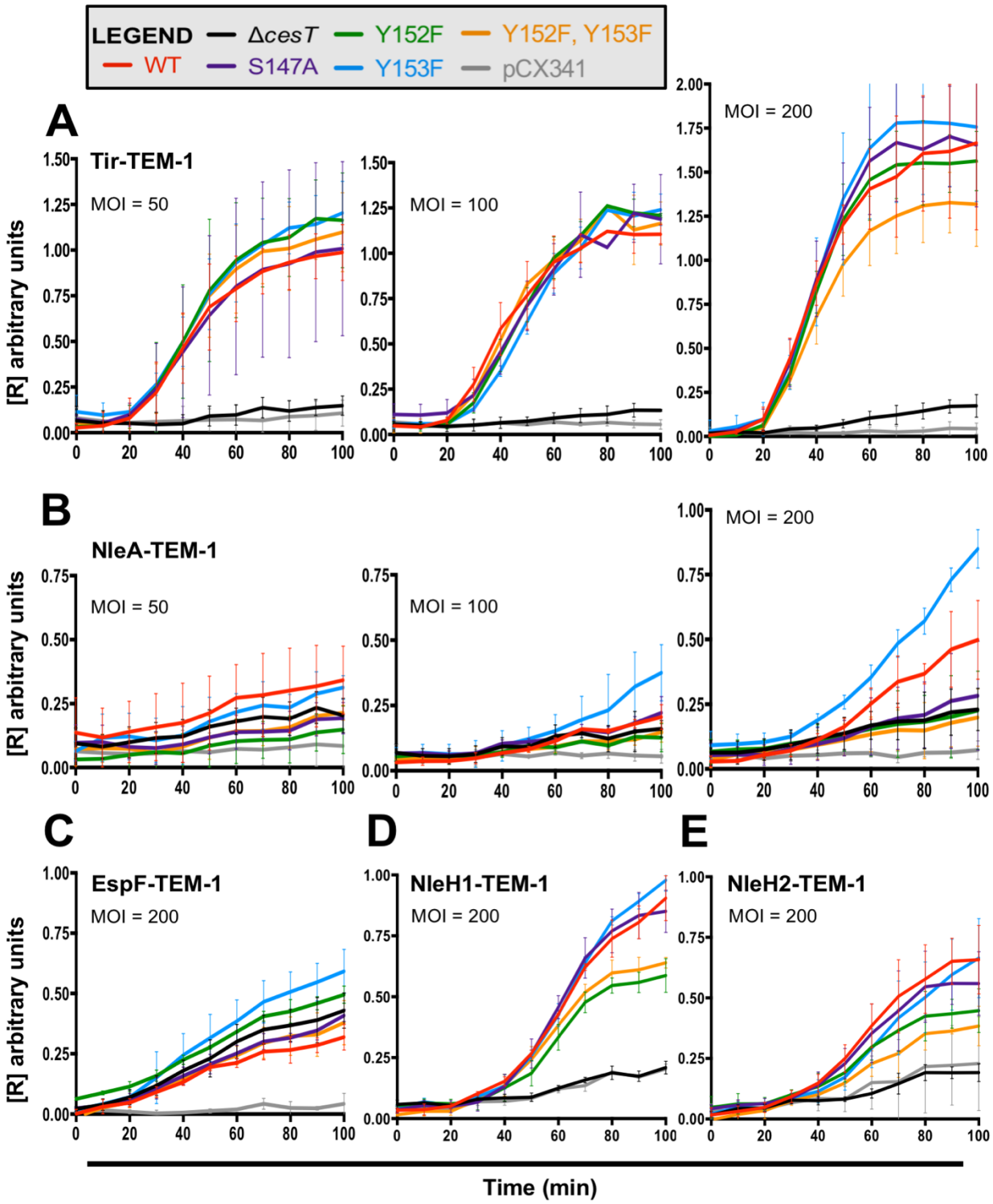

Figure 3.12: Site-specific amino acid substitutions within the CesT C-terminal domain impact effector translocation efficiencies. EPEC and *cesT* variant EPEC strains, each containing a single chromosomally encoded effector-*blaM* gene, were subjected to kinetic translocation analysis. HeLa cells were pre-loaded with CCF2/AM and infected at MOI = 50, 100, or 200 with bacterial strains 'pre-activated' in DMEM for 4

h. The [R] value (y-axis) is a quantitative ratio representative of effector-TEM-1 accumulation within infected HeLa cells. Wild type EPEC carrying pCX341 (expresses native, unfused TEM-1) was used as a negative control for non-T3SS-specific beta-lactamase translocation. The data is representative of three independent infection experiments carried out in duplicates. For data presentation clarity, statistically significant differences are noted in Table R4.

Table 3.4: Statistically significant differences observed during real-time analysis of effector translocation for CesT phosphosite variant strains.

Group	Compared CesT variants:	** (P < 0.01)	* (P < 0.05)
nleA::nleA-blaM	Y153F vs. Y152F	t = 70-100 min	t = 60-100 min
nleA::nleA-blaM	Y153F vs. Y152F, Y153F	t = 60-100 min	t = 60-100 min
nleA::nleA-blaM	Y153F vs. S147A	t = 80-100 min	t = 70-100 min
nleA::nleA-blaM	WT vs. Y152F	t = 90-100 min	t = 80-100 min
nleA::nleA-blaM	WT vs. Y153F	t = 90-100 min	t = 80-100 min
nleA::nleA-blaM	WT vs. Y152F, Y153F	t = 80-100 min	t = 70-100 min
nleA::nleA-blaM	WT vs. S147A	n.s.	t = 90-100 min
nleH1::nleH1-blaM	Y153F vs. Y152F	t = 70-100 min	t = 70-100 min
nleH1::nleH1-blaM	Y153F vs. Y152F, Y153F	t = 80-100 min	t = 70-100 min
nleH1::nleH1-blaM	S147A vs. Y152F	t = 70-100 min	t = 70-100 min
nleH1::nleH1-blaM	S147A vs. Y152F, Y153F	t = 70-100 min	t = 70-100 min
nleH2::nleH2-blaM	Y153F vs. Y152F	t = 90-100 min	t = 90-100 min
nleH2::nleH2-blaM	Y153F vs. Y152F, Y153F	t = 80-100 min	t = 80-100 min
nleH2::nleH2-blaM	S147A vs. Y152F, Y153F	t = 80-90 min	t = 70-100 min
espF::espF-blaM	WT vs. Y152F	t = 40-70min; t = 90-100 min	t = 40-100 min
espF::espF-blaM	WT vs. Y153F	t = 90 min	t = 60-100 min
espF::espF-blaM	Y152F vs. Y152F, Y153F	t = 40-50 min	t = 40-70 min
espF::espF-blaM	Y153F vs. Y152F, Y153F	n.s.	t = 90-100 min

Note: Statistical analyses were conducted with GraphPad Prism (6.0) using the unpaired t-test method to compare mean and standard deviation at individual time points. The range of time (min) over which the comparison was statistically significant is listed for two P values.

3.7 Analysis of the CesT Y152 relationship with NleA

Due to the striking requirement for CesT Y152 to support NleA translocation, I questioned why we had observed intermediate differences for the other CesT-interacting effectors when this phosphosite was mutated. As noted previously, it was recently

identified that NleA expression is controlled by the post-transcriptional regulator CsrA in a process involving CesT, and that NleA expression is induced upon EPEC attachment to host cells (Katsowich *et al.,* 2017). In the same study it was revealed that despite high translocation efficiency, the relative amount of intrabacterial NleA was low. We therefore considered the possibility that phosphosite Y152 contributes to improved protein expression of NleA which in turn leads to greater translocation efficiency.

Under secretion inducing conditions, NleA expression was notably less for wild type EPEC compared to the *cesT* (Y153F) variant (Figure 3.13A). NleA expression was not detected for chromosomal *cesT* variants encoding the Y152F mutation. Upon collection of total lysates recovered from a 2 h HeLa infection, NleA was only detectable for wild type and the *cesT* (Y153F) variant conditions (Figure 3.13B). Similar to the real-time translocation data, NleA was greater in the *cesT* (Y153F) variant than wild type. Tir was evident for the *cesT* (Y152F) and (Y152F, Y153F) strains, indicating that despite an NleA defect, these strains are translocation competent (Figure 3.13B).

To gain insight into post-transcriptional regulatory control of NleA expression, we obtained plasmid-encoded CsrA from the ASKA library (a complete set of *E. coli* K-12 ORF archive). This high copy pCsrA construct is controlled by the Isopropyl β-D-1-thiogalactopyranoside (IPTG)-inducible $P_{T5\text{-}lac}$ promoter. Upon establishment of this plasmid within EPEC *nleA::nleA-blaM* and the derivative *cesT* variant strains, we conducted *in vitro* secretion assays and used the real-time translocation system to address whether CsrA overexpression alters NleA expression and secretion in context of CesT phosphosite mutations (Figure 3.13C-E). Without IPTG-induced overexpression of

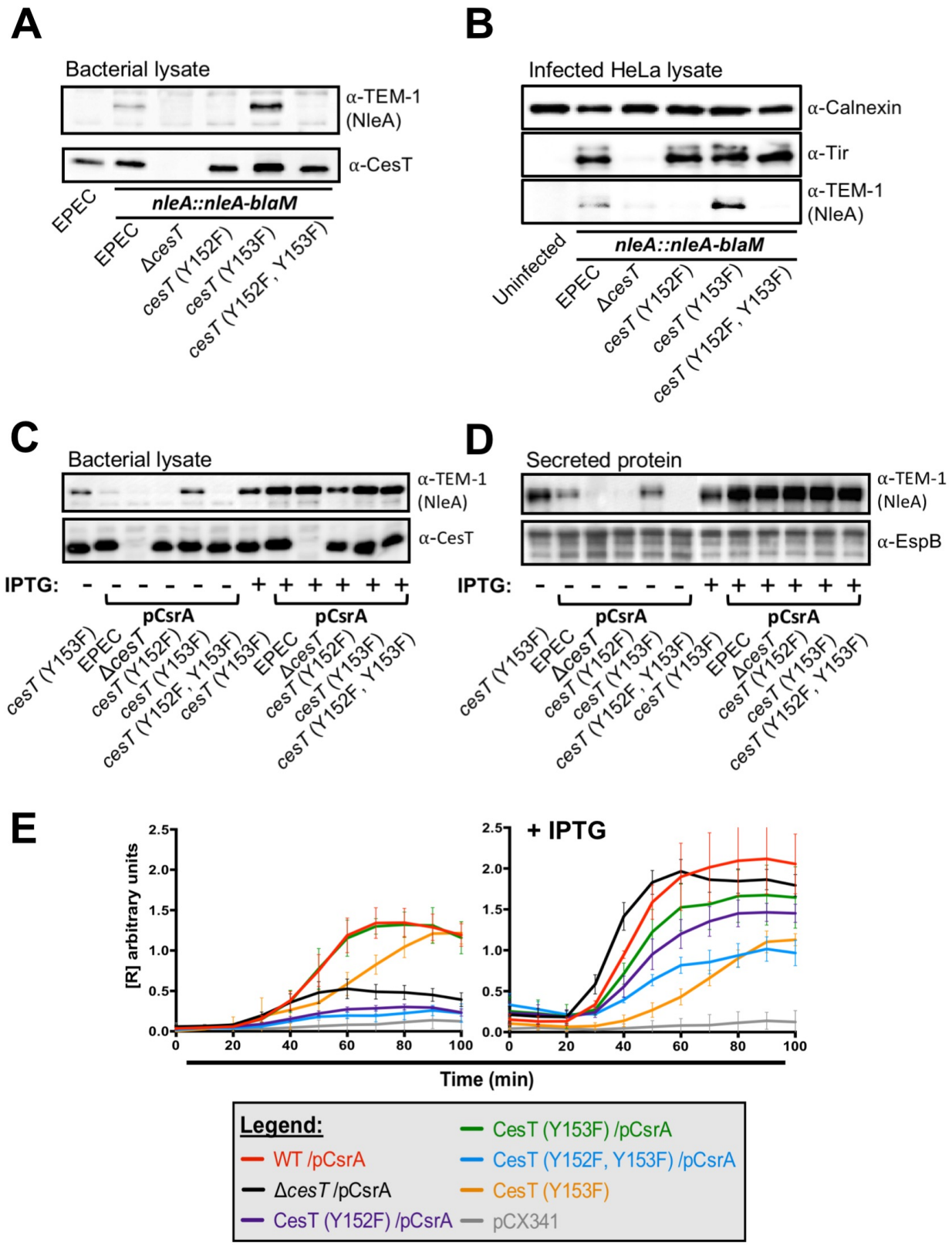

Figure 3.13: NleA expression is dependent on CesT Y152 and can be artificially induced by CsrA overexpression. (A) The indicated EPEC parent or *nleA::nleA-blaM* derivative strains were cultured in DMEM +2mM EGTA for 6 h. Protein expression from

whole cell lysates was detected by immunoblot with α-CesT or α-TEM-1 antibodies. (B) Total lysates were collected after 2 h from mock infected or HeLa cells inoculated at MOI 200 with the indicated *nleA::nleA-blaM* strains pre-activated for 4 h in DMEM. Calnexin served as a loading control for immunoblot analysis. (C) Bacterial lysates or (D) total secreted protein were collected from the indicated strains cultured in DMEM +2mM EGTA with or without addition of 0.4 mM IPTG to induce CsrA overexpression. Immunoblot images are representative of two independent experiments. (E) Kinetic analysis of NleA translocation in context of CsrA overexpression using the *blaM* reporter system. HeLa cells were infected (MOI 200) in the presence or absence of IPTG with bacterial strains pre-activated for 4 h in DMEM. Data is representative of three independent infection experiments carried out in duplicates. For presentation clarity, statistically significant differences are noted in Table 3.5.

CsrA, the NleA expression pattern remained identical to the *cesT* variant strains without the plasmid (Figure 3.13A). However, upon CsrA overexpression by addition of 0.4 mM IPTG, NleA expression was noted for all *cesT* variants, including Δ*cesT* (Figure 3.13C). As a control, the *cesT* (Y153F) variant without pCsrA was included and showed no change in context of NleA expression or secretion when IPTG was added. Secretion of the T3SS translocon component EspB was not influenced by CsrA overexpression; however, NleA secretion was induced independent of CesT or CesT phosphosites (Figure 3.13D). Collectively, these data illustrate that NleA expression is dependent on the CesT Y152 phosphosite; however CsrA overexpression induced NleA expression and secretion by a CesT-independent mechanism.

Subsequent analysis of CsrA overexpression was conducted with the *blaM* reporter assay. Divergent from an endpoint immunoblot with sensitive TEM-1 antibody, this kinetic assay provided detailed insight toward NleA translocation dynamics in the presence of CsrA overexpression and the CesT phosphosite variants in an infection setting. Without IPTG-induced CsrA overexpression, NleA was efficiently translocated into HeLa cells by wild type or the *cesT* (Y153F) variant (Figure 3.13E), as seen previously

in Figure 3.12. Under this condition, rapid translocation of NleA began by 40 min post-infection for EPEC strains containing pCsrA. Through addition of IPTG to the infection media, rapid NleA translocation began at the earlier time point of 30 min post- infection for strains containing pCsrA (Figure 3.13E). For figure clarity, statistical analyses to compare the data are described in Table 3.5. The *cesT* (Y152F, Y153F) variant, while able to translocate NleA in the presence of IPTG, was significantly impaired ($P < 0.01$; relative to wild type and Δ*cesT*) from 40-100 min post-infection in terms of the translocation rate. The *cesT* (Y152F) variant was significantly impaired ($P < 0.01$; relative to wild type and Δ*cesT*) for the NleA translocation rate from 50-100 min post-infection. The difference observed for *cesT* (Y153F) was not statistically significant. Taken together, these data indicate that despite CsrA overexpression, which stimulated NleA expression and secretion by a CesT independent mechanism, there is significant inhibition of the NleA translocation rate when CesT is present and cannot be phosphorylated at Y152.

Table 3.5: Statistical analyses summary for NleA-TEM-1 translocation comparisons in context of *cesT* variants with or without IPTG induced overexpression of CsrA.

Comparison (without IPTG) *nleA::nleA-blaM* /pCsrA *cesT* variants	**** (P < 0.01)**	*** (P < 0.05)**
wild type vs. ΔcesT	60-100 min	50-100 min
wild type vs. Y152F	50-100 min	40-100 min
wild type vs. Y153F	n.s.	n.s.
wild type vs. Y152F, Y153F	50-100 min	40-100 min
wild type vs. *Y153F *without pCsrA*	50-70 min	50-70 min
Y153F vs. *Y153F *without pCsrA*	50-70 min	50-70 min
Comparison (+0.4 mM IPTG) *nleA::nleA-blaM* /pCsrA *cesT* variants	**** (P < 0.01)**	*** (P < 0.05)**
wild type vs. ΔcesT	n.s.	n.s.
wild type vs. Y152F	50-100 min	40-100 min
wild type vs. Y153F	n.s	n.s
wild type vs. Y152F, Y153F	40-100 min	40-100 min
wild type vs. *Y153F *without pCsrA*	40-100 min	40-100 min
Y152F vs. *Y153F *without pCsrA*	40-100 min	40-100 min
Y153F vs. *Y153F *without pCsrA*	40-100 min	40-100 min
Y152F, Y153F vs. *Y153F *without pCsrA*	40-60 min	40-60 min

Note: Statistical analyses were conducted with GraphPad Prism (6.0) using the unpaired t-test method to compare mean and standard deviation at individual time points. The range of time (min) over which the comparison was statistically significant is listed for two P values. Unless noted (*), EPEC *cesT* variant strains with chromosomal *nleA::nleA-blaM* contained the high copy number pCsrA plasmid (IPTG inducible) obtained from the ASKA library.

3.8 *Citrobacter rodentium* is Attenuated by Phosphodeficient CesT Expression in a Natural Model of A/E Pathogenesis

Given the observations of functional significance for the CesT phosphosites to EPEC effector injection into host cells during *in vitro* infection, an analysis with *cesT* variant *C. rodentium* strains was designed to assess significance *in vivo*. *C. rodentium* has been previously used for a natural small animal model of A/E pathogenesis to demonstrate the role of many EPEC and EHEC virulence factors, including the T3SS, LEE-encoded, and non-LEE-encoded genes. Specifically, *ΔcesT C. rodentium* is highly

attenuated for mouse intestinal colonization and disease. To investigate the importance of CesT Y152 and Y153 for *C. rodentium* mouse infection, healthy female C57BL/6 mice (n = 5) were infected by oral gavage with established control strains (wild type, *ΔcesT*, *ΔnleA*) or CesT phosphosite substitution variants that express i) Y152F, ii) Y153F, or iii) Y152F, Y153F. The experiment was monitored relative to an uninfected control group over 9 days, and stool samples were collected at 3, 5, 7, and 9 days post-infection to assess *C. rodentium* shedding. None of the mice from the experimental groups showed a significant weight loss over the course of the infection (Appendix D).

A pilot experiment revealed that at day 9 post-infection the burden of *C. rodentium* in the stool and colon tissue was markedly less for the CesT Y152F, Y153F variant in comparison to wild type (Figure 3.14). Specifically in the colon tissue, wild type infection

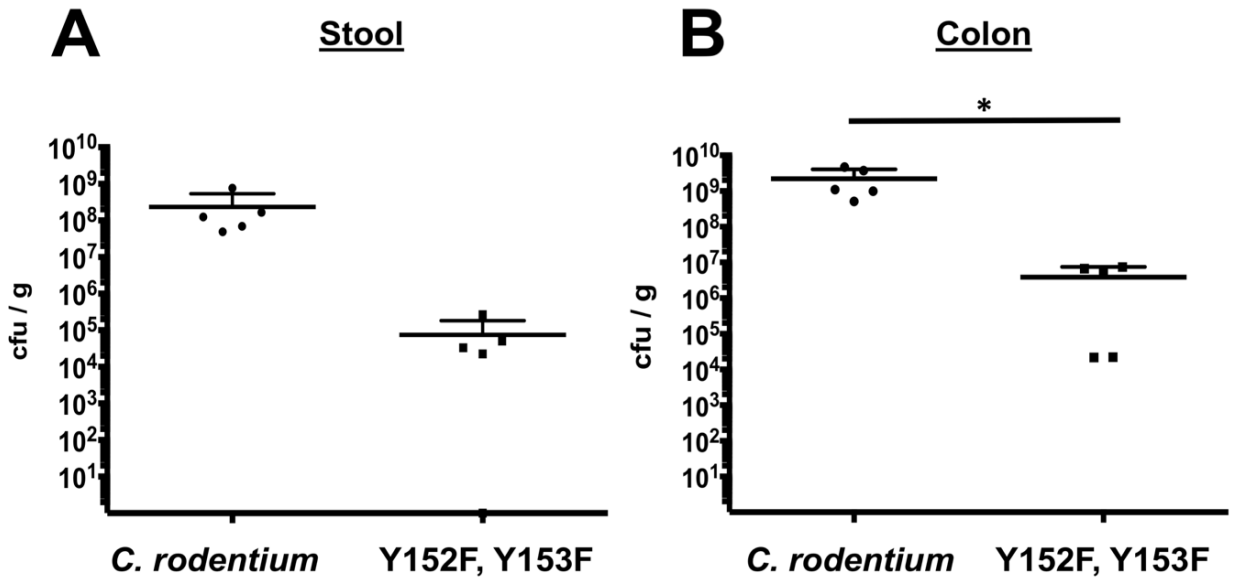

Figure 3.14 Endpoint analysis of *C. rodentium* colonization at day 9 post-infection from the pilot experiment with wild type and the CesT Y152F, Y153F double phosphosite substitution variant. (A) Stool or (B) colon tissue was homogenized, subjected to serial dilution, and plated to determine colony forming units per gram (cfu / g). Statistical significance determined by the unpaired t-test method is indicated by an asterisk (*, P< 0.05).

achieved a mean of $2.2x10^9$ cfu/g whereas the CesT Y152F, Y153F variant reached a mean of $3.9x10^6$ cfu/g, an approximate 3-Log (99.8%) statistically significant difference (P = 0.03). To contextualize the significant colonization defect of the CesT double phosphosite mutant with *cesT* or *nleA* null *C. rodentium* strains, a second independent experiment was conducted. The shedding of live *C. rodentium* in the mice stool was monitored for all strains during infection (Figure 3.15A & B). Throughout the experiment, the wild type and CesT Y153F mutant strains clustered at the highest relative level on each day (Figure 3.15). The *ΔcesT* strain never exceeded 10^5 cfu/g, which was always lower than wild type (10^7–10^8 cfu/g) despite only achieving statistical significance at 7 days post-infection. The CesT Y152F and Y152F, Y153F mutants were delayed in achieving their maximal shedding point, yet were consistently shed at a level greater than Δ*cesT* (Figure 3.15B). Shedding of wild type and each of the CesT phosphosite variant *C. rodentium* strains was maximal by day 7 (mean range: $6.6x10^7$-$2.2x10^8$ cfu/g). However, only one of the five mice infected with CesT Y152F, Y153F produced a cfu/g count greater than 10^6 on this day (Figure 3.15A). By day 9, the mean level of CesT Y152F, Y153F ($2.2x10^6$ cfu/g) in stool was reduced by 99.3% from the wild type mean ($2.9x10^8$ cfu/g), however statistical tests did not achieve a significant P-value by an unpaired t-test. Live CesT Y152F, Y153F *C. rodentium* recovered from excised colon tissue at day 9 was 85% lower than wild type; and 98% less than either single CesT phosphosite mutant. The Δ*nleA* infection progressed to a maximal level of $3.0x10^6$ cfu/g by day 5. Power of the statistical tests was potentially limited by sample size and variability within the animal groups, however clear trends between the *C. rodentium* strains exist.

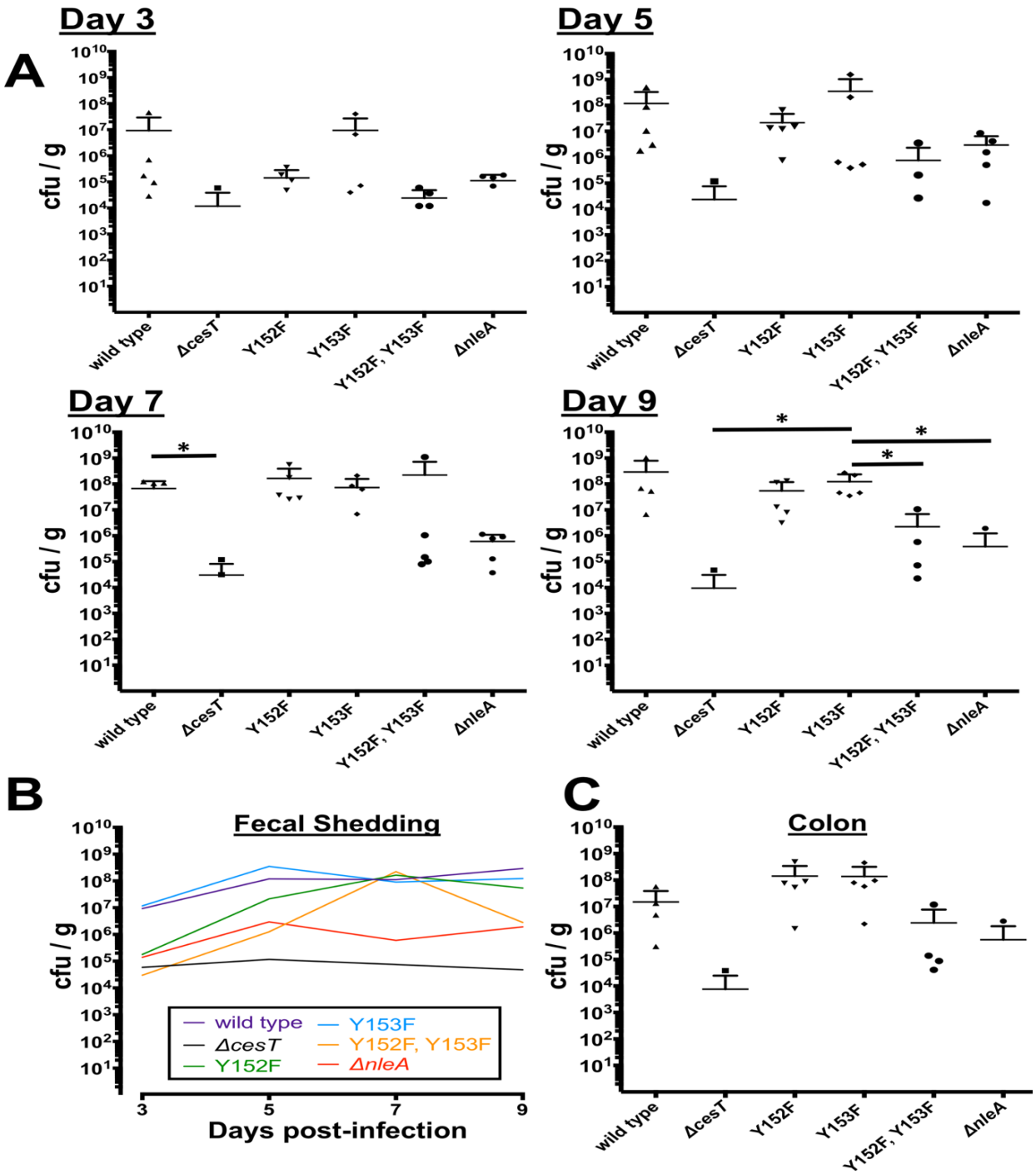

Figure 3.15 Shedding of *C. rodentium* strains determined from fecal samples of infected C57BL/6 mice. (A) Bacterial enumeration from feces collected at day 3, 5, 7, and 9 are represented with lines to indicate the mean + SD. (B) The dynamics of *C. rodentium* shedding is presented as the mean for each experimental group at each time point. (C) Live *C. rodentium* enumeration from excised colon tissue at day 9 post-infection. Statistically significant cfu/g differences were determined by multiple unpaired t-tests where indicated by asterisks (*P < 0.05; n=5 per group).

Collectively these data indicate that *C. rodentium* expressing CesT with both Y152 and Y153 phosphosites mutated are significantly attenuated for host colonization. This colonization defect is evidently less dramatic than what is imposed by outright deletion of *cesT*. As reported previously and in this study, *ΔcesT* strains are unable to translocate the effector Tir into host cells, which removes this essential colonization factor from the infection paradigm. Specific mutation of the CesT Y152 phosphosite had a negative effect on *C. rodentium* shedding levels at day 3 and day 5 post-infection, whereas the Y153F mutation had no noticeable defect, relative to wild type.

3.9 Development of a Genetic Screen for a Kinase that Phosphorylates CesT

The report by Hansen and colleagues revealed that CesT Y152 or Y153 can be phosphorylated by EHEC lacking the two known *E. coli* tyrosine kinases EtK and Wzc. The kinase(s) responsible for phosphorylation of CesT has yet to be identified in EPEC or EHEC, however its discovery would significantly improve our understanding of the regulatory nature of type III effector secretion coordinated through CesT. At this point, it is interesting to speculate that CesT phosphorylation at Y152 may occur upon host-cell contact in order to stimulate NleA expression and translocation. It was theorized that the NleA-TEM-1 fusion construct could provide a useful phenotypic output tool to use in a genetic screen for the kinase that phosphorylates CesT Y152. Expression of native β-lactamase TEM-1 from the low-copy pCX341 plasmid conferred increased ampicillin resistance for EPEC E2348/69 (Figure 3.16). To link this observation to CesT and specifically the Y152 phosphosite, the *cesT* variant *nleA::nleA-blaM* strains were cultured

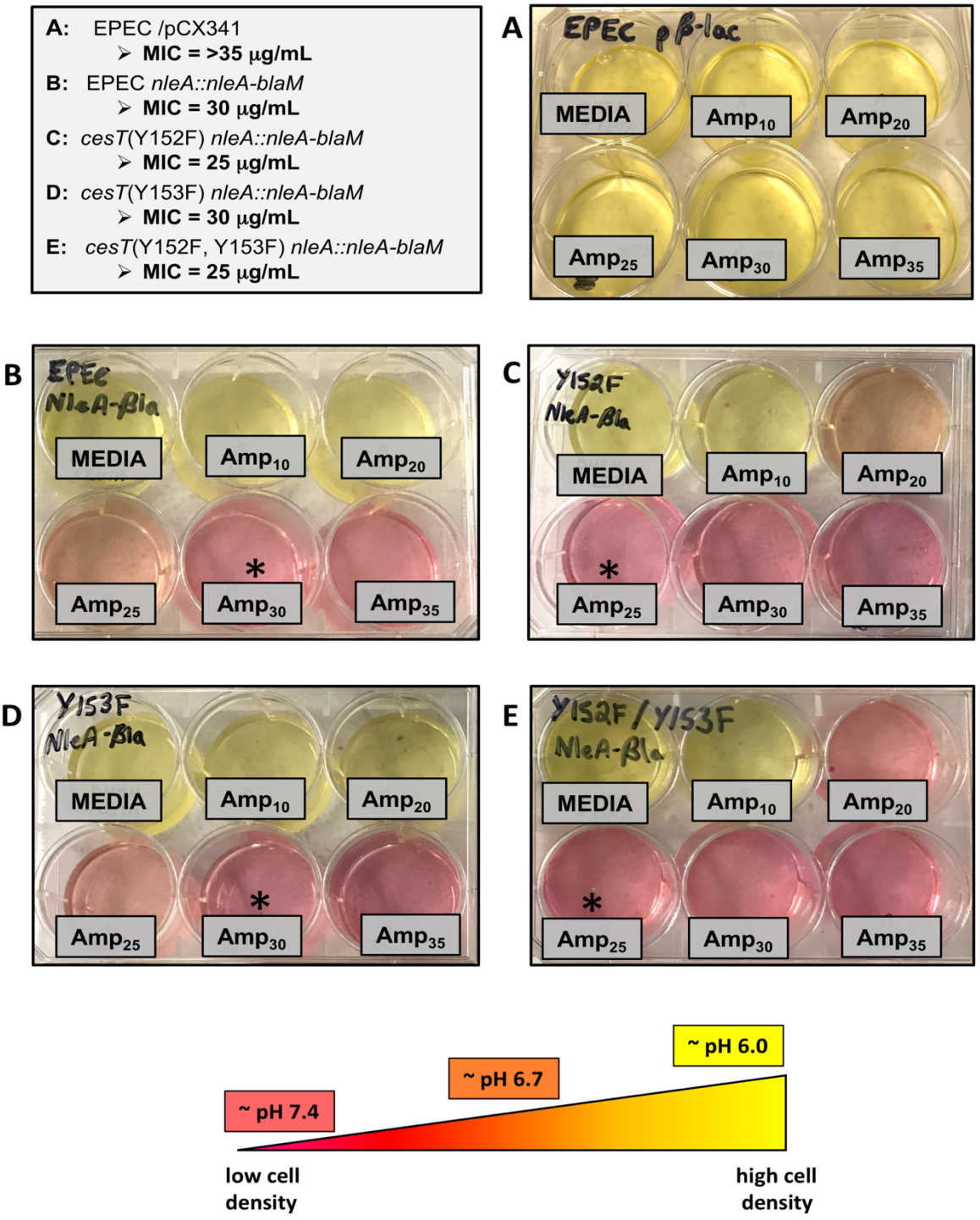

Figure 3.16: CesT Y152-dependent expression and secretion of NleA-TEM-1 increases resistance to ampicillin (Amp) for overnight culture growth in DMEM +2mM EGTA. Asterisks (*) note the minimum inhibitory concentration (MIC) of Amp (μg/μL) for the strains listed (A – E). Colour change from red to yellow indicates media acidification consistent with culture growth. Representative images from two independent experiments are shown.

overnight under a range of ampicillin concentrations to determine the minimum inhibitory concentration (MIC). No microbial growth of wild type EPEC E2348/69 was observed at Amp 20 μg/mL (data not shown), which was therefore established as the ampicillin MIC for EPEC independent of *nleA-blaM*. With mutation of the CesT Y152 phosphosite (CesT Y152F, or CesT Y152F, Y153F) in context of *nleA-blaM* expression, the MIC was established at 25 μg/mL (Figure 3.16C & E). For the wild type CesT sequence or the Y153F variant, the MIC was 30 μg/mL (Figure 3.16B & D). In theory, a transposon mutagenesis screen that successfully disrupted the expression of the unknown kinase for the CesT Y152 phosphosite would reduce the MIC of ampicillin due to a lack of NleA-TEM-1 expression and secretion.

By plating of ampicillin-susceptible *E. coli,* it was demonstrated that 30 μL of the filter-sterilized culture supernatant from EPEC *cesT* (Y153F) *nleA::nleA-blaM* was capable of inactivating 10 μg Ampicillin (Amp10) disks (Figure 3.17A). In complete contrast, the wild type EPEC E2348/69 supernatant did not inactivate the Amp10 disk, and a 20 (±1) mm zone of clearing diameter was observed. Based on the observation of β-lactamase activity in the supernatant it was hypothesized that an overnight pre-activation step in secretion-inducing media without antibiotic pressure followed by a subculture step into selective media might further increase the ampicillin MIC in a manner dependent on NleA-TEM-1. Strikingly, even the maximum ampicillin concentration tested (100 μg/mL) did not limit growth of the *cesT* (Y153F) *nleA::nleA-blaM* strain if it was initially pre-activated overnight in DMEM +2mM EGTA (Figure 3.17B). Pre-activation of wild type EPEC had no effect on its susceptibility to ampicillin.

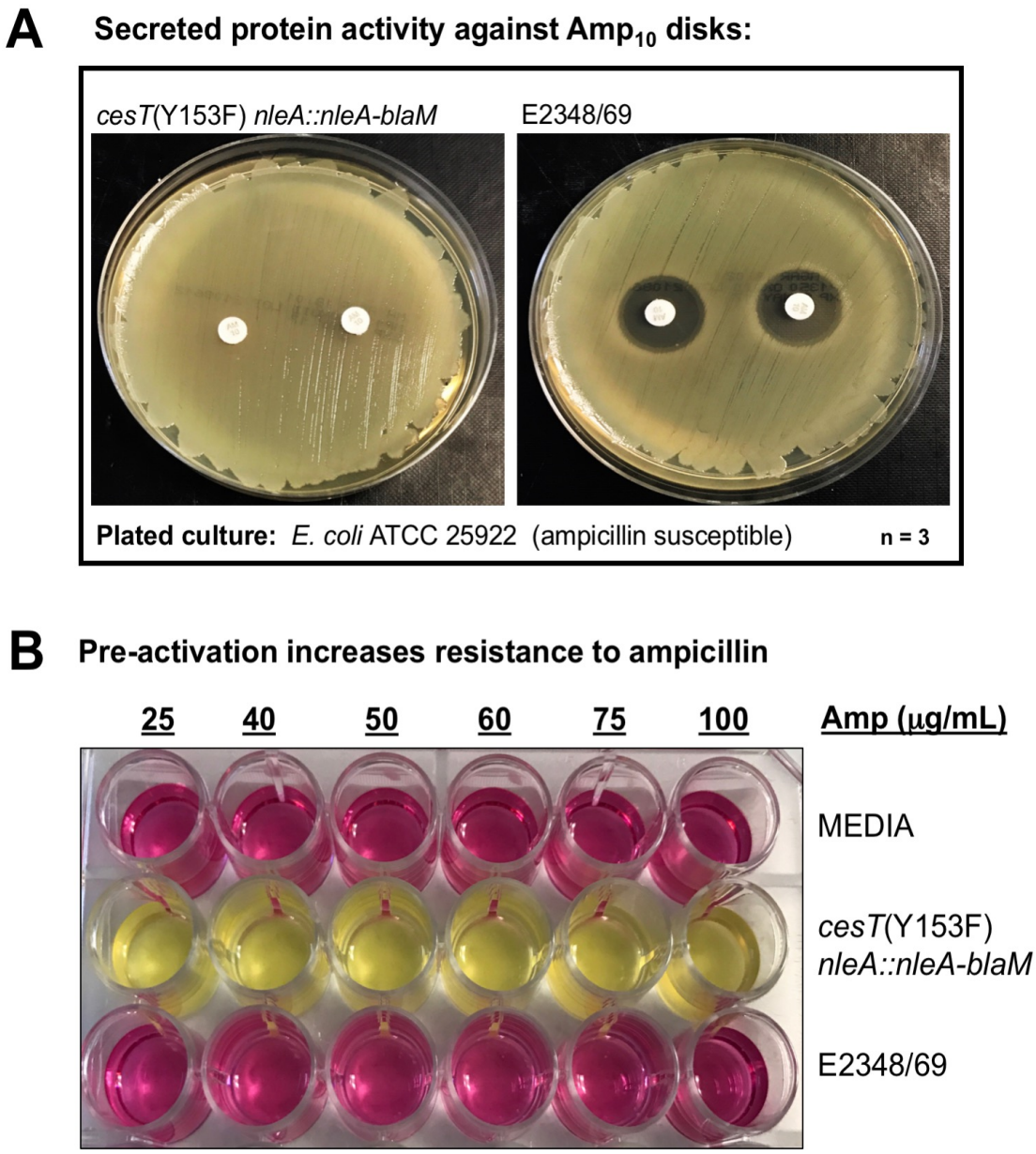

Figure 3.17: Overnight culture supernatant from *cesT* Y153F *nleA::nleA-blaM* inactivates Amp10 disks and promotes an elevated Amp MIC for liquid culture growth. (A) A 30 μL volume of liquid overnight culture supernatant (f/s) from the indicated strain was spotted on each Amp10 disk. A liquid suspension of ampicillin susceptible *E. coli* was plated prior to addition of the Amp10 disks and subsequent culture supernatant. The diameter of the clearing zone around three disks per plate was measured manually. (B) The ampicillin MIC is increased from 30 μg/mL to >100 μg/mL if *cesT*(Y153F) *nleA::nleA-blaM* is pre-activated in non-selective secretion inducing media (1/50 subculture). No growth of the EPEC E2348/69 control was observed above its previously identified MIC at Amp 10 μg/mL.

The results presented in this section collectively indicate that a transposon mutant library generated from the *cesT* (Y153F) *nleA::nleA-blaM* parent strain could be phenotypically screened for a kinase that phosphorylates CesT Y152 by applying ampicillin pressure during growth of library isolates. Disruption of the kinase gene expression would limit expression and secretion of NleA-TEM-1, abolishing EPEC growth at elevated ampicillin levels. Certain limitations and their potential solutions, such as the impact of transposon disruption of T3SS structural genes, will be discussed in greater detail in the next chapter of this thesis.

CHAPTER 4. DISCUSSION

4.1 The CesT Tyrosine Phosphosites Impact T3SS Effector Hierarchy

Since its initial characterization as the molecular chaperone for the effector Tir, several features of CesT have been identified that point toward its central role in A/E pathogenesis. It is well established that through binding to their respective effector proteins, multicargo T3SCs contribute to spatiotemporal regulation of effector secretion events (Thomas *et al.,* 2012). CesT is no exception in this regard, as it is known to interact with at least 11 effectors within the bacterial cytoplasm to coordinate a secretion hierarchy required for intimate attachment to the epithelial surface and modulation of host cell signalling pathways (Mills *et al*. 2013; Raymond *et al.,* 2013; Thomas *et al.,* 2007). The exact molecular mechanisms behind CesT-mediated effector regulation have yet to be fully elucidated, however the evidence presented in this thesis indicates that two specific tyrosine phosphosites critically impact CesT function. This study presents the first observation of a functional role for a T3SC phosphorylation site. Given the requirement of CesT for fulminant EPEC and EHEC virulence and this newly identified phosphosite-specific regulatory modification that influences CesT activity, we have identified a new research direction to investigate limitation of A/E pathogenesis.

The CesT amino acid sequence (156 aa) is highly conserved across many EPEC and STEC serotypes and clinical isolates (95-100% identity). Without exception the amino acid positions 152 and 153 are conserved tyrosines, yet they are located within a predicted disordered domain of the protein (Luo *et al.,* 2001; Ramu *et al.,* 2013). Disordered regions of proteins typically have a higher rate of positional amino acid sequence mutation than structured parts of the same protein (but not always) (Uversky &

Dunker, 2013). An intriguing and perhaps rare finding of the EHEC proteome analysis was the separate and distinct phosphorylation of adjacent tyrosines within the unstructured CesT C-terminal domain (Hansen *et al.,* 2013). The evidence presented in this study extends observation of these two phosphosites to EPEC, and indicate that by preventing site-specific phosphorylation with phenylalanine substitution at the adjacent phosphosite, the remaining phosphorylatable tyrosine contributed to distinct functional outcomes for type III effector secretion. In general, many cases of post-translational modification within intrinsically disordered protein (IDP) domains confers a functional versatility of the protein (Babu, Kriwacki, & Pappu, 2012). Taxonomically, across all domains of life it is estimated that 25-50% of all proteins contain functionally important IDP domains, which often have high polarity in the amino acid sequence that is biased away from hydrophobicity, suggesting the region would fail to fold (Hongbo Xie *et al.,* 2007; Pavlović-Lažetić *et al.,* 2011; Uversky & Dunker, 2013). For the case of the CesT unstructured C-terminus (-SSDNKHYYAGR *'C*; local charge = +2), it is clear that the paradigm of IDP domain functionality could be extended to this specific prokaryotic example. Through post translational modification, IDP domains may undergo disorder-to-order transitions (or vice versa) where the biochemical properties of the protein are changed in such a way that facilitates protein-protein interactions, conformational changes, or promotes stabilization or destabilization of secondary structure (Bah & Forman-Kay, 2016; Uversky & Dunker, 2013; Vihinen *et al.,* 1987). The evident functional significance of CesT phosphorylation has identified a new direction to explore how this site-specific modification affects chaperone interaction with T3SS apparatus components and other cytoplasmic regulatory proteins such as CsrA. In this study a functional

significance for CesT phosphorylation within the C-terminal IDP domain is established. Future insights into the predicted protein-protein interactions required for and established by this post-translational modification through molecular biology, genetics, and biophysical approaches such as NMR, and quantitative mass spectrometry, will have an enormous benefit for expanding our current knowledge of the complex T3SS regulatory network.

At a transcriptional level, *cesT* mRNA is controlled by two independent promoter elements within the LEE. The LEE5 operon co-transcribes *tir-cesT-eae* mRNA in response to Ler and GrlA activation, while an internal *cesT* promoter (cesTp) exists within the *tir-cesT* intrageneic region that is active independent of Ler and GrlA (Brouwers, Ma, & Thomas, 2012). Activity of cesTp has been demonstrated at earlier time points than LEE5 promoter activity, indicating that early CesT expression may be required to prime the cell ahead of Ler- and GrlA- mediated activation of the LEE (Brouwers, Ma, & Thomas, 2012). Post-translational dimerization of CesT is considered a prerequisite for chaperone-effector binding, and involves the helical α2 domain encoded from P63-E78 (Delahay *et al.,* 2002; Luo *et al.,* 2001). Specific amino acid substitutions within this region have been demonstrated to reduce CesT stability (Ramu *et al.,* 2013). The amphipathic α3 domain of CesT (P106-G131) contains a number of surface exposed hydrophobic residues that are predicted to mediate direct contact with putative chaperone-binding domains of the CesT-interacting effectors (Delahay *et al.,* 2002; Luo *et al.,* 2001; Ramu *et al.,* 2013; Thomas *et al.,* 2007). The evidence presented in this thesis indicates that site-specific protein phosphorylation at the unique C-terminal domain (S146-R156) of CesT is required to control efficient delivery of EPEC virulence proteins into host cells during infection.

Collective analyses ranging from genetic manipulation, mass spectrometry, and infection biology approaches implicate the CesT phosphosites Y152 and Y153 in the development of A/E pathogenesis. Furthermore, the general hierarchy of effector protein secretion is specifically influenced by the CesT Y152 phosphosite, which is the first evidence for impact of a phosphorylation-mediated regulatory mechanism of type III effector secretion.

Tyrosine phosphorylation is currently emerging as a widespread post-translational modification in the study of bacterial proteomes, however mechanistic roles related to virulence for this process are limited (refer to Chapter 1.4 or 4.3). In context of the A/E human pathogens EPEC and EHEC, only two examples relating the functional consequence of tyrosine phosphorylation to virulence factors have been established in the literature. The first example involves synthesis of the exopolysaccharide capsule and the conserved family of bacterial tyrosine autokinases that include Etk and Wzc, which are structurally distinct from eukaryotic transmembrane kinases (Grangeasse, 2016; Nadler *et al.,* 2012; Peleg *et al.,* 2005; Vincent *et al.,* 2000; Wugeditsch *et al.,* 2001). In addition to expanding the known repertoire of the *E. coli* phosphotyrosine proteome, the recent study from Hansen and colleagues identified a positive functional role for tyrosine phosphorylation of SspA Y92 (Hansen *et al.,* 2013). The regulator SspA had been previously demonstrated to positively impact T3SS expression by negatively controlling accumulation of the global regulator H-NS (Hansen & Jin, 2012). By phosphodeficient Y92F mutation of SspA, a negative impact on expression and secretion of T3SS proteins and a less pronounced A/E lesion phenotype was observed relative to wild type SspA (Hansen *et al.,* 2013). A similar methodology for phosphosite analysis was applied to this study of CesT. By the conservative site-specific tyrosine substitution with a phenylalanine

residue we have only imposed the localized removal of an oxygen atom critical for phosphorylation by an unknown kinase. These specific mutations should have no impact on overall 3D structure due to the location of the Y152 and Y153 phosphosites in an IDP domain of CesT (Luo *et al.,* 2001; Ramu *et al.,* 2013). Future studies seeking the identification of the kinase(s) that phosphorylate CesT will gain insight into the overall significance of this C-terminal domain with respect to kinase recognition and interaction with other cytosolic proteins, such as CsrA or T3SS apparatus components at the cytoplasmic face of the injectisome complex.

With the lack of a kinase in mind, a model for the role of CesT phosphorylation in regulation of EPEC virulence factors is proposed in Figure 4.1. We have quantitative evidence to suggest there is only a moderate reduction in hierarchical Tir translocation into HeLa cells during infection if both CesT phosphosites are abolished. It is therefore evident that a significant portion of 'early' Tir translocation occurs independent of CesT phosphorylation. However, the reduced injection rate of other CesT-interacting effectors by mutation of both phosphosites, and more significantly at position Y152, suggest that site-specific CesT phosphorylation regulates intrabacterial effector trafficking and type III secretion (T3S). Protein expression of the effector NleA was recently connected to T3SS-mediated host cell contact and a CesT-dependent mechanism (Katsowich *et al.,* 2017). The native *nleA* 5' untranslated region (5' UTR) of EPEC, EHEC and *Citrobacter* strains has three conserved putative binding sites for CsrA (GGA in a predicted RNA hairpin) within a 100 base pair region upstream of the transcriptional start site (Katsowich *et al.*, 2017). The first CsrA binding sequence beginning at the +9 position directly overlaps the ribosomal binding site, which was implicated through gel mobility shift assays as one of

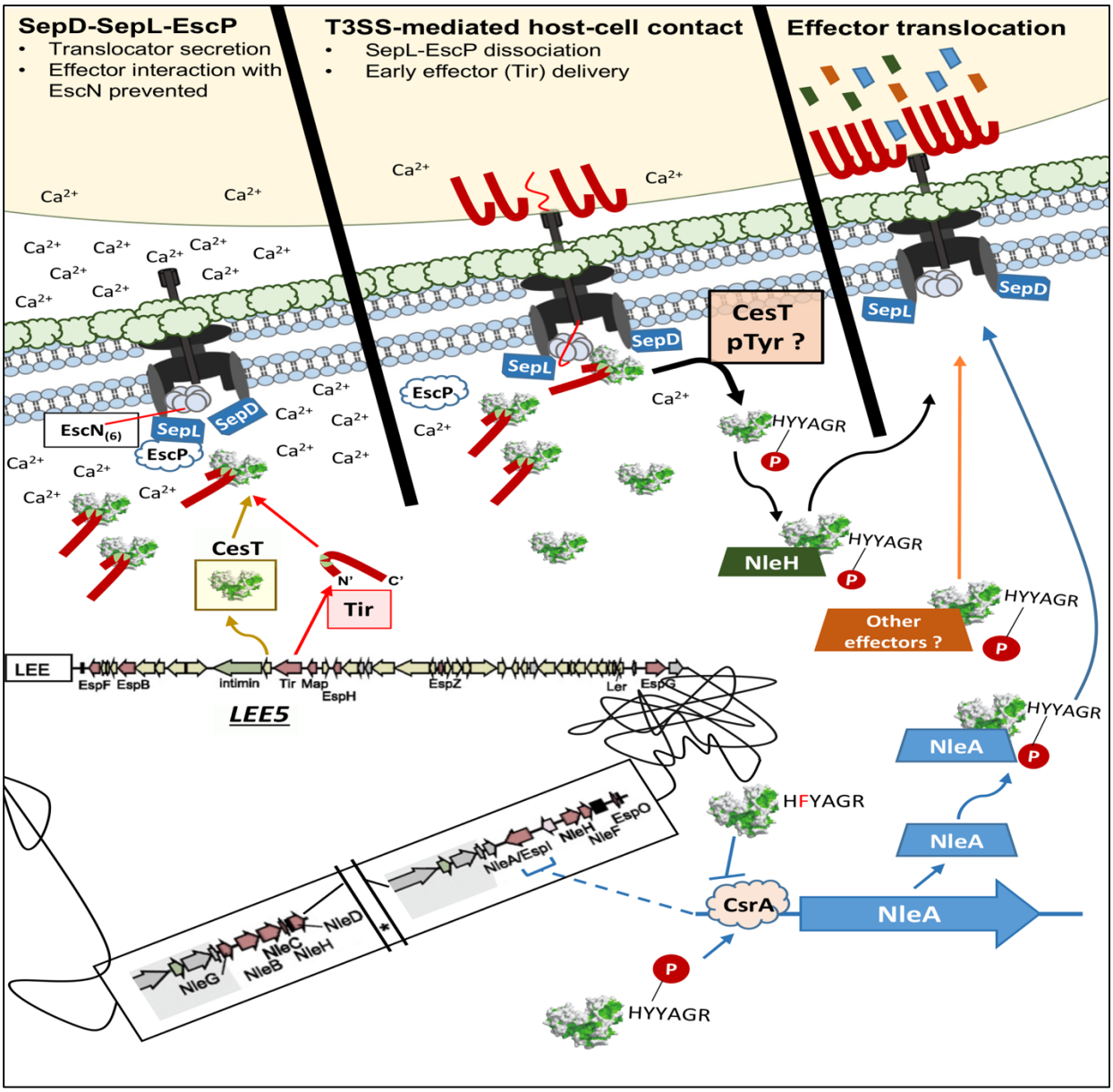

Figure 4.1 CesT is a critical factor for EPEC pathogenesis. (A) Translocator proteins (EspA, EspB, EspD) are secreted through the needle following EscU autocleavage. At this stage the gatekeepers SepD and SepL-EscP prevent premature interaction of CesT-effector complexes with the T3SS ATPase EscN. The T3S of translocators and effectors by EPEC and other pathogens is regulated by the concentration of Ca^{2+} [Ca^{2+}]. Recent evidence suggests that an assembling T3SS is exposed to extracellular [Ca^{2+}] that is elevated relative to the intracellular [Ca^{2+}] sensed following completion of the conduit from the host cytosol to the bacterium. (B) Following completion of the continuous T3SS channel, the decrease in [Ca^{2+}] sensed by EscP prompts dissociation of the SepL-EscP complex, which permits CesT-Tir access to EscN at the T3SS sorting platform to initiate effector secretion. The evidence presented in this thesis demonstrates that C-terminal CesT phosphorylation at Y152 or Y153 is not required for secretion of Tir. NleA is expressed following host cell contact or *in vitro* calcium chelation in a CesT Y152

dependent manner. The CesT Y153F mutation localizes the phosphosite to Y152 only, which was demonstrated to elevate overall effector secretion. Discovery of a kinase that phosphorylates CesT was beyond the scope of this study, however it is hypothesized that this enzyme is active toward CesT Y152 upon host cell contact or calcium depletion. Future studies will aim to identify the kinase(s) and characterize the importance of each CesT phosphosite with respect to secretion of the other CesT-interacting T3S effectors.

---

the two CsrA binding sites on the *nleA* 5'UTR mRNA (Katsowich *et al.,* 2017). The model proposed by Katsowich *et al.,* 2017 implicates a pool of 'freed' CesT in the bacterial cytoplasm post T3SS-mediated host cell contact that is directly responsible for interacting with CsrA to alleviate its binding to the *nleA* 5'UTR to thereby result in NleA translation (Katsowich *et al.,* 2017). The findings of this study confirm that CesT is required for NleA expression in EPEC, and extend this requirement to the CesT Y152 phosphosite. By chromosomal CesT Y152F mutation we have only imposed the loss of an oxygen atom from an unstructured region of the protein while maintaining single-copy CesT regulation. Strikingly, CesT Y152F, or Y152F, Y153F mutation abolished NleA translocation and expression to Δ*cesT* levels (Figure 3.12B, 3.13A). It is therefore predicted that phosphorylation at Y152 changes the biochemical nature of the CesT C-terminus to promote interaction with CsrA to stimulate translation of the *nleA* mRNA.

Our analysis of NleA expression and translocation into host cells led to subsequent study of CsrA overexpression in context of the CesT phosphosite mutants. Strikingly, by elevating CsrA levels we effectively pushed the EPEC system into a CesT-independent mechanism of NleA expression (Figure 3.13). Under CsrA overexpression the most efficient NleA translocation into HeLa cells occurred from the EPEC *ΔcesT* strain. It is well established that Tir stability is severely impaired by deletion of *cesT*, which would increase access to the T3SS for other effectors trafficking via CesT-independent

mechanisms (Delahay *et al.,* 2002; Elliott *et al.,* 1999). Unlike Tir, intrabacterial stability of NleA does not require effector binding to CesT (Katsowich *et al.,* 2017). Due to the pleiotropic nature of CsrA, the effect of its overexpression is questionable at a global regulatory scale (Romeo, Vakulskas, & Babitzke, 2013). CsrA activity is antagonized by small non-coding mRNAs, CsrB and CsrC, which contain multiple CsrA binding sites (Romeo, 1998). Changing the overall CsrABC stoichiometry undoubtedly influences the regulatory equilibrium of multiple signalling pathways. CsrA remodeling of mRNA translation initiation regions can negatively impact protein expression, or promote mRNA stability and ribosome binding to activate expression (Patterson-Fortin *et al.,* 2013; Yakhnin *et al.,* 2013). It is clear that at the level of CsrA overexpression analyzed in this study under a low calcium growth condition we have artificially activated NleA protein expression independent of CesT. Despite this CesT-independent mechanism, evidence that the NleA translocation rate was significantly reduced by CesT Y152F, Y153F indicates that if CesT is present and not phosphorylated, NleA trafficking to the T3SS is impaired (Figure 3.13E). The single CesT Y152F phosphosite substitution induced a more dramatic reduction in NleA translocation than the CesT Y153F variant, which might indicate that site-specific tyrosine phosphorylation is important for CesT docking at the cytoplasmic face of the T3SS apparatus. Both single phosphosite substitution variants reduced NleA translocation relative to wild type CesT (Figure 3.13E). Collectively, this artificial CsrA overexpression approach provided another piece of statistically significant evidence that phosphodeficient CesT Y152F, Y153F impairs effector translocation.

By incorporating the effectors NleH1, NleH2, and EspF into the quantitative beta-lactamase (*blaM*; TEM-1) fluorescence reporter system we have extended our CesT

phosphosite analysis to a broadened context of CesT-interacting effectors. It is certainly possible that unique phosphosite-specific relationships exist between the effector-CesT combinations that were not explored in this study. Therefore time and resources dedicated to construction of single-copy *espG-, espH-, espZ-, map-, nleG-,* and *nleF-blaM* fusions into the chromosomal *cesT* phosphosite variant strains would be a useful tool to establish a complete picture of how the CesT phosphosites contribute to secretion of specific effectors and their respective translocation kinetics.

Analysis of EspF injection into host cells revealed that limited statistically significant differences are imposed on the translocation efficiency by mutation of either CesT phosphosite, or both. EspF is unique to other CesT-interacting effectors in that it also interacts with its own dedicated T3SC, CesF, which is conserved by A/E pathogens (Elliott *et al.,* 2002). The expression of two distinct molecular chaperones for a single effector highlight the importance of EspF to EPEC infection. In recent years EspF has been classified as a multifunctional bacterial effector that plays a role in many disruptive host cell processes, including nucleolus destruction, mitochondrial dysfunction, disruption of cytoskeletal dynamics and the intestinal epithelial barrier, and cell death by apoptosis (Ugalde-Silva *et al.,* 2016). Previous work has demonstrated EspF translocation is significantly reduced relative to wild type by a *cesF* mutant (Mills *et al.,* 2013). Additionally, *C. rodentium* virulence in mice was reduced by a *cesF* or *espF* mutant (Deng *et al.,* 2004). We have added to evidence in the literature that indicates there is only a minor role for CesT mediated EspF translocation (Mills *et al.,* 2013). Interestingly, our kinetic translocation analysis demonstrated that the CesT Y153F variant supported EspF injection into host cells better than all other *cesT* variant EPEC strains. Keep in mind that

this observation was not statistically significant, however it does suggest a general importance of the CesT Y152 phosphosite to promoting effector injection via the T3SS.

This study has provided significant evidence that expression and translocation of NleA requires the CesT Y152 phosphosite (Figure 3.7, 3.9, 3.10, 3.12B, 3.13). By interacting with Nod-Like Receptor 3 (NLRP3) in the host cytoplasm, NleA interrupts a critical de-ubiquitination step that is required for NLRP3 inflammasome activation (Yen *et al.,* 2015). As a result, the NLRP3 inflammasome formation is suppressed, preventing caspase-1 activation which dampens secretion of the pro-inflammatory cytokines IL-1β and IL-18 (Yen, Sugimoto, & Tobe 2015). NleH1 and NleH2 are two additional non-LEE-encoded EPEC effectors that dampen host innate immune signaling which were incorporated into the kinetic translocation analysis of the CesT phosphosites. We observed a significant reduction in NleH1 and NleH2 injection into host cells by mutation of CesT Y152, which contributes to the body of evidence that indicates CesT phosphosite Y152 is of central importance to efficient effector translocation. Unlike NleA translocation, the NleH effectors were not strictly dependent on CesT Y152 (Figure 3.9, 3.12 D-E). The CesT Y152F or Y152F, Y153F variants translocated NleH1 and NleH2 at a level significantly greater than a Δ*cesT* mutant. NleH1 and NleH2 share 84% sequence identity and a similar functional role for EHEC and EPEC subversion of host signalling; however *C. rodentium* only carries one copy of NleH that is functionally equivalent to NleH1 (Gao *et al.,* 2009; Petty *et al.,* 2010). Following injection into host cells, NleH1 and NleH2 modulate the expression of immune response genes regulated through NF-κB by targeting of ribosomal protein S3 (RPS3) (Pham *et al.,* 2012; Royan *et al.,* 2010). RPS3 is a subunit of nuclear NF-κB complexes that confers regulatory specificity on a subset of

NF-κB regulated genes (Wan *et al.,* 2011). At the bacterial level, targeting of immune signalling pathways by effector injection is a critical aspect of pathogenesis (Galán *et al.,* 2009). The data within this thesis implicates the requirement of CesT phosphosite Y152 for NleA expression and translocation, and for efficient NleH translocation. Given that NleA, NleH1, and NleH2 impact host immunomodulatory signalling (Gao *et al.,* 2009; Pham *et al.,* 2012; Thanabalasuriar *et al.,* 2010; Yen *et al.,* 2015), and that NleA expression is only induced upon host cell contact (Katsowich *et al*., 2017), we suggest that CesT phosphorylation at Y152 triggers a switch that leads to efficient translocation of effectors required to dampen the host innate immune response.

In support of this hypothesis, we have obtained evidence that a significant portion of Tir translocation does not require CesT phosphorylation at Y152 or Y153 (Figure 3.12A). Notably, the rate of Tir translocation was modestly reduced for EPEC CesT Y152F, Y153F relative to wild type, although this difference was not statistically significant ($P< 0.05$). Tir is well established as the hierarchical T3SS effector, meaning that it is secreted or translocated into host cells at earlier time points and with greater efficiency than each of the other EPEC effectors by a mechanism that critically requires CesT (Mills *et al.,* 2013; Thomas *et al.,* 2007). The real-time translocation data presented in Figure 3.11 validates the Tir hierarchy, which confirmed this system as a reliable tool for analysis of effector translocation efficiencies in context of the CesT phosphosites. Additionally, we confirmed that the unstructured C-terminal region of CesT (S146-R156) and the CesT phosphosites are not required for effector binding or Tir stability (Appendix C). Reports in the literature indicate that CesT-Tir complexes cannot access the T3SS ATPase EscN until a conformational change in the gatekeeper SepD, SepL proteins is induced by

calcium dependent EscP-SepL dissociation (Shaulov *et al.,* 2017). The completion of the T3SS injectisome by EspBD translocon pore formation in the host membrane is the proposed event that decreases intrabacterial calcium to switch the secretion paradigm from translocators to effectors (Shaulov *et al.,* 2017). Following this secretion switch, hierarchical Tir translocation and insertion into the host cell plasma membrane mediates actin cytoskeletal rearrangements to facilitate intimate bacterial attachment to the host surface (DeVinney *et al.,* 1999; Kenny *et al.,* 1997). Data presented in this thesis indicates that hierarchical translocation of Tir into host cells does not strictly require a CesT phosphosite. However, the secondary effector group, which includes NleA, NleH1, NleH2, and EspF, requires the CesT Y152 phosphosite for efficient translocation**.** From this evidence in combination with NleA expression upon EPEC or EHEC host cell contact from Katsowich *et al.,* 2017, it is hypothesized here that CesT phosphorylation at Y152 might only occur after intimate, Tir-mediated, bacterial contact with the host cell is established to stimulate more efficient injection of the wave of effectors that dampen innate immune signalling.

4.2 The CesT Y152 or Y153 Phosphosite is Required for Fulminant Pathogenesis *in vitro* and *in vivo*

Actin pedestal formation on cultured epithelial cells, or A/E lesion formation *in vivo,* is strictly dependent on efficient Tir accumulation within the host membrane to form an intimin binding site (Campellone & Leong, 2005; Kenny *et al.,* 1997; Schüller *et al.,* 2007). This process additionally requires the two Tir cytoplasmic domains that drive a host signalling cascade to promote actin polymerization underneath the attached bacterium (Cantarelli *et al.,* 2001; Caron *et al.,* 2006; Valérie F. Crepin *et al.,* 2010; Goosney *et al.,*

2000). In this study an *in vitro* fluorescence microscopy-based infection assay was conducted to assess the impact of each CesT phosphosite on EPEC intimate attachment to HeLa cells. An advantage of the pedestal assay in comparison to the quantitative kinetic effector translocation analyses is that we gain insight to a host cell driven process influenced by pathogenic fitness of the bacterial strain. Actin pedestal formation strictly requires Tir accumulation within the host cell membrane, however there are other translocated CesT-interacting effectors such as Map, EspG, and EspH, that contribute to EPEC modulation of host-actin dynamics (Navarro-Garcia, Serapio-Palacios, Ugalde-Silva, Tapia-Pastrana, Chavez-Dueñas, *et al*., 2013).

Using an established binding index and fluorescent actin staining after a 3 h infection, it was determined that EPEC with one tyrosine phosphosite (Y152 or Y153) abolished at the CesT C-terminus did not negatively impact pedestal formation (Figure 3.8). However, mutation of both phosphosites, in the case of *cesT* Y152F, Y153F, significantly reduced pedestal formation by 75% relative to wild type. A more severe reduction in pedestal formation on HeLa cells (5%) was observed for the Δ*cesT* strain. Critically, this was established using single-copy *cesT* variant EPEC strains with the native *LEE5* regulatory region and *tir-cesT* intragenic *cesT* promoter intact. Conducting the same assay with EPEC or EHEC *cesT* phosphosite variants expressed from plasmids (pCesT) demonstrated that pedestal formation by the pCesT Y152F, Y153F variant was unaffected relative to wild type pCesT (data not shown). In agreement with the kinetic Tir translocation data, this demonstrated that by mutation of both CesT phosphosites we have negatively impacted effector injection efficiency, but have not outright abolished the ability of the bacteria to induce pedestal formation. These results collectively indicate that

the interplay of CesT protein expression under tightly regulated native levels along with one of the two C-terminal tyrosine phosphosites are critical to EPEC virulence *in vitro*. It was therefore critical to establish if mutation of the CesT phosphosites in an experiment where the same chromosomal organization was maintained led to virulence defects with an *in vivo* infection model.

C. rodentium is commonly used to study EPEC and EHEC infection in a small animal model of A/E pathogenesis, as it shares several virulence factors including the LEE-encoded T3SS, CesT, and many of the LEE and non-LEE-encoded effectors (Petty *et al.,* 2010). Infection of C3H/HeJ mice with *C. rodentium* results in high mortality due to exaggerated infectious diarrhea, however the C57BL/6 mice strain is useful in the study of a natural host-pathogen combination, in which the mice are capable of clearing the infection by enterocyte shedding at 2-3 weeks post-infection (Collins *et al.,* 2014; Wiles *et al.,* 2004). With the C57BL/6 infection model, the mice develop infectious colitis characterized by reduction in abundance and diversity of the normal host microbiota and significant overgrowth of *C. rodentium*; approximately 10^9 cfu/g by day 7 post-infection (Crepin *et al.,* 2016). Post oral inoculation, *C. rodentium* initially colonizes the caecal patch, which is a lymphoid region of the gastrointestinal tract at the proximal end of the colon. Here the adherent bacteria undergo a virulence switch that includes activation of T3SS genes required for colonization of the distal colon and rectum (Collins *et al.,* 2014).

In the two independent analyses of *C. rodentium* colonization dynamics within C57BL/6 mice (healthy, adult females), a significant average cfu/g reduction of bacterial burden in stool (99.2 – 99.8%) and within the colon (81.9 – 99.8%) was observed relative to wild type if both CesT phosphosites were mutated to phenylalanine (Y152F, Y153F).

Increased variation for the overall bacterial burden was observed during the second independent *Citrobacter* experiment. In this second experiment we additionally included each of the single CesT phosphosite variant strains (Y152F, or Y153F), as well as the Δ*cesT*, and Δ*nleA* CR strains (Figure 3.15). These last two groups were included in the second experiment to provide a reference to previously published observations for attenuated *C. rodentium* strains (Deng *et al.,* 2004). In this experiment the level of wild type bacterial burden in the colon at day 9 post-infection had achieved an average of $1.5x10^7$ cfu/g (n =5), with a greater observed bacterial burden range for each individual mouse ($3.1x10^5$ – $5.6x10^7$). Despite adhering to standard guidelines for conducting animal experiments (including ordering mice from the same supplier and pre-experiment blinding of the mice groups), it is worth noting that the mice were housed for an additional two weeks upon arrival at the IWK Animal Care Facility prior to infection in this second experiment. It is possible, however unlikely, that this may have had an unknown impact on the pathogen-free gastrointestinal microbiota and thereby affected *C. rodentium* colonization dynamics within the mice. Nonetheless, we observed a pronounced reduction in bacterial burden among the mice infected with *cesT* Y152F, Y153F, which was consistent with the first pilot experiment where the colonization levels clustered with more uniformity between individual mice within a group (Figure 3.14). Collectively, the two independent *Citrobacter* experiments provided clear evidence that a CesT phosphosite is required for efficient *C. rodentium* colonization of mice.

Consistent with established reports in the literature, the Δ*cesT C. rodentium* infection group was severely attenuated (Deng *et al.,* 2004). In addition to colonic burden at day 9, fecal shedding of live bacteria was monitored from day 3 to 9 during the second

in vivo experiment (Figure 3.15). Despite a lack of statistically significant differences between groups throughout the experiment (except for day 9 post-infection), biologically relevant trends consistent with certain *in vitro* experiments emerged. At day 3 post-infection, the *cesT* Y152F, Y153F burden was similar to Δ*cesT* (~10^4 cfu/g), which was lower than Δ*nleA* and *cesT* Y152F (~10^5 cfu/g), and wild type and cesT Y153F (~10^7 cfu/g). The Δ*cesT* infection group consistently maintained a burden less than 10^5 cfu/g throughout the experiment. By day 5 post-infection, stool levels of *cesT* Y152F, Y153F had eclipsed the Δ*cesT* infection, and clustered at levels similar to the Δ*nleA* group (10^6 cfu/g). By this point in the infection, wild type, *cesT* Y152F, and *cesT* Y153F were established beyond 10^7 cfu/g, and by day 7 these groups clustered at 10^8 cfu/g. A clear difference at day 7 was observed for the *cesT* Y152F, Y153F group, in which 4 out of 5 mice shed CR at 10^5 cfu/g; while the other individual within the group shed *Citrobacter* at 10^9 cfu/g; drastically altering the average cfu/g value overall. At day 9, all mice infected with *cesT* Y152F, Y153F had reduced bacterial loads in the stool (<10^7 cfu/g), while wild type, *cesT* Y152F, and *cesT* Y153F remained at ~10^8 cfu/g. To summarize, fecal shedding of the *C. rodentium cesT* Y152F, Y153F group was consistently lower than wild type, *cesT* Y152F, or *cesT* Y153F; but elevated compared to Δ*cesT* (other than at day 3). A similar 'intermediate' trend for *cesT* Y152F, Y153F existed for the *in vitro* EPEC pedestal assay data (figure 3.8), where these bacteria were attenuated but not to the level of Δ*cesT*. A minor decrease in stool burden of *C. rodentium* was observed at day 3 post-infection for the *cesT* Y152F variant relative to wild type and *cesT* Y153F CR. Collectively, these data suggest that the CesT Y152 phosphosite is important for early *in vivo* infection,

however the bacteria are able to colonize at levels identical to wild type by the peak of infection as long as one CesT phosphosite exists.

We understand that while CesT expression is critical, neither the unstructured C-terminal domain (-SSDNKHYYAGR ‘C) nor the encompassed Y152 or Y153 phosphosites are required for maintaining protein levels of the essential colonization factor Tir (Figure 3.13B), or for CesT-Tir interaction (Appendix C) and subsequent Tir injection into host cells (Figure 3.12A). However, the rate of Tir translocation into host cells is modestly reduced if CesT cannot be tyrosine phosphorylated at its C-terminus (CesT Y152F, Y153F) (Figure 3.12A). The outcome of this Tir-directed paradigm is exemplified by the *in vitro* pedestal formation data (Figure 3.8) and the *in vivo* infection (Figure 3.14 & 3.15). When CesT is present, host actin rearrangements required for intimate bacterial attachment are able to occur, and this process is efficient as long as one of the two CesT phosphosites (Y152 or Y153) are intact (Figure 3.8). *In vivo*, Δ*cesT C. rodentium* colonization is strongly reduced in infected mice relative to the *cesT* Y152F, Y153F strain (Figure 3.15). Relative to wild type CR, the *cesT* Y152F, Y153F variant is significantly attenuated (Figure 3.14), however not to the baseline level of Δ*cesT*. Taken together, these results demonstrate that a CesT Y152F, Y153F variant is significantly attenuated to an intermediate level relative to Δ*cesT* (low) and wild type (high) controls *in vitro* and *in vivo,* which highlights the importance of a CesT phosphorylation mechanism for complete A/E pathogenesis.

4.3 Phosphoproteomic Studies are Critical to our Understanding of Bacterial Phosphorylation in Context of Virulence

To date, there are a number of prokaryotic phosphoproteomic datasets available (reviewed in Table 4.1). From those published prior to 2011, serine and threonine phosphosites were identified with higher frequency than tyrosine phosphosites. However, recent phosphoproteomic profiling of *E. coli*, *S. flexneri, Bacillus subtilis* and *Klebsiella pneumoniae* has revealed the incidence of Tyr phosphorylation is perhaps higher than what was previously understood (Hansen *et al.,* 2013; Lin *et al.,* 2015; Standish *et al.,* 2016). This body of evidence has significantly contributed to an increasing notion that STY phosphorylation serves as a fundamental regulatory mechanism in all domains of life (Aivaliotis *et al.,* 2009; Hunter, 2009). To continue to integrate newly identified sites of phosphorylation into diverse protein signalling networks, careful analysis of phosphosite mutation(s) is required to determine if functional significance exists (Dephoure *et al.,* 2013). This is particularly important for reported virulence factors that are identified by mass spectrometry-based phosphoproteomic profiling, such as CesT.

An established example of STY phosphorylation regulates cell division and production of the pneumococcal exopolysaccharide capsule, which is an essential virulence factor for *S. pneumoniae* (Kadioglu *et al.,* 2008). STY phosphorylation is regulated by the activity of StkP, a traditional eukaryotic-like serine/threonine kinase, and CpsD, a BYK (Grangeasse, 2016). StkP is a transmembrane protein with kinase activity at its cytoplasmic domain, and its extracellular peptidoglycan-binding domains are required to coordinate cell elongation and division (Massidda, Nováková, & Vollmer, 2013). The CpsD kinase is a BYK structurally similar to Wzc and Etk from *E. coli,* and CapB of *Staphylococcus aureus*, and thus its mechanism of autophosphorylation is predicted to be similar (Grangeasse, 2016).

Table 4.1: STY phosphoproteome datasets reveal a higher prevalence for serine and threonine phosphorylation compared to tyrosine for prokaryotes and the Archeon *Halobacterium salinarum*.

Organism	# of phospho-peptides	# of phospho-sites	% Ser	% Thr	% Tyr	Reference
E. coli (*K12*)	105	81	68.9	23.5	8.6	Macek *et al.,* 2008
E. coli (K12 & EHEC O157:H7)	342	512 p-Tyr sites	N/A	N/A	N/A	* Hansen *et al.,* 2013
E. coli (K12)	392	1088	69.5	21.8	7.7	Lin *et al.,* 2015
S. flexneri	573	905 p-Tyr sites	N/A	N/A	N/A	* Standish *et al.,* 2016
M. tuberculosis	301	516	34	62	4	Kusebauch *et al.,* 2014; Prisic *et al.,* 2010
Campylobacter jejuni	58	35	30.3	72.7	9.1	Voisin *et al.,* 2007
K. pneumoniae	117	93	31.2	15.1	25.8	Lin *et al.,* 2009
K. pneumoniae	663	559	72.9	13.7	12.9	Lin *et al.,* 2015
L. lactis	102	79	46.5	50.6	2.7	Soufi *et al.,* 2008
B. subtilis	103	78	69.2	20.5	10.3	Macek *et al.,* 2007
B. subtilis	441	339	74.8	17.7	7.1	Lin *et al.,* 2015
Helicobacter pylori	80	124	42.8	38.7	18.5	Ge *et al.,* 2011
Mycoplasma pneumoniae	15	15	53.3	46.7	0	Schmidl *et al.,* 2010
Pseudomonas putida	56	53	52.8	39.6	7.5	Ravichandran *et al.,* 2009
P. aeruginosa	57	55	52.7	32.7	14.5	Ravichandran *et al.,* 2009
Streptococcus pneumoniae	102	163	47.2	43.8	9	Sun *et al.,* 2010
Streptomyces coelicolor	44	44	34.1	52.3	13.6	Parker *et al.,* 2010
H. salinarum	42	31	84	16	0	Aivaliotis *et al.,* 2009

Note: References noted by an asterisk (*) indicate a study of the pTyr proteome only.

Capsule assembly is an essential virulence determinant for *S. pneumoniae*, as its formation is critically linked to cell division (Grangeasse, 2016). Phosphorylation of CpsD is promoted by its interaction with CpsC of the transmembrane capsule assembly machinery. One substrate of CpsD phosphorylation is CpsE, which accelerates capsule subunit export (Grangeasse, 2016; Henriques *et al.,* 2011). Additionally, phosphorylated CpsD dissociates from ParB for proper chromosome segregation leading up to cell

division (Nourikyan *et al.,* 2015). CpsD and StkP phosphorylate additional substrates that are involved in regulation of iron intake, pilus synthesis, cell lysis, and competence; therefore indicating that these two kinases are essential to a complex signalling node that controls multiple aspects of cell cycle and virulence (Grangeasse, 2016).

While we currently do not know the kinase(s) that phosphorylates CesT, the evidence presented in this thesis demonstrates that CesT is integral to a phosphosignalling pathway involved in virulence regulation. Similar to the nature of CpsD and StkP of *S. pneumoniae,* it is possible that this unknown kinase for CesT also phosphorylates multiple targets. The study by Hansen and colleagues identified several EHEC T3SS proteins phosphorylated on tyrosine, including the Class II chaperone CesA, the effector EspJ, and the translocators EspA, EspB, and EspD (Hansen *et al.,* 2013). Another tyrosine phosphorylated LEE1 encoded protein (of unknown function at the time; *orf4*) has since been characterized as EscK; a component of the T3SS cytoplasmic sorting platform that interacts with EscQ (Soto *et al.,* 2017). Tyrosine phosphorylated EspA was additionally detected in the BYK double mutant EHEC (*Δetk Δwzc*) strain (Hansen *et al.,* 2013). It is perhaps unlikely that one of these T3SS-associated proteins is a kinase that phosphorylates CesT, yet CesT is importantly one of eight tyrosine phosphorylated T3SS proteins. Together with CesT-specific evidence presented in this thesis, this might suggest that tyrosine phosphorylation serves to recruit these proteins to the cytoplasmic face of the T3SS.

Mycobacterium tuberculosis was once thought to be devoid of tyrosine phosphorylation due to a lack of traditional BYKs and previous unsuccessful attempts to identify tyrosine phosphosites with early phosphoproteomic studies (Kusebauch *et al.,*

2014; Prisic *et al.,* 2010; Sherman & Grundner, 2014). Considering the significance of tyrosine phosphorylation for *M. tuberculosis* despite the absence of BYKs, and the recently expanded *E. coli* phosphotyrosine proteome*,* in which 115 unique pTyr sites were identified in a BYK deficient EHEC strain (Δ*etk*Δ*wzc*) (Hansen *et al.,* 2013); it is likely that DSPK enzymes or unidentified BYKs confer a more significant contribution to the pTyr proteome than what was once thought. DSPKs are particularly important to yeast and certain eukaryotes, yet in addition to *M. tuberculosis,* they have only been described amongst prokaryotes for *Bacillus spp.* and *C. pneumoniae,* to date (Arora *et al.,* 2012; Johnson & Mahony, 2007; Lee *et al.,* 1996; Miller, 2012). Therefore further work will be required to identify and characterize conserved features of novel DSPK and BYK enzymes that contribute to the expanded repertoire of prokaryotic phosphosignalling. Site-specific, high-confidence mass spectrometry data presented in this thesis indicates that the recombinant CesT-FLAG protein can be phosphorylated on Serine-160 (Table 3.1). This evidence suggests that the kinase(s) for CesT phosphorylation may in fact function with relaxed site-specificity. Through imposing the C-terminal FLAG tag (-2 net charge at neutral pH) for immunoprecipitation and downstream LysC digestion, we have altered the local biochemical nature of the CesT C-terminus; which affected CesT functionality (Figure 3.2) and perhaps CesT-kinase interactions. Therefore future identification of a kinase that phosphorylates CesT at Y152 and/or Y153 should also seek to address if serine and threonine residues, of CesT or other protein substrates, may also be phosphorylated.

Mass spectrometry technology has commonly been employed for extensive study of protein phosphorylation in eukaryotic cells. Bacterial phosphoproteomes are less well

established, yet emerging; and phosphorylation dependent signalling mechanisms are expected to be promising targets for new drugs to combat the antibiotic resistance crisis (Lin *et al.,* 2015; Mijakovic & Macek, 2012). Kinase-substrate specificity is typically based on the amino acid sequence surrounding the phosphorylation site. We are only beginning to understand the nature bacterial STY phosphosite motifs, yet distinct differences and some similarities to eukaryotic phosphosites are apparent (Hansen *et al.,* 2013; Lin *et al.,* 2015; Standish *et al.,* 2016). Two high confidence bacterial phosphosite motifs are established that are distinct from eukaryotic motifs: a linear motif with lysine at the (-1) position of the phospho-acceptor Ser or Thr residue, or a position-based motif with the phosphosite near the N- or C-terminus of the protein (position-directed motif) (Lin *et al.,* 2015). Phosphotyrosine-specific motifs have recently been established for *E. coli* and *S. flexneri,* however only two motifs are conserved across both species: YxxxK, and YxxK (Hansen *et al.,* 2013; Standish *et al.,* 2016). Identification of high confidence phosphosite motifs unique to bacteria will be of paramount importance as phosphoproteomic datasets are established in future studies. Such motifs will be valuable for development of specific small molecules that seek to inhibit bacterial kinases, and for the continuous search for new phosphosites.

4.4 Future Research Directions

It is intriguing that differential mutations at neighbouring CesT phosphosites significantly altered T3S effector translocation outcomes. Given that the effector NleA is regulated by CsrA and CesT (Katsowich *et al.,* 2017), it is also evident that the CesT Y152 phosphosite is required to promote expression and translocation of NleA.

Collectively, these observations together with the *in vivo* significance of both CesT phosphosites characterized in this thesis have identified a new research direction: seeking the identification of a kinase that phosphorylates CesT. To approach this question, the EPEC *cesT* Y153F *nleA::nleA-blaM* reporter strain could be a valuable tool to employ. Under low calcium DMEM growth conditions it was demonstrated that NleA-TEM-1 confers increased EPEC resistance to ampicillin in a CesT Y152 phosphosite dependent manner (Figure 3.16B,D). Additionally an ampicillin-free overnight pre-activation in DMEM +2mM EGTA produced enzymatically active supernatant of the *cesT* Y153F *nleA::nleA-blaM* strain; which increased the ampicillin MIC from 30 μg/mL to ≥100 μg/mL for the strain (Figure 3.17). In theory, one could therefore use this strain as a conjugation recipient for transposon mutagenesis by way of the *E. coli* /pRL27 donor strain received from Bill Metcalf. This transposon system is a Tn5 derivative (Larsen *et al.,* 2002) and with an EPEC *cesT* Y153F *nleA::nleA-blaM* (*pir* negative) recipient, transposants can be selected with kanamycin (pRL27) and streptomycin (EPEC).

To phenotypically screen colonies of interest, one could grow cultures in 96-well plates in DMEM +2mM EGTA for 24 h, then subculture (1/50 v/v) into fresh media supplemented with 100 μg/mL ampicillin. Mutants unable to grow in selective media could also be screened by a simple 1:1 Bradford Assay from DMEM +2mM EGTA growth conditions to predict transposants with T3SS apparatus mutations. Valuable controls in this secondary screening experiment would be EPEC Δ*escN* (negative), *cesT* Y152F *nleA::nleA-blaM* (intermediate) and *cesT* Y153F *nleA::nleA-blaM* (positive). However it is important to understand the possible limitations of this approach; including the possibility that multiple kinases might contribute to CesT phosphorylation. Therefore this phenotypic

screen may not be informative if a single kinase gene is disrupted by the transposon and functional redundancy indeed exists for another kinase. Additionally, a single kinase may phosphorylate multiple targets, and there could be negative pleiotropic effects, such as major growth deficiencies, if such a kinase is mutated (Dephoure *et al.,* 2013). Altogether, an ideal candidate transposant colony (Kan^RSt^R) would display i) no major growth defect in non-selective secretion inducing media, ii) susceptibility to ampicillin following subculture, and iii) overall secreted protein levels greater than the Δ*escN* negative control; possibly at levels similar to the *cesT* Y152F *nleA::nlaA-blaM* strain.

One of the major challenges that researchers will face in continuing the study of CesT phosphorylation, upon identification of the responsible kinase and phosphatase enzymes, is to conduct future mass spectrometry experiments that shed light on the stoichiometry that exists between phosphorylation at CesT Y152 or CesT Y153. Careful consideration must be applied to development and execution of such a protocol; beyond the chemical (isobaric tags for relative and absolute quantification (iTRAQ), or dimethyl iTRAQ (mTRAQ)), or metabolic labelling technique (stable isotope labelling with amino acids in cell culture (SILAC)), or label-free quantitation method chosen (Bantscheff, *et al.*, 2012). Given the challenges faced to accomplish detection of each phosphorylated CesT tyrosine phosphosite in this thesis, in all likelihood largely due to the low abundance or stability of the phosphorylated CesT protein, I would recommend implementing a scaled-up gel-free approach with the following three major guidelines. First of all, careful consideration of different culture growth conditions (i.e. DMEM, DMEM +2mM EGTA, or during *in vitro* or *in vivo* infection) must be applied to address the possibility that the phosphorylation status of CesT changes with respect to EPEC environmental sensing. A

secondary important consideration to such an analysis is the lysate generation and subsequent protein or phosphopeptide enrichment strategy. Ideally, two synthetic CesT phosphopeptides (i.e. EEISSSDNKHY^{P}YAGR and EEISSSDNKHYY^{P}AGR; available through ThermoFisher Custom Peptide Synthesis Service) could be used to raise high affinity monospecific antibodies that would be highly valuable for sample enrichment prior to mass spectrometry. The synthetic phosphopeptides would also serve as valuable internal standards for downstream mass spectrometry experiments to control for multiple experimental aspects, including i) PSM comparisons, ii) determination of the ideal ionization energy for phosphopeptide MS/MS fragmentation, and iii) to account for potential differences between phosphopeptide stability with respect to the phosphorylation modification at CesT site Y152 or Y153.

A final important consideration for the workflow is the enzyme for protease digestion, which is largely dependent on the nature of CesT in the analysis. This study demonstrated functional limitations for NleA translocation (but not Tir) imposed by the CesT-FLAG protein expressed within a Δ*cesT* genetic background, indicating this recombinant peptide tag may not be suitable for more in-depth analysis of the CesT phosphorylation status. The unfortunate small C-terminal peptide originating from a wild type CesT protein sequence that is generated by complete trypsin digestion (HYYAGR) encompasses both phosphosites, and has yet to be observed in phosphorylated form (either by our analysis in EPEC or by Hansen and colleagues in EHEC). Alternative proteases, such as GluC (for sequence cleavage at glutamic acid or aspartic acid depending on buffer conditions), are available; or the conditions for incomplete tryptic digest could be optimized with the use of an internal phosphopeptide standard and

subsequently applied to experimental samples. Collectively the continued analysis of CesT will not be trivial if we seek to understand the dynamics and abundance of phosphorylation at one tyrosine phosphosite relative to its neighbour. With a combination of both mass spectrometry-based quantitation of CesT phosphorylation abundance under different physiological conditions and, with some good fortune, the identification of kinase and phosphatase enzymes responsible for catalyzing the reversible modification, we will gain a tremendous understanding of how A/E pathogens have specifically evolved a unique mechanism to regulate type III effector secretion to promote enteric disease.

To further strengthen the body of evidence that suggests a CesT phosphosite is important during infection, one might consider a fluorescence microscopy-based live-cell imaging assay to assess pedestal formation or effector translocation kinetics *in vitro.* Such an experiment is logistically within our grasp at Dalhousie with the use of the Invitrogen EVOS FL Auto Cell Imaging System (catalog #: AMC1000) if a project collaboration or agreement is reached with Dr. Brendan Leung (Faculty of Dentistry). The experimental setup would differ from the pedestal assay conducted in this thesis, as HeLa cell F-actin would need to be pre-labelled with a fluorescent marker, such as the SiR-actin Kit (CY-SC001), or loaded with the cytosolic CCF2-AM substrate for an effector-TEM-1 translocation assay. This EVOS FL imaging system would allow a researcher to use a sterile 24-well glass bottom culture plate to conduct the experiment in a controlled environment (built-in incubator), and capture images of specified locations (known as “beacons”) at time points of interest or in time-lapse mode to create a video. The pedestal assay described in this thesis captured an established infection endpoint, which was evidently valuable but limited in terms of assessing kinetics of EPEC intimate attachment.

An alternative combination of fluorophores could combine the CCF2-AM (green/blue) labelled human cell line with PhusionRed-labelled bacteria (red fluorescent). This would allow for simultaneous analysis of intimate bacterial attachment, EPEC microcolony formation, and translocation kinetics of a specific effector-TEM-1 fusion in a live cell imaging experiment. This would be particularly interesting in context of real-time NleA translocation following EPEC attachment for wild type compared to the *cesT* Y153F variant. The kinetic NleA translocation analysis presented in Figure 3.12 does not account for the possibility that the *cesT* Y153F variant could induce actin pedestal formation more rapidly than wild type EPEC. If this were the case, the rate of NleA translocation would be expected to be more rapid. However, the collective effector-TEM-1 kinetic analyses (most importantly for Tir) and the 3 h pedestal assay suggest that host actin dynamics are not impacted by deletion of the CesT Y153 phosphosite.

The *Citrobacter* experiment could additionally be optimized in certain ways to create a more robust *in vivo* colonization dataset. While plating diluted fecal and colonic tissue resuspensions on MacConkey agar for cfu counts is the common technique to identify *Citrobacter* colonies, there is potential for masking of these colonies by other Gram-negative bacteria at lesser dilutions (i.e. at 10^{-2}, 10^{-3}; for plating of *C. rodentium* Δ*cesT*, Δ*nleA,* or *cesT* Y152F, Y153F). To improve upon this limitation a couple of options are available in addition to conducting *cesT* PCR tests to confirm *Citrobacter* colony identification. The first and possibly most straightforward improvement could be to plate the dilutions on Citrate media supplemented with bile salts to maintain Gram-positive inhibition. *Citrobacter* are capable of using citrate as their sole carbon source, while *E. coli* are citrate negative; therefore this test would provide a way differentiate between

these two species, but may not be a robust initial growth medium with other bacteria present in the fecal or tissue resuspensions. A second method to improve reliability of colony identification could be the use of a bioluminescent *C. rodentium* DBS100 derivative developed by Dr. Siouxsie Wiles and Dr. Gad Frankel (Wiles *et al.,* 2004). To prepare the necessary strains for a CesT phosphosite analysis this would require re-cloning the variant *cesT* alleles into this strain prior to beginning the experiment. The bioluminescent *C. rodentium* expresses the *luxCDABE* operon and kanamycin resistance cassette, inserted by transposon mutagenesis (mini-Tn5 vector) within a *xylE* gene homologue that is non-essential to *in vitro* or *in vivo* growth (Wiles *et al.,* 2004). This highly bioluminescent *C. rodentium* strain could be identified from the other bacterial colonies with the VersaDoc MP5000 (Bio-Rad) system for colony counting.

4.5 Concluding Remarks

My primary objective in this thesis was to functionally characterize the two reported CesT phosphosites, Y152 and Y153, which were originally identified by Hansen *et al.*, 2013, in a global phosphotyrosine proteome survey of EHEC O157:H7. Both Y152 and Y153 are always conserved in 1183 non-redundant NCBI database entries of the CesT protein (full-length) from A/E pathogen isolates from around the globe, including EPEC, STEC, and *Citrobacter*. Considering that Y152 and Y153 are located in an intrinsically disordered CesT domain previously identified as important for regulating effector secretion, it was suspected these phosphosites were critical for CesT function. As a multicargo (class IB) T3SC, it is well established that CesT interacts with at least 11 type III secreted effector proteins in EPEC. Robust experimental systems reported in the

literature including the *in vitro* protein secretion, pedestal, infected host-cell fractionation, and kinetic effector-TEM-1 translocation assays demonstrate that CesT is required for secretion of several of these effectors and that CesT contributes to establishing the hierarchy of effector secretion (Deng *et al.,* 2005; Mills *et al.,* 2008; 2013; Ramu *et al.,* 2013; Thomas *et al.,* 2005; 2007).

In this study I have shown that at least one of the two CesT tyrosine phosphosites are required for fulminant *in vivo* pathogenesis of *C. rodentium* and for efficient EPEC intimate attachment to host epithelial cells during *in vitro* infection. Under *in vitro* growth conditions that promote CesT-dependent type III effector secretion (i.e. EPEC Δ*sepD* liquid culture in DMEM, or growth in a wild type genetic background in low calcium DMEM) it is clear that if the CesT Y152 phosphosite is mutated to phenylalanine to prevent site-specific phosphorylation, there is a reduction in Tir and a complete loss of NleA secretion into culture supernatants. Additionally, an intact CesT Y152 phosphosite is required for NleA expression in context of HeLa cell infection or EPEC growth in low calcium DMEM. The CesT Y153 phosphosite alone (i.e. CesT Y152F) is sufficient to maintain reasonable Tir secretion and actin pedestal formation on infected epithelial cells, but does not support NleA expression or secretion.

In agreement with these findings, the real time effector translocation analyses using the *blaM* reporter system demonstrated that if EPEC CesT can only support phosphorylation at Y152 (i.e. CesT Y153F) the rate of NleA injection into host cells is significantly increased relative to wild type. In general, the CesT Y152 phosphosite appears to promote increased translocation of other CesT-interacting effectors into host cells; including NleH1, NleH2, Tir, and EspF (in addition to NleA). This finding suggests

that CesT phosphorylated at Y152, rather than Y153, might be a more suitable substrate for interaction with a functionally important yet currently unidentified protein domain at the cytoplasmic face of the T3SS. Additionally, a genetic screen conducted earlier had identified that a CesT S147A mutation does not support NleA secretion or translocation into host cells, which was confirmed with the *blaM* reporter system in this thesis. NleA expression and translocation into host cells was recently demonstrated to be regulated by a post-transcriptional process involving CsrA and CesT; with CesT responsible for alleviating CsrA-mediated repression of *nleA* mRNA translation initiation (Katsowich *et al.,* 2017). Given that NleH1, NleH2, and Tir translocation is not impacted by the CesT S147A mutation, I hypothesize that this site-specific C-terminal mutation does not abolish CesT phosphorylation at Y152, but rather alters the ability of CesT to interact with CsrA to promote NleA expression and subsequent injection into host cells. Future mass spectrometry-based analyses will therefore be required to identify if a CesT S147A variant can still be phosphorylated at Y152.

The secondary research objective of this thesis was to extend the EHEC site-specific observations of CesT phosphorylation at Y152 or Y153 to the closely related A/E pathogen EPEC. Indeed both CesT phosphosites were validated using an independent enrichment approach to what was conducted for the EHEC phosphotyrosine proteome survey (Hansen *et al.,* 2013). This analysis utilized the stable, recombinant FLAG epitope C-terminally fused in frame to CesT (CesT-GTRSVDYKDDDDK). Although this epitope tag functionally impaired NleA translocation, it provided a high affinity interaction “handle” to pull down CesT from complex lysates with FLAG antibody, and generated optimal peptides for LC-MS/MS following digestion with LysC (lysine cleavage only). We

observed high confidence, site-specific phosphorylation at CesT Y153 for 8 peptide-spectrum matches (PSMs) across two independent experiments. CesT Y152 phosphorylation was observed for 5 PSMs across two independent experiments in context of CesT(Y153F)-FLAG. Importantly, peptides corresponding to the non-phosphorylated form of the identified phosphopeptides were also observed and invaluable for comparative purposes between MS and MS/MS spectra.

This thesis has collectively generated insight into the regulatory impact of site-specific tyrosine phosphorylation on CesT function. It is highly likely that once phosphorylated at Y152, the CesT C-terminus confers protein:protein interactions between i) CesT and CsrA, and ii) for CesT with an unidentified T3SS component. It is extremely rare to observe neighbouring amino acid residues as separate phosphorylation targets with each specific site having an impact on overall protein function. This study is the first to assign a regulatory impact for tyrosine phosphorylation to a type III secretion chaperone, and therefore presents a new research direction in bacterial pathogenesis. The *in vivo* relevance of the tyrosine phosphosites for CesT function in combination with their conservation among all A/E pathogens suggests that once a kinase for CesT is discovered, specific inhibitors that prevent its catalytic activity could be developed to help limit EPEC and EHEC pathogenesis.

REFERENCES

Abby, S. S., & Rocha, E. P. C. (2012). The non-flagellar type III secretion system evolved from the bacterial flagellum and diversified into host-cell adapted systems. *PLoS Genetics*, *8*(9), e1002983. http://doi.org/10.1371/journal.pgen.1002983

Abe, A., De Grado, M., Pfuetzner, R. A., Sánchez-SanMartín, C., DeVinney, R., Puente, J. L., … Finlay, B. B. (1999). Enteropathogenic *Escherichia coli* translocated intimin receptor, Tir, requires a specific chaperone for stable secretion. *Molecular Microbiology*, *33*, 1162–1175. http://doi.org/10.1046/j.1365-2958.1999.01558.x

Aivaliotis, M., Macek, B., Gnad, F., Reichelt, P., Mann, M., Oesterhelt, D., … Oesterhelt, D. (2009). Ser/Thr/Tyr Protein Phosphorylation in the Archaeon *Halobacterium salinarum*—A Representative of the Third Domain of Life. *PLoS ONE*, *4*(3), e4777. http://doi.org/10.1371/journal.pone.0004777

Akeda, Y., & Galán, J. E. (2005). Chaperone release and unfolding of substrates in type III secretion. *Nature*, *437*(7060), 911–915. http://doi.org/10.1038/nature03992

Allen-Vercoe, E., Waddell, B., Livingstone, S., Deans, J., & Devinney, R. (2006). Enteropathogenic *Escherichia coli* Tir translocation and pedestal formation requires membrane cholesterol in the absence of bundle-forming pili. *Cellular Microbiology*, *8*(4), 613–624. http://doi.org/10.1111/j.1462-5822.2005.00654.x

Arenas-Hernández, M. M. P., Martínez-Laguna, Y., & Torres, A. G. (2012). Clinical Implications of Enteroadherent *Escherichia coli*. *Current Gastroenterology Reports*, *14*(5), 386–394. http://doi.org/10.1007/s11894-012-0277-1

Arnold, R., Brandmaier, S., Kleine, F., Tischler, P., Heinz, E., Behrens, S., … Rattei, T. (2009). Sequence-based prediction of type III secreted proteins. *PLoS Pathogens*, *5*(4), e1000376. http://doi.org/10.1371/journal.ppat.1000376

Arora, G., Sajid, A., Arulanandh, M. D., Singhal, A., Mattoo, A. R., Pomerantsev, A. P., … Singh, Y. (2012). Unveiling the novel dual specificity protein kinases in Bacillus anthracis: identification of the first prokaryotic dual specificity tyrosine phosphorylation-regulated kinase (DYRK)-like kinase. *The Journal of Biological Chemistry*, *287*(32), 26749–63. http://doi.org/10.1074/jbc.M112.351304

Babu, M. M., Kriwacki, R. W., & Pappu, R. V. (2012). Versatility from Protein Disorder. *Science*, *337*(6101). Retrieved from http://science.sciencemag.org/content/337/6101/1460.long

Bah, A., & Forman-Kay, J. D. (2016). Modulation of Intrinsically Disordered Protein Function by Post-translational Modifications. *The Journal of Biological Chemistry*, *291*(13), 6696–705. http://doi.org/10.1074/jbc.R115.695056

Bantscheff, M., Lemeer, S., Savitski, M. M., & Kuster, B. (2012). Quantitative mass spectrometry in proteomics: critical review update from 2007 to the present. *Analytical and Bioanalytical Chemistry*, *404*(4), 939–965. http://doi.org/10.1007/s00216-012-6203-4

Barba, J., Bustamante, V. H., Flores-Valdez, M. A., Deng, W., Finlay, B. B., & Puente, J. L. (2005). A Positive Regulatory Loop Controls Expression of the Locus of Enterocyte Effacement-Encoded Regulators Ler and GrlA. *JOURNAL OF BACTERIOLOGY*, *187*(23), 7918–7930. http://doi.org/10.1128/JB.187.23.7918–7930.2005

Beld, M. J. C., & Reubsaet, F. A. G. (2012). Differentiation between Shigella, enteroinvasive *Escherichia coli* (EIEC) and noninvasive *Escherichia coli* . *European Journal of Clinical Microbiology & Infectious Diseases*, *31*(6), 899–904. http://doi.org/10.1007/s10096-011-1395-7

Berdichevsky, T., Friedberg, D., Nadler, C., Rokney, A., Oppenheim, A., & Rosenshine, I. (2005). Ler Is a Negative Autoregulator of the LEE1 Operon in Enteropathogenic *Escherichia coli* . *JOURNAL OF BACTERIOLOGY*, *187*(1), 349–357. http://doi.org/10.1128/JB.187.1.349–357.2005

Bhatt, S., Edwards, A. N., Nguyen, H. T. T., Merlin, D., Romeo, T., & Kalman, D. (2009). The RNA binding protein CsrA is a pleiotropic regulator of the locus of enterocyte effacement pathogenicity island of enteropathogenic *Escherichia coli* . *Infection and Immunity*, *77*(9), 3552–68. http://doi.org/10.1128/IAI.00418-09

Bhatt, S., Egan, M., Jenkins, V., Muche, S., & El-Fenej, J. (2016). The Tip of the Iceberg: On the Roles of Regulatory Small RNAs in the Virulence of Enterohemorrhagic and Enteropathogenic *Escherichia coli* . *Frontiers in Cellular and Infection Microbiology*, *6*, 105. http://doi.org/10.3389/fcimb.2016.00105

Bhavsar, A. P., Guttman, J. a, & Finlay, B. B. (2007). Manipulation of host-cell pathways by bacterial pathogens. *Nature*, *449*(7164), 827–834. http://doi.org/10.1038/nature06247

Bouzari, S., Jafari, A., & Aslani, M. M. (2012). *Escherichia coli* : A brief review of diarrheagenic pathotypes and their role in diarrheal diseases in Iran. *Iranian Journal of Microbiology*.

Bronstein, P. A., Miao, E. A., & Miller, S. I. (2000). InvB is a type III secretion chaperone specific for SspA. *Journal of Bacteriology*, *182*(23), 6638–44. http://doi.org/10.1128/JB.182.23.6638-6644.2000

Brouwers, E., Ma, I., & Thomas, N. A. (2012). Dual temporal transcription activation mechanisms control cesT expression in enteropathogenic *Escherichia coli* . *Microbiology*, *158*(Pt_9), 2246–2261. http://doi.org/10.1099/mic.0.059444-0

Burkinshaw, B. J., Deng, W., Lameignère, E., Wasney, G. A., Zhu, H., Worrall, L. J., … Strynadka, N. C. J. (2015). Structural analysis of a specialized type III secretion system peptidoglycan-cleaving enzyme. *The Journal of Biological Chemistry*, *290*(16), 10406–17. http://doi.org/10.1074/jbc.M115.639013

Burkinshaw, B. J., & Strynadka, N. C. J. (2014). Assembly and structure of the T3SS. *Biochimica et Biophysica Acta (BBA) - Molecular Cell Research*, *1843*(8), 1649–1663. http://doi.org/10.1016/j.bbamcr.2014.01.035

Burridge, K., & Wennerberg, K. (2004). Rho and Rac Take Center Stage. *Cell*, *116*(2), 167–179. http://doi.org/10.1016/S0092-8674(04)00003-0

Bustamante, V. H., Santana, F. J., Calva, E., & Puente, J. L. (2001). Transcriptional regulation of type III secretion genes in enteropathogenic *Escherichia coli* : Ler antagonizes H-NS-dependent repression. *Molecular Microbiology*, *39*(3), 664–678. http://doi.org/10.1046/j.1365-2958.2001.02209.x

Bustamante, V. H., Villalba, M. I., García-Angulo, V. A., Vázquez, A., Martínez, L. C., Jiménez, R., & Puente, J. L. (2011). PerC and GrlA independently regulate Ler expression in enteropathogenic *Escherichia coli* . *Molecular Microbiology*, *82*(2), 398–415. http://doi.org/10.1111/j.1365-2958.2011.07819.x

Büttner, D., Gürlebeck, D., Noël, L. D., & Bonas, U. (2004). HpaB from *Xanthomonas campestris* pv. vesicatoria acts as an exit control protein in type III-dependent protein secretion. *Molecular Microbiology*, *54*(3), 755–768. http://doi.org/10.1111/j.1365-2958.2004.04302.x

Büttner, D., & He, S. Y. (2009). Type III protein secretion in plant pathogenic bacteria. *Plant Physiology*, *150*(4), 1656–64. http://doi.org/10.1104/pp.109.139089

Büttner, D., Noël, L., Stuttmann, J., & Bonas, U. (2007). Characterization of the Nonconserved *hpaB-hrpF* Region in the *hrp* Pathogenicity Island from *Xanthomonas campestris* pv. *vesicatoria*. *Molecular Plant-Microbe Interactions*, *20*(9), 1063–1074. http://doi.org/10.1094/MPMI-20-9-1063

Campellone, K. G., Giese, A., Tipper, D. J., & Leong, J. M. (2002). A tyrosine-phosphorylated 12-amino-acid sequence of enteropathogenic *Escherichia coli* Tir binds the host adaptor protein Nck and is required for Nck localization to actin pedestals. *Molecular Microbiology*, *43*(5), 1227–1241. http://doi.org/10.1046/j.1365-2958.2002.02817.x

Campellone, K. G., & Leong, J. M. (2005). Nck-independent actin assembly is mediated by two phosphorylated tyrosines within enteropathogenic *Escherichia coli* Tir. *Molecular Microbiology*, *56*(2), 416–432. http://doi.org/10.1111/j.1365-2958.2005.04558.x

Campellone, K. G., Rankin, S., Pawson, T., Kirschner, M. W., Tipper, D. J., & Leong, J. M. (2004). Clustering of Nck by a 12-residue Tir phosphopeptide is sufficient to trigger localized actin assembly. *Journal of Cell Biology*, *164*(3), 407–416. http://doi.org/10.1083/jcb.200306032

Canadian Food Inspection Agency's (CFIA) Investigation into *E. coli* O121 in Flour and Flour Products - Food - Canadian Food Inspection Agency. Retrieved June 26, 2017, from http://www.inspection.gc.ca/food/information-for-consumers/food-safety-investigations/e-coli-o121/eng/1492621159359/1492621214587

Canova, M. J., & Molle, V. (2014). Bacterial Serine/Threonine Protein Kinases in Host-Pathogen Interactions. *Journal of Biological Chemistry*, *289*(14), jbc.R113.529917. http://doi.org/10.1074/jbc.R113.529917

Cantarelli, V. V, Takahashi, A., Yanagihara, I., Akeda, Y., Imura, K., Kodama, T., … Honda, T. (2001). Talin, a host cell protein, interacts directly with the translocated intimin receptor, Tir, of enteropathogenic *Escherichia coli* , and is essential for pedestal formation. *Cellular Microbiology*, *3*(11), 745–51. Retrieved from http://www.ncbi.nlm.nih.gov/pubmed/11696034

Caron, E., Crepin, V. F., Simpson, N., Knutton, S., Garmendia, J., & Frankel, G. (2006). Subversion of actin dynamics by EPEC and EHEC. *Current Opinion in Microbiology*, *9*(1), 40–45. http://doi.org/10.1016/j.mib.2005.12.008

Charpentier, X., & Oswald, E. (2004). Identification of the secretion and translocation domain of the enteropathogenic and enterohemorrhagic *Escherichia coli* effector Cif, using TEM-1 ??-lactamase as a new fluorescence-based reporter. *Journal of Bacteriology*, *186*, 5486–5495. http://doi.org/10.1128/JB.186.16.5486-5495.2004

Chen, J. W., Romero, P., Uversky, V. N., & Dunker, A. K. (2006). Conservation of intrinsic disorder in protein domains and families: I. A database of conserved predicted disordered regions. *Journal of Proteome Research*, *5*(4), 879–87. http://doi.org/10.1021/pr060048x

Chen, L., Ai, X., Portaliou, A. G., Minetti, C. A. S. A., Remeta, D. P., Economou, A., & Kalodimos, C. G. (2013). Substrate-Activated Conformational Switch on Chaperones Encodes a Targeting Signal in Type III Secretion. *Cell Reports*, *3*(3), 709–715. http://doi.org/10.1016/j.celrep.2013.02.025

Chen, Y.-S., Bastidas, R. J., Saka, H. A., Carpenter, V. K., Richards, K. L., Plano, G. V., & Valdivia, R. H. (2014). The *Chlamydia trachomatis* Type III Secretion Chaperone Slc1 Engages Multiple Early Effectors, Including TepP, a Tyrosine-phosphorylated Protein Required for the Recruitment of CrkI-II to Nascent Inclusions and Innate Immune Signaling. *PLoS Pathogens*, *10*(2), e1003954. http://doi.org/10.1371/journal.ppat.1003954

Cieśla, J., Frączyk, T., & Rode, W. (2011). Phosphorylation of basic amino acid residues in proteins: important but easily missed. *Acta Biochimica Polonica*, *58*(2), 137–48. Retrieved from http://www.ncbi.nlm.nih.gov/pubmed/21623415

Collins, J. W., Keeney, K. M., Crepin, V. F., Rathinam, V. a K., Fitzgerald, K. a, Finlay, B. B., & Frankel, G. (2014). *Citrobacter rodentium*: infection, inflammation and the microbiota. *Nature Reviews. Microbiology*, *12*(9), 612–623. http://doi.org/10.1038/nrmicro3315

Contreras, T. J. O. and C. a. (2011). Enteropathogenic *E. coli* (EPEC) infection in children. *Curr Opin Infect Dis*, *; 24(5):*(10.1097/QCO.0b013e32834a8b8b), pages 478–483. http://doi.org/10.1097/QCO.0b013e32834a8b8b.Enteropathogenic

Cooper, C. A., Zhang, K., Andres, S. N., Fang, Y., Kaniuk, N. A., Hannemann, M., … Coombes, B. K. (2010). Structural and biochemical characterization of SrcA, a multi-cargo type III secretion chaperone in *Salmonella* required for pathogenic association with a host. *PLoS Pathogens*, *6*. http://doi.org/10.1371/journal.ppat.1000751

Costa, T. R. D., Felisberto-Rodrigues, C., Meir, A., Prevost, M. S., Redzej, A., Trokter, M., & Waksman, G. (2015). Secretion systems in Gram-negative bacteria: structural and mechanistic insights. *Nature Reviews Microbiology*, *13*(6), 343–359. http://doi.org/10.1038/nrmicro3456

Cozzone, A. J. (2006). Role of protein phosphorylation on serine/threonine and tyrosine in the virulence of bacterial pathogens. *Journal of Molecular Microbiology and Biotechnology*. http://doi.org/10.1159/000089648

Cozzone, A. J., Grangeasse, C., Doublet, P., & Duclos, B. (2004). Protein phosphorylation on tyrosine in bacteria. *Archives of Microbiology*. http://doi.org/10.1007/s00203-003-0640-6

Creasey, E. A., Delahay, R. M., Bishop, A. A., Shaw, R. K., Kenny, B., Knutton, S., & Frankel, G. (2003). CesT is a bivalent enteropathogenic *Escherichia coli* chaperone required for translocation of both Tir and Map. *Molecular Microbiology*, *47*, 209–221. http://doi.org/10.1046/j.1365-2958.2003.03290.x

Creasey, E. A., Friedberg, D., Shaw, R. K., Umanski, T., Knutton, S., Rosenshine, I., & Frankel, G. (2003). CesAB is an enteropathogenic *Escherichia coli* chaperone for the type-III translocator proteins EspA and EspB. *Microbiology*, *149*(12), 3639–3647. http://doi.org/10.1099/mic.0.26735-0

Crepin, V. F., Collins, J. W., Habibzay, M., & Frankel, G. (2016). *Citrobacter rodentium* mouse model of bacterial infection. *Nature Protocols*, *11*(10), 1851–76. http://doi.org/10.1038/nprot.2016.100

Crepin, V. F., Girard, F., Schüller, S., Phillips, A. D., Mousnier, A., & Frankel, G. (2010). Dissecting the role of the Tir:Nck and Tir:IRTKS/IRSp53 signalling pathways *in vivo*. *Molecular Microbiology*, *75*(2), 308–323. http://doi.org/10.1111/j.1365-2958.2009.06938.x

Crepin, V. F., Shaw, R., Abe, C. M., Knutton, S., & Frankel, G. (2005). Polarity of enteropathogenic *Escherichia coli* EspA filament assembly and protein secretion. *Journal of Bacteriology*, *187*(8), 2881–9. http://doi.org/10.1128/JB.187.8.2881-2889.2005

Cunha, L. D., & Zamboni, D. S. (2013). Subversion of inflammasome activation and pyroptosis by pathogenic bacteria. *Frontiers in Cellular and Infection Microbiology*, *3*, 76. http://doi.org/10.3389/fcimb.2013.00076

Darwin, K. H., & Miller, V. L. (1999). InvF is required for expression of genes encoding proteins secreted by the SPI1 type III secretion apparatus in *Salmonella* typhimurium. *Journal of Bacteriology*, *181*(16), 4949–54. Retrieved from http://www.ncbi.nlm.nih.gov/pubmed/10438766

Darwin, K. H., & Miller, V. L. (2001). Type III secretion chaperone-dependent regulation: activation of virulence genes by SicA and InvF in *Salmonella* typhimurium. *The EMBO Journal*, *20*(8), 1850–62. http://doi.org/10.1093/emboj/20.8.1850

de Grado, M., Abe, a, Gauthier, a, Steele-Mortimer, O., DeVinney, R., & Finlay, B. B. (1999). Identification of the intimin-binding domain of Tir of enteropathogenic *Escherichia coli* . *Cellular Microbiology*, *1*, 7–17. http://doi.org/10.1046/j.1462-5822.1999.00001.x

Dean, P., & Kenny, B. (2009). The effector repertoire of enteropathogenic *E. coli*: ganging up on the host cell. *Current Opinion in Microbiology*, *12*(1), 101–9. http://doi.org/10.1016/j.mib.2008.11.006

Delahay, R. M., Shaw, R. K., Elliott, S. J., Kaper, J. B., Knutton, S., & Frankel, G. (2002). Functional analysis of the enteropathogenic *Escherichia coli* type III secretion system chaperone CesT identifies domains that mediate substrate interactions. *Molecular Microbiology*, *43*, 61–73. http://doi.org/10.1046/j.1365-2958.2002.02740.x

Dell, A., Galadari, A., Sastre, F., & Hitchen, P. (2010). Similarities and differences in the glycosylation mechanisms in prokaryotes and eukaryotes. *International Journal of Microbiology*, *2010*, 148178. http://doi.org/10.1155/2010/148178

Deng, W., Li, Y., Hardwidge, P. R., Frey, E. A., Pfuetzner, R. A., Lee, S., … Finlay, B. B. (2005). Regulation of type III secretion hierarchy of translocators and effectors in attaching and effacing bacterial pathogens. *Infection and Immunity*, *73*(4), 2135–46. http://doi.org/10.1128/IAI.73.4.2135-2146.2005

Deng, W., Marshall, N. C., Rowland, J. L., McCoy, J. M., Worrall, L. J., Santos, A. S., … Finlay, B. B. (2017). Assembly, structure, function and regulation of type III secretion systems. *Nature Reviews Microbiology*. http://doi.org/10.1038/nrmicro.2017.20

Deng, W., Puente, J. L., Gruenheid, S., Li, Y., Vallance, B. A., Vázquez, A., … Finlay, B. B. (2004). Dissecting virulence: systematic and functional analyses of a pathogenicity island. *Proceedings of the National Academy of Sciences of the United States of America*, *101*, 3597–602. http://doi.org/10.1073/pnas.0400326101

Deng, W., Vallance, B. A., Li, Y., Puente, J. L., & Finlay, B. B. (2003). *Citrobacter rodentium* translocated intimin receptor (Tir) is an essential virulence factor needed for actin condensation, intestinal colonization and colonic hyperplasia in mice. *Molecular Microbiology*, *48*, 95–115. http://doi.org/10.1046/j.1365-2958.2003.03429.x

Deng, W., Yu, H. B., Li, Y., & Finlay, B. B. (2015). SepD/SepL-dependent secretion signals of the type III secretion system translocator proteins in enteropathogenic *Escherichia coli* . *Journal of Bacteriology*, *197*(7). http://doi.org/10.1128/JB.02401-14

Dephoure, N., Gould, K. L., Gygi, S. P., & Kellogg, D. R. (2013). Mapping and analysis of phosphorylation sites: a quick guide for cell biologists. *Molecular Biology of the Cell*, *24*(5), 535–42. http://doi.org/10.1091/mbc.E12-09-0677

Deutscher, J., & Saier Jr., M. H. (2006). Ser/Thr/Tyr Protein Phosphorylation in Bacteria – For Long Time Neglected, Now Well Established. *Journal of Molecular Microbiology and Biotechnology*, *9*(3–4), 125–131. http://doi.org/10.1159/000089641

DeVinney, R., Stein, M., Reinscheid, D., Abe, A., Ruschkowski, S., & Brett Finlay, B. (1999). Enterohemorrhagic *Escherichia coli* O157:H7 produces Tir, which is translocated to the host cell membrane but is not tyrosine phosphorylated. *Infection and Immunity*, *67*(5), 2389–2398.

Ehrbar, K., Friebel, A., Miller, S. I., & Hardt, W. D. (2003). Role of the *Salmonella* Pathogenicity Island 1 (SPI-1) Protein InvB in Type III Secretion of SopE and SopE2, Two *Salmonella* Effector Proteins Encoded Outside of SPI-1. *Journal of Bacteriology*, *185*(23), 6950–6967. http://doi.org/10.1128/JB.185.23.6950-6967.2003

Ehrbar, K., Hapfelmeier, S., Stecher, B., & Hardt, W. D. (2004). InvB Is Required for Type III-Dependent Secretion of SopA in *Salmonella enterica* Serovar Typhimurium. *Journal of Bacteriology*, *186*(4), 1215–1219. http://doi.org/10.1128/JB.186.4.1215-1219.2004

Elliott, S. J., Hutcheson, S. W., Dubois, M. S., Mellies, J. L., Wainwright, L. A., Batchelor, M., … Kaper, J. B. (1999). Identification of CesT, a chaperone for the type III secretion of Tir in enteropathogenic *Escherichia coli* . *Molecular Microbiology*, *33*, 1176–1189. http://doi.org/10.1046/j.1365-2958.1999.01559.x

Elliott, S. J., O'Connell, C. B., Koutsouris, A., Brinkley, C., Donnenberg, M. S., Hecht, G., & Kaper, J. B. (2002). A gene from the locus of enterocyte effacement that is required for enteropathogenic *Escherichia coli* to increase tight-junction permeability encodes a chaperone for EspF. *Infection and Immunity*, *70*(5), 2271–7. http://doi.org/10.1128/IAI.70.5.2271-2277.2002

Elliott, S. J., Wainwright, L. A., McDaniel, T. K., Jarvis, K. G., Deng, Y., Lai, L.-C., … Kaper, J. B. (2002). The complete sequence of the locus of enterocyte effacement (LEE) from enteropathogenic *Escherichia coli* E2348/69. *Molecular Microbiology*, *28*(1), 1–4. http://doi.org/10.1046/j.1365-2958.1998.00783.x

Faherty, C. S., & Maurelli, A. T. (2009). Spa15 of *Shigella flexneri* is secreted through the type III secretion system and prevents staurosporine-induced apoptosis. *Infection and Immunity*, *77*(12), 5281–90. http://doi.org/10.1128/IAI.00800-09

Feria, J. M., García-Gómez, E., Espinosa, N., Minamino, T., Namba, K., & González-Pedrajo, B. (2012). Role of escp (Orf16) in Injectisome Biogenesis and Regulation of Type III Protein Secretion in Enteropathogenic *Escherichia coli* . *Journal of Bacteriology*. http://doi.org/10.1128/JB.01215-12

Fíla, J., & Honys, D. (2012). Enrichment techniques employed in phosphoproteomics. *Amino Acids*, *43*(3), 1025–47. http://doi.org/10.1007/s00726-011-1111-z

Frankel, G., Phillips, A. D., Novakova, M., Field, H., Candy, D. C., Schauer, D. B., … Dougan, G. (1996). Intimin from enteropathogenic *Escherichia coli* restores murine virulence to a *Citrobacter rodentium* eaeA mutant: induction of an immunoglobulin A response to intimin and EspB. *Infection and Immunity*, *64*(12), 5315–25. Retrieved from http://www.ncbi.nlm.nih.gov/pubmed/8945583

Frenzen, P. D., Drake, A., Angulo, F. J., & Emerging Infections Program FoodNet Working Group. (2005). Economic cost of illness due to *Escherichia coli* O157 infections in the United States. *Journal of Food Protection*, *68*(12), 2623–30. Retrieved from http://www.ncbi.nlm.nih.gov/pubmed/16355834

Friedberg, D., Umanski, T., Fang, Y., & Rosenshine, I. (1999). Hierarchy in the expression of the locus of enterocyte effacement genes of enteropathogenic *Escherichia coli* . *Molecular Microbiology*, *34*(5), 941–52. Retrieved from http://www.ncbi.nlm.nih.gov/pubmed/10594820

Fujii, T., Cheung, M., Blanco, A., Kato, T., Blocker, A. J., & Namba, K. (2012). Structure of a type III secretion needle at 7-Å resolution provides insights into its assembly and signaling mechanisms. *Proceedings of the National Academy of Sciences of the United States of America*, *109*(12), 4461–6. http://doi.org/10.1073/pnas.1116126109

Galán, J. E., Lara-Tejero, M., Marlovits, T. C., & Wagner, S. (2014). Bacterial Type III Secretion Systems: Specialized Nanomachines for Protein Delivery into Target Cells. *Annual Review of Microbiology*, *68*(1), 415–438. http://doi.org/10.1146/annurev-micro-092412-155725

Galán, J. E., Li, H., Hu, L., Wang, J., Zhou, Y., Pang, Z., … al., et. (2009). Common themes in the design and function of bacterial effectors. *Cell Host & Microbe*, *5*(6), 571–9. http://doi.org/10.1016/j.chom.2009.04.008

Galán, J. E., & Wolf-Watz, H. (2006). Protein delivery into eukaryotic cells by type III secretion machines. *Nature*, *444*(7119), 567–573. http://doi.org/10.1038/nature05272

Gall, T. L., Mavris, M., Martino, M. C., Bernardini, M. L., Denamur, E., & Parsot, C. (2005). Analysis of virulence plasmid gene expression defines three classes of effectors in the type III secretion system of *Shigella flexneri*. *Microbiology*, *151*(3), 951–962. http://doi.org/10.1099/mic.0.27639-0

Gao, X., Wan, F., Mateo, K., Callegari, E., Wang, D., Deng, W., … Hardwidge, P. R. (2009). Bacterial effector binding to ribosomal protein s3 subverts NF-kappaB function. *PLoS Pathogens*, *5*(12), e1000708–e1000708. http://doi.org/10.1371/journal.ppat.1000708

Garib, F. Y., Rizopulu, A. P., Kuchmiy, A. A., & Garib, V. F. (2016). Inactivation of inflammasomes by pathogens regulates inflammation. *Biochemistry (Moscow)*, *81*(11), 1326–1339. http://doi.org/10.1134/S0006297916110109

Gauthier, A., De Grado, M., & Finlay, B. B. (2000). Mechanical fractionation reveals structural requirements for enteropathogenic *Escherichia coli* Tir insertion into host membranes. *Infection and Immunity*, *68*, 4344–4348. http://doi.org/10.1128/IAI.68.7.4344-4348.2000

Gauthier, A., & Finlay, B. B. (2003). Translocated intimin receptor and its chaperone interact with ATPase of the type III secretion apparatus of enteropathogenic *Escherichia coli* . *Journal of Bacteriology*, *185*(23), 6747–55. http://doi.org/10.1128/JB.185.23.6747-6755.2003

Gauthier, A., Robertson, M. L., Lowden, M., Ibarra, J. A., Puente, J. L., & Finlay, B. B. (2005). Transcriptional inhibitor of virulence factors in enteropathogenic *Escherichia coli* . *Antimicrobial Agents and Chemotherapy*, *49*(10), 4101–4109. http://doi.org/10.1128/AAC.49.10.4101-4109.2005

Ge, R., Sun, X., Xiao, C., Yin, X., Shan, W., Chen, Z., & He, Q.-Y. (2011). Phosphoproteome analysis of the pathogenic bacterium *Helicobacter pylori* reveals over-representation of tyrosine phosphorylation and multiply phosphorylated proteins. *PROTEOMICS*, *11*(8), 1449–1461. http://doi.org/10.1002/pmic.201000649

General Mills; 07/26/2016. (2016). General Mills Expands Retail Flour Recall. Retrieved June 26, 2017, from https://www.fda.gov/Safety/Recalls/ucm513288.htm

Girón, J. a, Ho, a S., & Schoolnik, G. K. (1991). An inducible bundle-forming pilus of enteropathogenic *Escherichia coli*. *Science (New York, N.Y.)*, *254*(5032), 710–713. http://doi.org/10.1126/science.1683004

Glotfelty, L. G., & Hecht, G. A. (2012). Enteropathogenic E. coli effectors EspG1/G2 disrupt tight junctions: new roles and mechanisms. *Annals of the New York Academy of Sciences*, *1258*(1), 149–158. http://doi.org/10.1111/j.1749-6632.2012.06563.x

Goldberg, M. D., Johnson, M., Hinton, J. C., & Williams, P. H. (2001). Role of the nucleoid-associated protein Fis in the regulation of virulence properties of enteropathogenic *Escherichia coli*. *Molecular Microbiology*, *41*(3), 549–59. Retrieved from http://www.ncbi.nlm.nih.gov/pubmed/11532124

Goldwater, P. N., & Bettelheim, K. a. (2012). Treatment of enterohemorrhagic *Escherichia coli* (EHEC) infection and hemolytic uremic syndrome (HUS). *BMC Medicine*, *10*(1), 12. http://doi.org/10.1186/1741-7015-10-12

Goosney, D. L., DeVinney, R., Pfuetzner, R. A., Frey, E. A., Strynadka, N. C., & Finlay, B. B. (2000). Enteropathogenic *E. coli* translocated intimin receptor, Tir, interacts directly with alpha-actinin. *Current Biology : CB*, *10*(12), 735–8. Retrieved from http://www.ncbi.nlm.nih.gov/pubmed/10873808

Goosney, D. L., Knoechel, D. G., & Finlay, B. B. (1999). Enteropathogenic *E. coli*, Salmonella, and Shigella: masters of host cell cytoskeletal exploitation. *Emerging Infectious Diseases*, *5*(2), 216–23. http://doi.org/10.3201/eid0502.990205

Government of Canada, P. H. A. of C. (2012). Public Health Notice: *E. coli* O157 illness related to beef - Food Safety - Public Health Agency of Canada. Retrieved from http://www.phac-aspc.gc.ca/fs-sa/phn-asp/ecoli-1012-eng.php

Grangeasse, C. (2016). Rewiring the Pneumococcal Cell Cycle with Serine/Threonine- and Tyrosine-kinases. *Trends in Microbiology*, *24*(9), 713–724. http://doi.org/10.1016/j.tim.2016.04.004

Grangeasse, C., Nessler, S., & Mijakovic, I. (2012). Bacterial tyrosine kinases: evolution, biological function and structural insights. *Philosophical Transactions of the Royal Society B: Biological Sciences*, *367*(1602), 2640–2655. http://doi.org/10.1098/rstb.2011.0424

Grangeasse, C., Stülke, J., & Mijakovic, I. (2015). Regulatory potential of post-translational modifications in bacteria. *Frontiers in Microbiology*, *6*, 500. http://doi.org/10.3389/fmicb.2015.00500

Gruenheid, S., Devinney, R., Bladt, F., Goosney, D., Gelkop, S., Gish, G. D., … Finlay, B. B. (2001). Enteropathogenic *E . coli* Tir binds Nck to initiate actin pedestal formation in host cells. *Nature Cell Biology*, *3*(September), 856–859. http://doi.org/10.1038/ncb0901-856

Gruenheid, S., Sekirov, I., Thomas, N. A., Deng, W., O'Donnell, P., Goode, D., … Finlay, B. B. (2004). Identification and characterization of NleA, a non-LEE-encoded type III translocated virulence factor of enterohaemorrhagic *Escherichia coli* O157:H7. *Molecular Microbiology*, *51*, 1233–1249. http://doi.org/10.1046/j.1365-2958.2003.03911.x

Guignot, J., Segura, A., & Tran Van Nhieu, G. (2015). The Serine Protease EspC from Enteropathogenic *Escherichia coli* Regulates Pore Formation and Cytotoxicity Mediated by the Type III Secretion System. *PLoS Pathogens*, *11*(7). http://doi.org/10.1371/journal.ppat.1005013

Hachani, A., Biskri, L., Rossi, G., Marty, A., Ménard, R., Sansonetti, P., … Allaoui, A. (2008). IpgB1 and IpgB2, two homologous effectors secreted via the Mxi-Spa type III secretion apparatus, cooperate to mediate polarized cell invasion and inflammatory potential of Shigella flexenri. *Microbes and Infection*, *10*(3), 260–268. http://doi.org/10.1016/j.micinf.2007.11.011

Hacker, J., & Kaper, J. B. (2000). Pathogenicity islands and the evolution of microbes. *Annual Review Microbiology*, *54*, 641–679. http://doi.org/10.1146/annurev.micro.54.1.641 [doi]\r54/1/641 [pii]

Hall, A. (1998). Rho GTPases and the Actin Cytoskeleton. *Science*, *279*(5350). Retrieved from http://science.sciencemag.org/content/279/5350/509?ijkey=3aa3e5fdeef04371500436618f81470aa4c59f54&keytype2=tf_ipsecsha

Hansen, A.-M., Chaerkady, R., Sharma, J., Díaz-Mejía, J. J., Tyagi, N., Renuse, S., … Pandey, A. (2013). The *Escherichia coli* Phosphotyrosine Proteome Relates to Core Pathways and Virulence. *PLoS Pathogens*, *9*(6), e1003403. http://doi.org/10.1371/journal.ppat.1003403

Hansen, A.-M., & Jin, D. J. (2012). SspA up-regulates gene expression of the LEE pathogenicity island by decreasing H-NS levels in enterohemorrhagic *Escherichia coli* . *BMC Microbiology*, *12*, 231. http://doi.org/10.1186/1471-2180-12-231

Hartl, F. U., & Hayer-Hartl, M. (2002). Molecular Chaperones in the Cytosol: from Nascent Chain to Folded Protein. *Science*, *295*(5561), 1852–1858. http://doi.org/10.1126/science.1068408

Hartland, E. L., Batchelor, M., Delahay, R. M., Hale, C., Matthews, S., Dougan, G., … Frankel, G. (1999). Binding of intimin from enteropathogenic *Escherichia coli* to Tir and to host cells. *Molecular Microbiology*, *32*(1), 151–158. http://doi.org/10.1046/j.1365-2958.1999.01338.x

Haugum, K., Brandal, L. T., Lindstedt, B.-A., Wester, A. L., Bergh, K., & Afset, J. E. (2014). PCR-based detection and molecular characterization of shiga toxin-producing *Escherichia coli* strains in a routine microbiology laboratory over 16 years. *Journal of Clinical Microbiology*, *52*(9), 3156–63. http://doi.org/10.1128/JCM.00453-14

Hazen, T. H., Donnenberg, M. S., Panchalingam, S., Antonio, M., Hossain, A., Mandomando, I., … Nataro, J. P. (2016). Genomic diversity of EPEC associated with clinical presentations of differing severity. *Nature Microbiology*, *1*(2), 15014. http://doi.org/10.1038/nmicrobiol.2015.14

Hazen, T. H., Sahl, J. W., Fraser, C. M., Donnenberg, M. S., Scheutz, F., & Rasko, D. a. (2013). Refining the pathovar paradigm via phylogenomics of the attaching and effacing *Escherichia coli* . *Proceedings of the National Academy of Sciences of the United States of America*, *110*(31). http://doi.org/10.1073/pnas.1306836110

Henriques, M. X., Rodrigues, T., Carido, M., Ferreira, L., & Filipe, S. R. (2011). Synthesis of capsular polysaccharide at the division septum of *Streptococcus pneumoniae* is dependent on a bacterial tyrosine kinase. *Molecular Microbiology*, *82*(2), 515–534. http://doi.org/10.1111/j.1365-2958.2011.07828.x

Hicks, S., Frankel, G., Kaper, J. B., Dougan, G., & Phillips, A. D. (1998). Role of Intimin and Bundle-Forming Pili in Enteropathogenic *Escherichia coli* Adhesion to Pediatric Intestinal Tissue in Vitro. *Infection and Immunity*, *66*(4), 1570–1578. http://doi.org/0019-9567/98

Ho, O., Rogne, P., Edgren, T., Wolf-Watz, H., Login, F. H., & Wolf-Watz, M. (2017). Characterization of the Ruler Protein Interaction Interface on the Substrate Specificity Switch Protein in the *Yersinia* Type III Secretion System. *The Journal of Biological Chemistry*, *292*(8), 3299–3311. http://doi.org/10.1074/jbc.M116.770255

Hongbo Xie, †, Slobodan Vucetic, †, Lilia M. Iakoucheva, ‡, Christopher J. Oldfield, #, A. Keith Dunker, #, Zoran Obradovic, † and, & Vladimir N. Uversky*, #,§. (2007). Functional Anthology of Intrinsic Disorder. 3. Ligands, Post-Translational Modifications, and Diseases Associated with Intrinsically Disordered Proteins. http://doi.org/10.1021/PR060394E

Hueck, C. J. (1998). Type III protein secretion systems in bacterial pathogens of animals and plants. *Microbiology and Molecular Biology Reviews : MMBR*, *62*(2), 379–433. Retrieved from http://www.ncbi.nlm.nih.gov/pubmed/9618447

Hunter, T. (2009). Tyrosine phosphorylation: thirty years and counting. *Current Opinion in Cell Biology*. http://doi.org/10.1016/j.ceb.2009.01.028

Iyoda, S., Koizumi, N., Satou, H., Lu, Y., Saitoh, T., Ohnishi, M., & Watanabe, H. (2006). The GrlR-GrlA regulatory system coordinately controls the expression of flagellar and LEE-encoded type III protein secretion systems in enterohemorrhagic *Escherichia coli* . *Journal of Bacteriology*, *188*(16), 5682–92. http://doi.org/10.1128/JB.00352-06

Izoré, T., Job, V., & Dessen, A. (2011). Biogenesis, regulation, and targeting of the type III secretion system. *Structure (London, England : 1993)*, *19*(5), 603–12. http://doi.org/10.1016/j.str.2011.03.015

Jarvis, K. G., Girón, J. a, Jerse, a E., McDaniel, T. K., Donnenberg, M. S., & Kaper, J. B. (1995). Enteropathogenic *Escherichia coli* contains a putative type III secretion system necessary for the export of proteins involved in attaching and effacing lesion formation. *Proceedings of the National Academy of Sciences of the United States of America*, *92*(August), 7996–8000. http://doi.org/10.1073/pnas.92.17.7996

Jin, J., & Pawson, T. (2012). Modular evolution of phosphorylation-based signalling systems. *Philosophical Transactions of the Royal Society B: Biological Sciences*, *367*(1602), 2540–2555. http://doi.org/10.1098/rstb.2012.0106

Johnson, D. L., & Mahony, J. B. (2007). Chlamydophila pneumoniae PknD Exhibits Dual Amino Acid Specificity and Phosphorylates Cpn0712, a Putative Type III Secretion YscD Homolog. *Journal of Bacteriology*, *189*(21), 7549–7555. http://doi.org/10.1128/JB.00893-07

Kadioglu, A., Weiser, J. N., Paton, J. C., & Andrew, P. W. (2008). The role of *Streptococcus pneumoniae* virulence factors in host respiratory colonization and disease. *Nature Reviews Microbiology*, *6*(4), 288–301. http://doi.org/10.1038/nrmicro1871

Kaneko, T., Joshi, R., Feller, S. M., & Li, S. S. (2012). Phosphotyrosine recognition domains: the typical, the atypical and the versatile. *Cell Communication and Signaling : CCS*, *10*(1), 32. http://doi.org/10.1186/1478-811X-10-32

Kaper JB, Nataro JP, M. H. . (2004). Pathogenic *Escherichia coli* . *Nat. Rev. Microbiol*, *2*, 123–140.

Katsowich, N., Elbaz, N., Pal, R. R., Mills, E., Kobi, S., Kahan, T., & Rosenshine, I. (2017). Host cell attachment elicits posttranscriptional regulation in infecting enteropathogenic bacteria. *Science*, *355*(6326). Retrieved from http://science.sciencemag.org/content/355/6326/735.long

Kendall, M. M., Rasko, D. A., & Sperandio, V. (2010). The LysR-type regulator QseA regulates both characterized and putative virulence genes in enterohaemorrhagic *Escherichia coli* O157:H7. *Molecular Microbiology*, *76*(5), 1306–1321. http://doi.org/10.1111/j.1365-2958.2010.07174.x

Kenny, B., DeVinney, R., Stein, M., Reinscheid, D. J., Frey, E. A., & Finlay, B. B. (1997). Enteropathogenic *E. coli* (EPEC) transfers its receptor for intimate adherence into mammalian cells. *Cell*, *91*, 511–520. http://doi.org/10.1016/S0092-8674(00)80437-7

Kenny, B., & Valdivia, R. (2009). Host–microbe interactions: bacteria. *Current Opinion in Microbiology*, *12*(1), 1–3. http://doi.org/10.1016/j.mib.2009.01.002

Kim, Y.-I., Boyd, J. S., Espinosa, J., & Golden, S. S. (2015). Detecting KaiC phosphorylation rhythms of the cyanobacterial circadian oscillator in vitro and in vivo. *Methods in Enzymology*, *551*, 153–73. http://doi.org/10.1016/bs.mie.2014.10.003

Kinoshita, E., Kinoshita-Kikuta, E., & Koike, T. (2009). Separation and detection of large phosphoproteins using Phos-tag SDS-PAGE. *Nature Protocols*, *4*(10), 1513–21. http://doi.org/10.1038/nprot.2009.154

Kinoshita, E., Kinoshita-Kikuta, E., & Koike, T. (2012). Phos-tag SDS-PAGE systems for phosphorylation profiling of proteins with a wide range of molecular masses under neutral pH conditions. *Proteomics*, *12*(2), 192–202. http://doi.org/10.1002/pmic.201100524

Kitagawa, M., Ara, T., Arifuzzaman, M., Ioka-Nakamichi, T., Inamoto, E., Toyonaga, H., & Mori, H. (2006). Complete set of ORF clones of *Escherichia coli* ASKA library (A Complete Set of *E. coli* K-12 ORF Archive): Unique Resources for Biological Research. *DNA Research*, *12*(5), 291–299. http://doi.org/10.1093/dnares/dsi012

Klink, B. U., Barden, S., Heidler, T. V, Borchers, C., Ladwein, M., Stradal, T. E. B., … Heinz, D. W. (2010). Structure of Shigella IpgB2 in complex with human RhoA: implications for the mechanism of bacterial guanine nucleotide exchange factor mimicry. *The Journal of Biological Chemistry*, *285*(22), 17197–208. http://doi.org/10.1074/jbc.M110.107953

Kodama, T., Rokuda, M., Park, K.-S., Cantarelli, V. V., Matsuda, S., Iida, T., & Honda, T. (2007). Identification and characterization of VopT, a novel ADP-ribosyltransferase effector protein secreted via the *Vibrio parahaemolyticus* type III secretion system 2. *Cellular Microbiology*, *9*(11), 2598–2609. http://doi.org/10.1111/j.1462-5822.2007.00980.x

Kusebauch, U., Ortega, C., Ollodart, A., Rogers, R. S., Sherman, D. R., Moritz, R. L., & Grundner, C. (2014). *Mycobacterium tuberculosis* supports protein tyrosine phosphorylation. *Proceedings of the National Academy of Sciences of the United States of America*, *111*(25), 9265–70. http://doi.org/10.1073/pnas.1323894111

Laemmli, U. K. (1970). Cleavage of structural proteins during the assembly of the head of bacteriophage T4. *Nature*, *227*, 680–685. http://doi.org/10.1038/227680a0

Lara-Ochoa, C., Oropeza, R., & Huerta-Saquero, A. (2010). Regulation of the LEE-pathogenicity island in attaching and effacing bacteria. Retrieved from http://www.formatex.info/microbiology2/635-645.pdf

Larsen, R., Wilson, M., Guss, A., & Metcalf, W. (2002). Genetic analysis of pigment biosynthesis in *Xanthobacter autotrophicus* Py2 using a new, highly efficient transposon mutagenesis system that is functional in a wide variety of bacteria. *Archives of Microbiology*, *178*(3), 193–201. http://doi.org/10.1007/s00203-002-0442-2

LeBlanc, J. J. (2003). Implication of virulence factors in *Escherichia coil* O157:H7 pathogenesis. *Critical Reviews in Microbiology*, *29*(4), 277–96. http://doi.org/10.1080/713608014

Lee, K., Du, C., Horn, M., & Rabinow, L. (1996). Activity and autophosphorylation of LAMMER protein kinases. *The Journal of Biological Chemistry*, *271*(44), 27299–303. http://doi.org/10.1074/JBC.271.44.27299

Levine, M. M., Bergquist, E. J., Nalin, D. R., Waterman, D. H., Hornick, R. B., Young, C. R., & Sotman, S. (1978). *Escherichia coli* strains that cause diarrhoea but do not produce heat-labile or heat-stable enterotoxins and are non-invasive. *Lancet*, *1*(8074), 1119–22. Retrieved from http://www.ncbi.nlm.nih.gov/pubmed/77415

Lin, M.-H., Hsu, T.-L., Lin, S.-Y., Pan, Y.-J., Jan, J.-T., Wang, J.-T., … Wu, S.-H. (2009). Phosphoproteomics of *Klebsiella pneumoniae* NTUH-K2044 Reveals a Tight Link between Tyrosine Phosphorylation and Virulence. *Molecular & Cellular Proteomics*, *8*(12), 2613–2623. http://doi.org/10.1074/mcp.M900276-MCP200

Lin, M.-H., Sugiyama, N., & Ishihama, Y. (2015). Systematic profiling of the bacterial phosphoproteome reveals bacterium-specific features of phosphorylation. *Science Signaling*, *8*(394). Retrieved from http://stke.sciencemag.org/content/8/394/rs10.long

Luo, Y., Bertero, M. G., Frey, E. A., Pfuetzner, R. A., Wenk, M. R., Creagh, L., … Strynadka, N. C. (2001). Structural and biochemical characterization of the type III secretion chaperones CesT and SigE. *Nature Structural Biology*, *8*, 1031–1036. http://doi.org/10.1038/nsb717

Macek, B., Gnad, F., Soufi, B., Kumar, C., Olsen, J. V, Mijakovic, I., & Mann, M. (2008). Phosphoproteome analysis of *E. coli* reveals evolutionary conservation of bacterial Ser/Thr/Tyr phosphorylation. *Molecular & Cellular Proteomics : MCP*, *7*(2), 299–307. http://doi.org/10.1074/mcp.M700311-MCP200

Macek, B., & Mijakovic, I. (2011). Site-specific analysis of bacterial phosphoproteomes. *Proteomics*. http://doi.org/10.1002/pmic.201100012

Macek, B., Mijakovic, I., Olsen, J. V., Gnad, F., Kumar, C., Jensen, P. R., & Mann, M. (2007). The Serine/Threonine/Tyrosine Phosphoproteome of the Model Bacterium *Bacillus subtilis. Molecular & Cellular Proteomics*, *6*(4), 697–707. http://doi.org/10.1074/mcp.M600464-MCP200

Massidda, O., Nováková, L., & Vollmer, W. (2013). From models to pathogens: how much have we learned about *Streptococcus pneumoniae* cell division? *Environmental Microbiology*, *15*(12), 3133–3157. http://doi.org/10.1111/1462-2920.12189

Mavris, M., Page, A.-L., Tournebize, R., Demers, B., Sansonetti, P., & Parsot, C. (2002). Regulation of transcription by the activity of the *Shigella flexneri* type III secretion apparatus. *Molecular Microbiology*, *43*(6), 1543–53. Retrieved from http://www.ncbi.nlm.nih.gov/pubmed/11971264

McDaniel, T. K., Jarvis, K. G., Donnenberg, M. S., & Kaper, J. B. (1995). A genetic locus of enterocyte effacement conserved among diverse enterobacterial pathogens. *Proceedings of the National Academy of Sciences of the United States of America*, *92*(5), 1664–8. Retrieved from http://www.ncbi.nlm.nih.gov/pubmed/7878036

McDermott, J. E., Corrigan, A., Peterson, E., Oehmen, C., Niemann, G., Cambronne, E. D., … Heffron, F. (2011). Computational Prediction of Type III and IV Secreted Effectors in Gram-Negative Bacteria. *Infection and Immunity*, *79*(1), 23–32. http://doi.org/10.1128/IAI.00537-10

Mellies, J. L., Elliott, S. J., Sperandio, V., Donnenberg, M. S., & Kaper, J. B. (1999). The Per regulon of enteropathogenic *Escherichia coli* : identification of a regulatory cascade and a novel transcriptional activator, the locus of enterocyte effacement (LEE)-encoded regulator (Ler). *Molecular Microbiology*, *33*(2), 296–306. http://doi.org/10.1046/j.1365-2958.1999.01473.x

Mijakovic, I., & Macek, B. (2012). Impact of phosphoproteomics on studies of bacterial physiology. *FEMS Microbiology Reviews*, *36*(4), 877–892. http://doi.org/10.1111/j.1574-6976.2011.00314.x

Miller, W. T. (2012). Tyrosine kinase signaling and the emergence of multicellularity. *Biochimica et Biophysica Acta*, *1823*(6), 1053–7. http://doi.org/10.1016/j.bbamcr.2012.03.009

Mills, E., Baruch, K., Aviv, G., Nitzan, M., & Rosenshine, I. (2013). Dynamics of the type III secretion system activity of enteropathogenic *Escherichia coli* . *mBio*, *4*(4), e00303-13-. http://doi.org/10.1128/mBio.00303-13

Mills, E., Baruch, K., Charpentier, X., Kobi, S., & Rosenshine, I. (2008). Real-Time Analysis of Effector Translocation by the Type III Secretion System of Enteropathogenic *Escherichia coli*. *Cell Host & Microbe*, *3*(2), 104–113. http://doi.org/10.1016/j.chom.2007.11.007

Moon, H. W., Whipp, S. C., Argenzio, R. A., Levine, M. M., & Giannella, R. A. (1983). Attaching and effacing activities of rabbit and human enteropathogenic *Escherichia coli* in pig and rabbit intestines. *Infection and Immunity*, *41*(3), 1340–1351.

Muniesa, M., Hammerl, J. A., Hertwig, S., Appel, B., & Brüssow, H. (2012). Shiga toxin-producing *Escherichia coli* O104:H4: a new challenge for microbiology. *Applied and Environmental Microbiology*, *78*(12), 4065–73. http://doi.org/10.1128/AEM.00217-12

Nadler, C., Koby, S., Peleg, A., Johnson, A. C., Suddala, K. C., Sathiyamoorthy, K., … Rosenshine, I. (2012). Cycling of Etk and Etp Phosphorylation States Is Involved in Formation of Group 4 Capsule by *Escherichia coli*. *PLoS ONE*, *7*(6), e37984. http://doi.org/10.1371/journal.pone.0037984

Nans, A., Kudryashev, M., Saibil, H. R., & Hayward, R. D. (2015). Structure of a bacterial type III secretion system in contact with a host membrane in situ. *Nature Communications*, *6*, 10114. http://doi.org/10.1038/ncomms10114

Navarro-Garcia, F., Serapio-Palacios, A., Ugalde-Silva, P., Tapia-Pastrana, G., & Chavez-Dueñas, L. (2013). Actin cytoskeleton manipulation by effector proteins secreted by diarrheagenic *Escherichia coli* pathotypes. *BioMed Research International*. http://doi.org/10.1155/2013/374395

Neuhoff, V., Stamm, R., & Eibl, H. (1985). Clear background and highly sensitive protein staining with Coomassie Blue dyes in polyacrylamide gels: A systematic analysis. *Electrophoresis*, *6*(9), 427–448. http://doi.org/10.1002/elps.1150060905

Notti, R. Q., & Stebbins, C. E. (2016). The Structure and Function of Type III Secretion Systems. *Microbiology Spectrum*, *4*(1). http://doi.org/10.1128/microbiolspec.VMBF-0004-2015

Nourikyan, J., Kjos, M., Mercy, C., Cluzel, C., Morlot, C., Noirot-Gros, M.-F., … Grangeasse, C. (2015). Autophosphorylation of the Bacterial Tyrosine-Kinase CpsD Connects Capsule Synthesis with the Cell Cycle in *Streptococcus pneumoniae*. *PLOS Genetics*, *11*(9), e1005518. http://doi.org/10.1371/journal.pgen.1005518

Obrig, T. G., & Karpman, D. (2012). Shiga toxin pathogenesis: kidney complications and renal failure. *Current Topics in Microbiology and Immunology*, *357*, 105–36. http://doi.org/10.1007/82_2011_172

Ochoa, T. J., Barletta, F., Contreras, C., & Mercado, E. (2008). New insights into the epidemiology of enteropathogenic *Escherichia coli* infection. *Transactions of the Royal Society of Tropical Medicine and Hygiene*, *102*(9), 852–856. http://doi.org/10.1016/j.trstmh.2008.03.017

Ogawa, M., Handa, Y., Ashida, H., Suzuki, M., & Sasakawa, C. (2008). The versatility of *Shigella* effectors. *Nature Reviews Microbiology*, *6*(1), 11–16. http://doi.org/10.1038/nrmicro1814

Ohya, K., Handa, Y., Ogawa, M., Suzuki, M., & Sasakawa, C. (2005). IpgB1 Is a Novel *Shigella* Effector Protein Involved in Bacterial Invasion of Host Cells. *Journal of Biological Chemistry*, *280*(25), 24022–24034. http://doi.org/10.1074/jbc.M502509200

Okada, R., Zhou, X., Hiyoshi, H., Matsuda, S., Chen, X., Akeda, Y., … Kodama, T. (2014). The *Vibrio parahaemolyticus* effector VopC mediates Cdc42-dependent invasion of cultured cells but is not required for pathogenicity in an animal model of infection. *Cellular Microbiology*, *16*(6), 938–947. http://doi.org/10.1111/cmi.12252

Ortega, C., Liao, R., Anderson, L. N., Rustad, T., Ollodart, A. R., Wright, A. T., … Grundner, C. (2014). *Mycobacterium tuberculosis* Ser/Thr Protein Kinase B Mediates an Oxygen-Dependent Replication Switch. *PLoS Biology*, *12*(1), e1001746. http://doi.org/10.1371/journal.pbio.1001746

Ostrovsky, P. C., & Maloy, S. (1995). Protein phosphorylation on serine, threonine, and tyrosine residues modulates membrane-protein interactions and transcriptional regulation in *Salmonella* typhimurium. *Genes & Development*, *9*(16), 2034–41. Retrieved from http://www.ncbi.nlm.nih.gov/pubmed/7544316

Page, A.-L., Sansonetti, P., & Parsot, C. (2002). Spa15 of *Shigella flexneri*, a third type of chaperone in the type III secretion pathway. *Molecular Microbiology*, *43*(6), 1533–42. Retrieved from http://www.ncbi.nlm.nih.gov/pubmed/11952903

Pallen, M. J., Francis, M. S., & FÃ¼tterer, K. (2003). Tetratricopeptide-like repeats in type-III-secretion chaperones and regulators. *FEMS Microbiology Letters*, *223*(1), 53–60. http://doi.org/10.1016/S0378-1097(03)00344-6

Papadopoulos, J. S., & Agarwala, R. (2007). COBALT: constraint-based alignment tool for multiple protein sequences. *Bioinformatics*, *23*(9), 1073–1079. http://doi.org/10.1093/bioinformatics/btm076

Parker, J. L., Jones, A. M. E., Serazetdinova, L., Saalbach, G., Bibb, M. J., & Naldrett, M. J. (2010). Analysis of the phosphoproteome of the multicellular bacterium *Streptomyces coelicolor* A3(2) by protein/peptide fractionation, phosphopeptide enrichment and high-accuracy mass spectrometry. *PROTEOMICS*, *10*(13), 2486–2497. http://doi.org/10.1002/pmic.201000090

Parsot, C., Ageron, E., Penno, C., Mavris, M., Jamoussi, K., d'Hauteville, H., … Demers, B. (2005). A secreted anti-activator, OspD1, and its chaperone, Spa15, are involved in the control of transcription by the type III secretion apparatus activity in *Shigella flexneri*. *Molecular Microbiology*, *56*(6), 1627–1635. http://doi.org/10.1111/j.1365-2958.2005.04645.x

Parsot, C., Hamiaux, C., & Page, A.-L. (2003). The various and varying roles of specific chaperones in type III secretion systems. *Current Opinion in Microbiology*, *6*(1), 7–14. http://doi.org/10.1016/S1369-5274(02)00002-4

Patterson-Fortin, L. M., Vakulskas, C. A., Yakhnin, H., Babitzke, P., & Romeo, T. (2013). Dual Posttranscriptional Regulation via a Cofactor-Responsive mRNA Leader. *Journal of Molecular Biology*, *425*(19), 3662–3677. http://doi.org/10.1016/j.jmb.2012.12.010

Pavlović-Lažetić, G. M., Mitić, N. S., Kovačević, J. J., Obradović, Z., Malkov, S. N., & Beljanski, M. V. (2011). Bioinformatics analysis of disordered proteins in prokaryotes. *BMC Bioinformatics*, *12*(1), 66. http://doi.org/10.1186/1471-2105-12-66

Pearson, J. S., Giogha, C., Wong Fok Lung, T., & Hartland, E. L. (2016). The Genetics of Enteropathogenic *Escherichia coli* Virulence. *Annual Review of Genetics*, *50*(1), 493–513. http://doi.org/10.1146/annurev-genet-120215-035138

Peleg, A., Shifrin, Y., Ilan, O., Nadler-Yona, C., Nov, S., Koby, S., … Rosenshine, I. (2005). Identification of an *Escherichia coli* operon required for formation of the O-antigen capsule. *Journal of Bacteriology*, *187*(15), 5259–66. http://doi.org/10.1128/JB.187.15.5259-5266.2005

Petty, N. K., Bulgin, R., Crepin, V. F., Cerdeño-Tárraga, A. M., Schroeder, G. N., Quail, M. A., … Thomson, N. R. (2010). The *Citrobacter rodentium* genome sequence reveals convergent evolution with human pathogenic *Escherichia coli* . *Journal of Bacteriology*, *192*(2), 525–538. http://doi.org/10.1128/JB.01144-09

Pham, T. H., Gao, X., Tsai, K., Olsen, R., Wan, F., & Hardwidge, P. R. (2012). Functional differences and interactions between the *Escherichia coli* type III secretion system effectors NleH1 and NleH2. *Infection and Immunity*, *80*(6), 2133–40. http://doi.org/10.1128/IAI.06358-11

Pilonieta, M. C., & Munson, G. P. (2008). The chaperone IpgC copurifies with the virulence regulator MxiE. *Journal of Bacteriology*, *190*(6), 2249–51. http://doi.org/10.1128/JB.01824-07

Prisic, S., Dankwa, S., Schwartz, D., Chou, M. F., Locasale, J. W., Kang, C.-M., … Husson, R. N. (2010). Extensive phosphorylation with overlapping specificity by *Mycobacterium tuberculosis* serine/threonine protein kinases. *Proceedings of the National Academy of Sciences of the United States of America*, *107*(16), 7521–7526. http://doi.org/10.1073/pnas.0913482107

Radics, J., Königsmaier, L., & Marlovits, T. C. (2014). Structure of a pathogenic type 3 secretion system in action. *Nature Structural & Molecular Biology*, *21*(1), 82–7. http://doi.org/10.1038/nsmb.2722

Ramu, T., Prasad, M. E., Connors, E., Mishra, A., Thomassin, J.-L., Leblanc, J., … Thomas, N. A. (2013). A novel C-terminal region within the multicargo type III secretion chaperone CesT contributes to effector secretion. *Journal of Bacteriology*, *195*(4), 740–56. http://doi.org/10.1128/JB.01967-12

Ravichandran, A., Sugiyama, N., Tomita, M., Swarup, S., & Ishihama, Y. (2009). Ser/Thr/Tyr phosphoproteome analysis of pathogenic and non-pathogenic *Pseudomonas* species. *PROTEOMICS*, *9*(10), 2764–2775. http://doi.org/10.1002/pmic.200800655

Raymond, B., Young, J. C., Pallett, M., Endres, R. G., Clements, A., & Frankel, G. (2013). Subversion of trafficking, apoptosis, and innate immunity by type III secretion system effectors. *Trends in Microbiology*, *21*(8), 430–41. http://doi.org/10.1016/j.tim.2013.06.008

Reeves, A. Z., Spears, W. E., Du, J., Tan, K. Y., Wagers, A. J., & Lesser, C. F. (2015). Engineering *Escherichia coli* into a Protein Delivery System for Mammalian Cells. *ACS Synthetic Biology*, *4*(5), 644–654. http://doi.org/10.1021/acssynbio.5b00002

Rodgers, L., Mukerjea, R., Birtalan, S., Friedberg, D., & Ghosh, P. (2010). A solvent-exposed patch in chaperone-bound YopE is required for translocation by the type III secretion system. *Journal of Bacteriology*, *192*(12), 3114–22. http://doi.org/10.1128/JB.00113-10

Romeo, T. (1998). Global regulation by the small RNA-binding protein CsrA and the non-coding RNA molecule CsrB. *Molecular Microbiology*, *29*(6), 1321–30. Retrieved from http://www.ncbi.nlm.nih.gov/pubmed/9781871

Romeo, T., Vakulskas, C. A., & Babitzke, P. (2013). Post-transcriptional regulation on a global scale: form and function of Csr/Rsm systems. *Environmental Microbiology*, *15*(2), 313–324. http://doi.org/10.1111/j.1462-2920.2012.02794.x

Rosenshine, I., Umanski, T., & Friedberg, D. (2002). Thermoregulated expression of virulence genes in enteropathogenic *Escherichia coli*. *Microbiology*, *148*(9), 2735–2744. http://doi.org/10.1099/00221287-148-9-2735

Royan, S. V, Jones, R. M., Koutsouris, A., Roxas, J. L., Falzari, K., Weflen, A. W., … Hecht, G. A. (2010). Enteropathogenic *E. coli* non-LEE encoded effectors NleH1 and NleH2 attenuate NF-κB activation. *Molecular Microbiology*, *78*(5), 1232–45. http://doi.org/10.1111/j.1365-2958.2010.07400.x

Ruano-Gallego, D., Álvarez, B., & Fernández, L. Á. (2015). Engineering the Controlled Assembly of Filamentous Injectisomes in *E. coli* K-12 for Protein Translocation into Mammalian Cells. *ACS Synthetic Biology*, *4*(9), 1030–41. http://doi.org/10.1021/acssynbio.5b00080

Saibil, H. (2013). Chaperone machines for protein folding, unfolding and disaggregation. *Nature Reviews. Molecular Cell Biology*, *14*(10), 630–42. http://doi.org/10.1038/nrm3658

Sajid, A., Arora, G., Singhal, A., Kalia, V. C., & Singh, Y. (2015). Protein Phosphatases of Pathogenic Bacteria: Role in Physiology and Virulence. *Annual Review of Microbiology*, *69*(1), 527–547. http://doi.org/10.1146/annurev-micro-020415-111342

Sal-Man, N., Deng, W., & Finlay, B. B. (2012). EscI: a crucial component of the type III secretion system forms the inner rod structure in enteropathogenic *Escherichia coli* . *Biochemical Journal*, *442*(1), 119–125. http://doi.org/10.1042/BJ20111620

Salvadori, M. I., Sontrop, J. M., Garg, A. X., Moist, L. M., Suri, R. S., & Clark, W. F. (2009). Factors that led to the Walkerton tragedy. *Kidney International*, *75*(112), S33–S34. http://doi.org/10.1038/ki.2008.616

Schmidl, S. R., Gronau, K., Pietack, N., Hecker, M., Becher, D., & Stulke, J. (2010). The Phosphoproteome of the Minimal Bacterium *Mycoplasma pneumoniae:* ANALYSIS OF THE COMPLETE KNOWN SER/THR KINOME SUGGESTS THE EXISTENCE OF NOVEL KINASES. *Molecular & Cellular Proteomics*, *9*(6), 1228–1242. http://doi.org/10.1074/mcp.M900267-MCP200

Schmitz, A. M., Morrison, M. F., Agunwamba, A. O., Nibert, M. L., & Lesser, C. F. (2009). Protein interaction platforms: visualization of interacting proteins in yeast. *Nature Methods*, *6*(7), 500–2. http://doi.org/10.1038/nmeth.1337

Schroeder, G. N., & Hilbi, H. (2008). Molecular pathogenesis of *Shigella spp*.: controlling host cell signaling, invasion, and death by type III secretion. *Clinical Microbiology Reviews*, *21*(1), 134–56. http://doi.org/10.1128/CMR.00032-07

Schüller, S., Chong, Y., Lewin, J., Kenny, B., Frankel, G., & Phillips, A. D. (2007). Tir phosphorylation and Nck/N-WASP recruitment by enteropathogenic and enterohaemorrhagic *Escherichia coli* during ex vivo colonization of human intestinal mucosa is different to cell culture models. *Cellular Microbiology*, *9*, 1352–1364. http://doi.org/10.1111/j.1462-5822.2006.00879.x

Sekiya, K., Ohishi, M., Ogino, T., Tamano, K., Sasakawa, C., & Abe, A. (2001). Supermolecular structure of the enteropathogenic *Escherichia coli* type III secretion system and its direct interaction with the EspA-sheath-like structure. *Proc Natl Acad Sci U S A*, *98*(20), 11638–11643. http://doi.org/10.1073/pnas.191378598\r191378598 [pii]

Sellin, M. E., Müller, A. A., & Hardt, W.-D. (2017). Consequences of Epithelial Inflammasome Activation by Bacterial Pathogens. *Journal of Molecular Biology*. http://doi.org/10.1016/j.jmb.2017.03.031

Sharp, F. C., & Sperandio, V. (2007). QseA directly activates transcription of LEE1 in enterohemorrhagic *Escherichia coli*. *Infection and Immunity*, *75*(5), 2432–40. http://doi.org/10.1128/IAI.02003-06

Shaulov, L., Gershberg, J., Deng, W., Finlay, B. B., & Sal-Man, N. (2017). The Ruler Protein EscP of the Enteropathogenic *Escherichia coli* Type III Secretion System Is Involved in Calcium Sensing and Secretion Hierarchy Regulation by Interacting with the Gatekeeper Protein SepL. *mBio*, *8*(1), e01733-16. http://doi.org/10.1128/mBio.01733-16

Sherman, D. R., & Grundner, C. (2014). Agents of change - concepts in *Mycobacterium tuberculosis* Ser/Thr/Tyr phosphosignalling. *Molecular Microbiology*, *94*(2), 231–241. http://doi.org/10.1111/mmi.12747

Shevchenko, A., Tomas, H., Havli&sbreve;, J., Olsen, J. V, & Mann, M. (2007). In-gel digestion for mass spectrometric characterization of proteins and proteomes TL - 1. *Nature Protocols*, *1 VN-re*(6), 2856–2860. http://doi.org/10.1038/nprot.2006.468

Silver, A. C., Kikuchi, Y., Fadl, A. A., Sha, J., Chopra, A. K., & Graf, J. (2007). Interaction between innate immune cells and a bacterial type III secretion system in mutualistic and pathogenic associations. *Proceedings of the National Academy of Sciences of the United States of America*, *104*(22), 9481–6. http://doi.org/10.1073/pnas.0700286104

Sittka, A., Pfeiffer, V., Tedin, K., & Vogel, J. (2007). The RNA chaperone Hfq is essential for the virulence of *Salmonella* typhimurium. *Molecular Microbiology*, *63*(1), 193–217. http://doi.org/10.1111/j.1365-2958.2006.05489.x

Soto, E., Espinosa, N., Díaz-Guerrero, M., Gaytán, M. O., Puente, J. L., & González-Pedrajo, B. (2017). Functional Characterization of EscK (Orf4), a Sorting Platform Component of the Enteropathogenic *Escherichia coli* Injectisome. *Journal of Bacteriology*, *199*(1), e00538-16. http://doi.org/10.1128/JB.00538-16

Soufi, B., Gnad, F., Jensen, P. R., Petranovic, D., Mann, M., Mijakovic, I., & Macek, B. (2008). The Ser/Thr/Tyr phosphoproteome of *Lactococcus lactis* IL1403 reveals multiply phosphorylated proteins. *PROTEOMICS*, *8*(17), 3486–3493. http://doi.org/10.1002/pmic.200800069

Soufi, B., Krug, K., Harst, A., & Macek, B. (2015). Characterization of the *E. coli* proteome and its modifications during growth and ethanol stress. *Frontiers in Microbiology*, *6*, 103. http://doi.org/10.3389/fmicb.2015.00103

Spaeth, K. E., Chen, Y. S., & Valdivia, R. H. (2009). The *Chlamydia* type III secretion system C-ring engages a chaperone-effector protein complex. *PLoS Pathogens*, *5*. http://doi.org/10.1371/journal.ppat.1000579

Sperandio, V., Li, C. C., & Kaper, J. B. (2002). Quorum-sensing *Escherichia coli* regulator A: a regulator of the LysR family involved in the regulation of the locus of enterocyte effacement pathogenicity island in enterohemorrhagic *E. coli*. *Infection and Immunity*, *70*(6), 3085–93. http://doi.org/10.1128/IAI.70.6.3085-3093.2002

Stabb, E. V, & Ruby, E. G. (2002). RP4-based plasmids for conjugation between *Escherichia coli* and members of the *Vibrionaceae*. *Methods in Enzymology*, *358*, 413–26. Retrieved from http://www.ncbi.nlm.nih.gov/pubmed/12474404

Standish, A. J., Teh, M. Y., Tran, E. N. H., Doyle, M. T., Baker, P. J., & Morona, R. (2016). Unprecedented Abundance of Protein Tyrosine Phosphorylation Modulates *Shigella flexneri* Virulence. *Journal of Molecular Biology*, *428*(20), 4197–4208. http://doi.org/10.1016/j.jmb.2016.06.016

Stebbins, C. E., & Galán, J. E. (2001). Maintenance of an unfolded polypeptide by a cognate chaperone in bacterial type III secretion. *Nature*, *414*(6859), 77–81. http://doi.org/10.1038/35102073

Stebbins, C. E., & Galán, J. E. (2003). Opinion: Priming virulence factors for delivery into the host. *Nature Reviews Molecular Cell Biology*, *4*(9), 738–744. http://doi.org/10.1038/nrm1201

Sterzenbach, T., Nguyen, K. T., Nuccio, S.-P., Winter, M. G., Vakulskas, C. A., Clegg, S., … Bäumler, A. J. (2013). A novel CsrA titration mechanism regulates fimbrial gene expression in *Salmonella* typhimurium. *The EMBO Journal*, *32*(21), 2872–2883. http://doi.org/10.1038/emboj.2013.206

Sun, X., Ge, F., Xiao, C.-L., Yin, X.-F., Ge, R., Zhang, L.-H., & He, Q.-Y. (2010). Phosphoproteomic Analysis Reveals the Multiple Roles of Phosphorylation in Pathogenic Bacterium *Streptococcus pneumoniae*. *Journal of Proteome Research*, *9*(1), 275–282. http://doi.org/10.1021/pr900612v

Thanabalasuriar, A., Bergeron, J., Gillingham, A., Mimee, M., Thomassin, J. L., Strynadka, N., … Gruenheid, S. (2012). Sec24 interaction is essential for localization and virulence-associated function of the bacterial effector protein NleA. *Cellular Microbiology*, *14*, 1206–1218. http://doi.org/10.1111/j.1462-5822.2012.01789.x

Thanabalasuriar, A., Koutsouris, A., Weflen, A., Mimee, M., Hecht, G., & Gruenheid, S. (2010). The bacterial virulence factor NleA is required for the disruption of intestinal tight junctions by enteropathogenic *Escherichia coli*. *Cellular Microbiology*, *12*(1), 31–41. http://doi.org/10.1111/j.1462-5822.2009.01376.x

Thomas, N. A., Deng, W., Baker, N., Puente, J., & Finlay, B. B. (2007). Hierarchical delivery of an essential host colonization factor in enteropathogenic *Escherichia coli*. *Journal of Biological Chemistry*, *282*, 29634–29645. http://doi.org/10.1074/jbc.M706019200

Thomas, N. A., Deng, W., Puente, J. L., Frey, E. A., Yip, C. K., Strynadka, N. C. J., & Finlay, B. B. (2005). CesT is a multi-effector chaperone and recruitment factor required for the efficient type III secretion of both LEE- and non-LEE-encoded effectors of enteropathogenic *Escherichia coli*. *Molecular Microbiology*, *57*, 1762–1779. http://doi.org/10.1111/j.1365-2958.2005.04802.x

Thomas, N. A., Ma, I., Prasad, M. E., & Rafuse, C. (2012). Expanded roles for multicargo and class 1B effector chaperones in type III secretion. *Journal of Bacteriology*, *194*, 3767–3773. http://doi.org/10.1128/JB.00406-12

Thomassin, J.-L., He, X., & Thomas, N. a. (2011). Role of EscU auto-cleavage in promoting type III effector translocation into host cells by enteropathogenic *Escherichia coli*. *BMC Microbiology*, *11*(1), 205. http://doi.org/10.1186/1471-2180-11-205

Tobe, T., Hayashi, T., Han, C. G., Schoolnik, G. K., Ohtsubo, E., & Sasakawa, C. (1999). Complete DNA sequence and structural analysis of the enteropathogenic *Escherichia coli* adherence factor plasmid. *Infection and Immunity*, *67*(10), 5455–62. Retrieved from http://www.ncbi.nlm.nih.gov/pubmed/10496929

Trabulsi, L. R., Keller, R., & Gomes, T. A. T. (2002). Typical and Atypical Enteropathogenic *Escherichia coli*. *Emerging Infectious Diseases*, *8*(5), 508–513. http://doi.org/10.3201/eid0805.010385

Tucker, S. C., & Galán, J. E. (2000). Complex function for SicA, a *Salmonella enterica* serovar typhimurium type III secretion-associated chaperone. *Journal of Bacteriology*, *182*(8), 2262–8. Retrieved from http://www.ncbi.nlm.nih.gov/pubmed/10735870

Ugalde-Silva, P., Gonzalez-Lugo, O., & Navarro-Garcia, F. (2016). Tight Junction Disruption Induced by Type 3 Secretion System Effectors Injected by Enteropathogenic and Enterohemorrhagic *Escherichia coli* . *Frontiers in Cellular and Infection Microbiology*, *6*(August). http://doi.org/10.3389/fcimb.2016.00087

Uversky, V. N., & Dunker, A. K. (2013). The case for intrinsically disordered proteins playing contributory roles in molecular recognition without a stable 3D structure. *F1000 Biology Reports*, *5*, 1. http://doi.org/10.3410/B5-1

Uversky, V. N., Oldfield, C. J., & Dunker, A. K. (2005). Showing your ID: intrinsic disorder as an ID for recognition, regulation and cell signaling. *Journal of Molecular Recognition*, *18*(5), 343–384. http://doi.org/10.1002/jmr.747

van Eerde, A., Hamiaux, C., Pérez, J., Parsot, C., & Dijkstra, B. W. (2004). Structure of Spa15, a type III secretion chaperone from *Shigella flexneri* with broad specificity. *EMBO Reports*, *5*(5), 477–83. http://doi.org/10.1038/sj.embor.7400144

Vihinen, M., Mitić, N. S., Kovačević, J. J., Obradović, Z., Malkov, S. N., Beljanski, M. V, … Dunker, A. (1987). Relationship of protein flexibility to thermostability. *"Protein Engineering, Design and Selection," 1*(6), 477–480. http://doi.org/10.1093/protein/1.6.477

Vincent, C., Duclos, B., Grangeasse, C., Vaganay, E., Riberty, M., Cozzone, A. J., & Doublet, P. (2000). Relationship between exopolysaccharide production and protein-tyrosine phosphorylation in gram-negative bacteria. *Journal of Molecular Biology*, *304*(3), 311–21. http://doi.org/10.1006/jmbi.2000.4217

Vingadassalom, D., Campellone, K. G., Brady, M. J., Skehan, B., Battle, S. E., Robbins, D., … Leong, J. M. (2010). Enterohemorrhagic *E. coli* requires n-wasp for efficient type iii translocation but not for espfu-mediated actin pedestal formation. *PLoS Pathogens*, *6*, 57–58. http://doi.org/10.1371/journal.ppat.1001056

Voisin, S., Watson, D. C., Tessier, L., Ding, W., Foote, S., Bhatia, S., … Young, N. M. (2007). The cytoplasmic phosphoproteome of the Gram-negative bacterium *Campylobacter jejuni:* Evidence for modification by unidentified protein kinases. *PROTEOMICS*, *7*(23), 4338–4348. http://doi.org/10.1002/pmic.200700483

Wagner, M. J., Stacey, M. M., Liu, B. a., & Pawson, T. (2013). Molecular mechanisms of SH2- and PTB-Domain-containing proteins in receptor tyrosine kinase signaling. *Cold Spring Harbor Perspectives in Biology*, *5*(12), 1–19. http://doi.org/10.1101/cshperspect.a008987

Wagner, S., Königsmaier, L., Lara-Tejero, M., Lefebre, M., Marlovits, T. C., & Galán, J. E. (2010). Organization and coordinated assembly of the type III secretion export apparatus. *Proceedings of the National Academy of Sciences of the United States of America*, *107*(41), 17745–50. http://doi.org/10.1073/pnas.1008053107

Wan, F., Weaver, A., Gao, X., Bern, M., Hardwidge, P. R., & Lenardo, M. J. (2011). IKKβ phosphorylation regulates RPS3 nuclear translocation and NF-κB function during infection with *Escherichia coli* strain O157:H7. *Nature Immunology*, *12*(4), 335–343. http://doi.org/10.1038/ni.2007

Wang, D., Roe, A. J., McAteer, S., Shipston, M. J., & Gally, D. L. (2008). Hierarchal type III secretion of translocators and effectors from *Escherichia coli* O157:H7 requires the carboxy terminus of SepL that binds to Tir. *Molecular Microbiology*, *69*(6), 1499–1512. http://doi.org/10.1111/j.1365-2958.2008.06377.x

Wang, G., Clark, C. G., & Rodgers, F. G. (2002). Detection in *Escherichia coli* of the genes encoding the major virulence factors, the genes defining the O157:H7 serotype, and components of the type 2 Shiga toxin family by multiplex PCR. *Journal of Clinical Microbiology*, *40*(10), 3613–9. http://doi.org/10.1128/jcm.40.10.3613-3619.2002

Westermann, A. J., Förstner, K. U., Amman, F., Barquist, L., Chao, Y., Schulte, L. N., … Vogel, J. (2016). Dual RNA-seq unveils noncoding RNA functions in host–pathogen interactions. *Nature*, *529*(7587), 496–501. http://doi.org/10.1038/nature16547

Whitmore, S. E., & Lamont, R. J. (2012). Tyrosine phosphorylation and bacterial virulence. *International Journal of Oral Science*, *4*(1), 1–6. http://doi.org/10.1038/ijos.2012.6

WHO | WHO estimates of the global burden of foodborne diseases. (2017). *WHO*. Retrieved from http://www.who.int/foodsafety/publications/foodborne_disease/fergreport/en/

Wiles, S., Clare, S., Harker, J., Huett, A., Young, D., Dougan, G., & Frankel, G. (2004). Organ specificity, colonization and clearance dynamics in vivo following oral challenges with the murine pathogen *Citrobacter rodentium*. *Cellular Microbiology*, *6*(10), 963–972. http://doi.org/10.1111/j.1462-5822.2004.00414.x

Williams, M. D., Ouyang, T. X., & Flickinger, M. C. (1994). Starvation-induced expression of SspA and SspB: the effects of a null mutation in sspA on *Escherichia coli* protein synthesis and survival during growth and prolonged starvation. *Molecular Microbiology*, *11*(6), 1029–43. Retrieved from http://www.ncbi.nlm.nih.gov/pubmed/8022275

Wong, A. R. C., Clements, A., Raymond, B., Crepin, V. F., & Frankel, G. (2012). The interplay between the *Escherichia coli* Rho guanine nucleotide exchange factor effectors and the mammalian RhoGEF inhibitor EspH. *mBio*, *3*(1), e00250-11. http://doi.org/10.1128/mBio.00250-11

Wugeditsch, T., Paiment, A., Hocking, J., Drummelsmith, J., Forrester, C., & Whitfield, C. (2001). Phosphorylation of Wzc, a tyrosine autokinase, is essential for assembly of group 1 capsular polysaccharides in *Escherichia coli*. *The Journal of Biological Chemistry*, *276*(4), 2361–71. http://doi.org/10.1074/jbc.M009092200

Yakhnin, A. V., Baker, C. S., Vakulskas, C. A., Yakhnin, H., Berezin, I., Romeo, T., & Babitzke, P. (2013). CsrA activates *flhDC* expression by protecting *flhDC* mRNA from RNase E-mediated cleavage. *Molecular Microbiology*, *87*(4), 851–866. http://doi.org/10.1111/mmi.12136

Yen, H., Sugimoto, N., & Tobe, T. (2015). Enteropathogenic *Escherichia coli* Uses NleA to Inhibit NLRP3 Inflammasome Activation. *PLOS Pathogens*, *11*(9), e1005121. http://doi.org/10.1371/journal.ppat.1005121

Zarivach, R., Deng, W., Vuckovic, M., Felise, H. B., Nguyen, H. V., Miller, S. I., … Strynadka, N. C. J. (2008). Structural analysis of the essential self-cleaving type III secretion proteins EscU and SpaS. *Nature*, *453*(7191), 124–127. http://doi.org/10.1038/nature06832

Appendix A: Synthetic Gene Block Sequences for EPEC and *Citrobacter cesT* variants

EPEC *cesT* Y152F
GAATTCCATATGAAAATAGAGGAAATTAGCTCAAGCGATAATAAACATTTTTACGCC
GGAAGATAAAACTTATTTATTAGTATTAATTTACTACTCATTCTAACTCATTGTGGTG
GAGCCCAAACATGATTACTCATGGTTTTTATGCCCGGACCCGGCACAAGCATAAGC
TAAAAAAAACATTTATTATGCTTAGTGCTGGTTTAGGATTGTTTTTTTATGTTAATCA
GAATTCATTTGCAAATGGTGAAAATTATTTTAAATTGGGTTCGGATTCAAAACTGTTA
ACTCATAATAGCTATCAGAATCGCCTTTTTTATACGTTGAAAACAGGTGAAACTGTT
GCCGATCTTTCTAAATCGCAAGATATTAATTTATCGACGATTTGGTCGTTGAATAAG
CATTTATACAGTTCTGAAAGCGAAATGATGAAGGCCGAGCCTGGTCAGCAGATCAT
TTTGCCACTCAAAAAACTTCGGTACCTT

EPEC *cesT* Y153F
GAATTCCATATGAAAATAGAGGAAATTAGCTCAAGCGATAATAAACATTATTTCGCC
GGAAGATAAAACTTATTTATTAGTATTAATTTACTACTCATTCTAACTCATTGTGGTG
GAGCCCAAACATGATTACTCATGGTTTTTATGCCCGGACCCGGCACAAGCATAAGC
TAAAAAAAACATTTATTATGCTTAGTGCTGGTTTAGGATTGTTTTTTTATGTTAATCA
GAATTCATTTGCAAATGGTGAAAATTATTTTAAATTGGGTTCGGATTCAAAACTGTTA
ACTCATAATAGCTATCAGAATCGCCTTTTTTATACGTTGAAAACAGGTGAAACTGTT
GCCGATCTTTCTAAATCGCAAGATATTAATTTATCGACGATTTGGTCGTTGAATAAG
CATTTATACAGTTCTGAAAGCGAAATGATGAAGGCCGAGCCTGGTCAGCAGATCAT
TTTGCCACTCAAAAAACTTCGGTACCTT

EPEC *cesT* Y152F, Y153F
GAATTCCATATGAAAATAGAGGAAATTAGCTCAAGCGATAATAAACATTTTTTCGCC
GGAAGATAAAACTTATTTATTAGTATTAATTTACTACTCATTCTAACTCATTGTGGTG
GAGCCCAAACATGATTACTCATGGTTTTTATGCCCGGACCCGGCACAAGCATAAGC
TAAAAAAAACATTTATTATGCTTAGTGCTGGTTTAGGATTGTTTTTTTATGTTAATCA
GAATTCATTTGCAAATGGTGAAAATTATTTTAAATTGGGTTCGGATTCAAAACTGTTA
ACTCATAATAGCTATCAGAATCGCCTTTTTTATACGTTGAAAACAGGTGAAACTGTT
GCCGATCTTTCTAAATCGCAAGATATTAATTTATCGACGATTTGGTCGTTGAATAAG
CATTTATACAGTTCTGAAAGCGAAATGATGAAGGCCGAGCCTGGTCAGCAGATCAT
TTTGCCACTCAAAAAACTTCGGTACCTT

Citrobacter cesT Y152F
GAATTCCATATGAAAATAGAGGAAATTAGTTCAAACGATAATAAACATTTTTACGCC
GGAAGATAAAGAATTATTTATTAATATAATTTACTACTCATTCTAACTCATTGTGGTG
GAGCCTATAACATGATTATTCATGGTTTTTGCACCGGGACCCGGCACAAGCATAAG
TTAAGAAAAACATTTATTATGCTTGGTGCTGGTTTAGGATTGTTTTTTTCTGTTAACC
AGAACTCATTTGCAAATGGTGAAAATTACTTTAAGTTAAGAGCCGATTCTAAACTAA
TAAATAATAATATTGCTCAGGATCGTCTTTTTTATACCTTGAAAACGGGTGAAAGCG
TTGCTCAGCTTTCTAAATCACAAGGGATCAGCGTGCCGGTTATTTGGTCGCTGAAT
AAGCATTTATATAGCTCTGAAAGTGAAATGATGAAGGCTAGTCCTGGTCAGGTACC
TT

Citrobacter cesT Y153F

GAATTCCATATGAAAATAGAGGAAATTAGTTCAAACGATAATAAACATTATTTCGCC
GGAAGATAAAGAATTATTTATTAATATAATTTACTACTCATTCTAACTCATTGTGGTG
GAGCCTATAACATGATTATTCATGGTTTTTGCACCGGGACCCGGCACAAGCATAAG
TTAAGAAAAACATTTATTATGCTTGGTGCTGGTTTAGGATTGTTTTTTTCTGTTAACC
AGAACTCATTTGCAAATGGTGAAAATTACTTTAAGTTAAGAGCCGATTCTAAACTAA
TAAATAATAATATTGCTCAGGATCGTCTTTTTTATACCTTGAAAACGGGTGAAAGCG
TTGCTCAGCTTTCTAAATCACAAGGGATCAGCGTGCCGGTTATTTGGTCGCTGAAT
AAGCATTTATATAGCTCTGAAAGTGAAATGATGAAGGCTAGTCCTGGTCAGGTACC
TT

Citrobacter cesT Y152F, Y153F

GAATTCCATATGAAAATAGAGGAAATTAGTTCAAACGATAATAAACATTTTTTCGCC
GGAAGATAAAGAATTATTTATTAATATAATTTACTACTCATTCTAACTCATTGTGGTG
GAGCCTATAACATGATTATTCATGGTTTTTGCACCGGGACCCGGCACAAGCATAAG
TTAAGAAAAACATTTATTATGCTTGGTGCTGGTTTAGGATTGTTTTTTTCTGTTAACC
AGAACTCATTTGCAAATGGTGAAAATTACTTTAAGTTAAGAGCCGATTCTAAACTAA
TAAATAATAATATTGCTCAGGATCGTCTTTTTTATACCTTGAAAACGGGTGAAAGCG
TTGCTCAGCTTTCTAAATCACAAGGGATCAGCGTGCCGGTTATTTGGTCGCTGAAT
AAGCATTTATATAGCTCTGAAAGTGAAATGATGAAGGCTAGTCCTGGTCAGGTACC
TT

Appendix B: Multiple Sequence Alignment of Identified Class IB T3SC

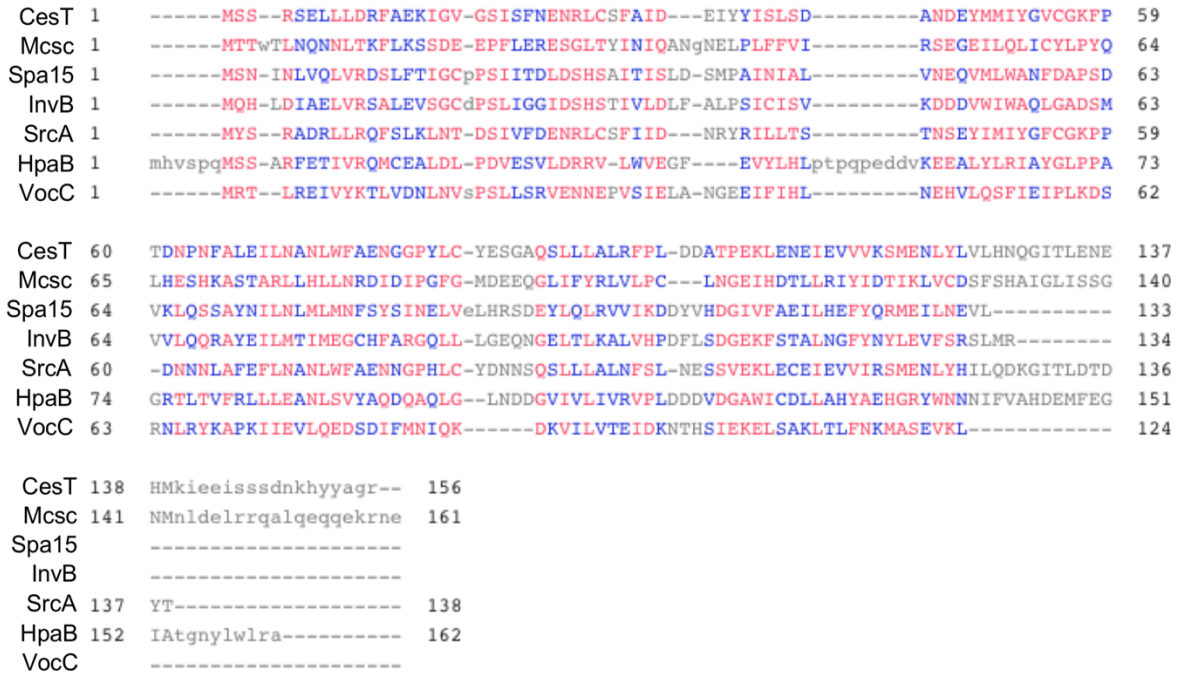

Figure: COBALT software from NCBI was used with default alignment parameters and a 2bit identity setting. Amino acids coloured red have a higher degree of conservation than those in blue. Across all seven class IB T3SC identified to date there is a low degree of sequence identity.

The COBALT algorithm computes a progressive multiple alignment of protein sequences. The alignment output is derived from a collection of pairwise constraints obtained from conserved domain database (CDD), protein motif database (PROSITE), and local sequence similarity using RPS-BLAST, BLASTP, and PHI-BLAST, respectively (Papadopoulos & Agarwala, 2007). The multiple cargo secretion chaperone (Mcsc) of *Chlamydia* spp. is the largest class IB T3SC identified to date (161 aa). Structural analysis of Mcsc has yet to be conducted, however it is predicted to form a dimer similar to other class IB chaperones based on a putative 3D model created with the folding prediction program I-TASSER (Spaeth *et al*., 2009). *Edwardsiella spp.* are occasionally opportunistic human pathogens that inhabit the intestinal tract of aquatic reptiles and fish. Closely related to *E. coli* within the Enterobacteriaceae family, *Edwardsiella* also encode a T3SS and CesT. Interestingly, in this context CesT Y153 is not conserved (substituted for F), however Y152 is maintained and a serine residue replaces alanine at position 154 (KNYFSAR).

Appendix C: Unpublished CesT Characterization from Dr. Nikhil Thomas

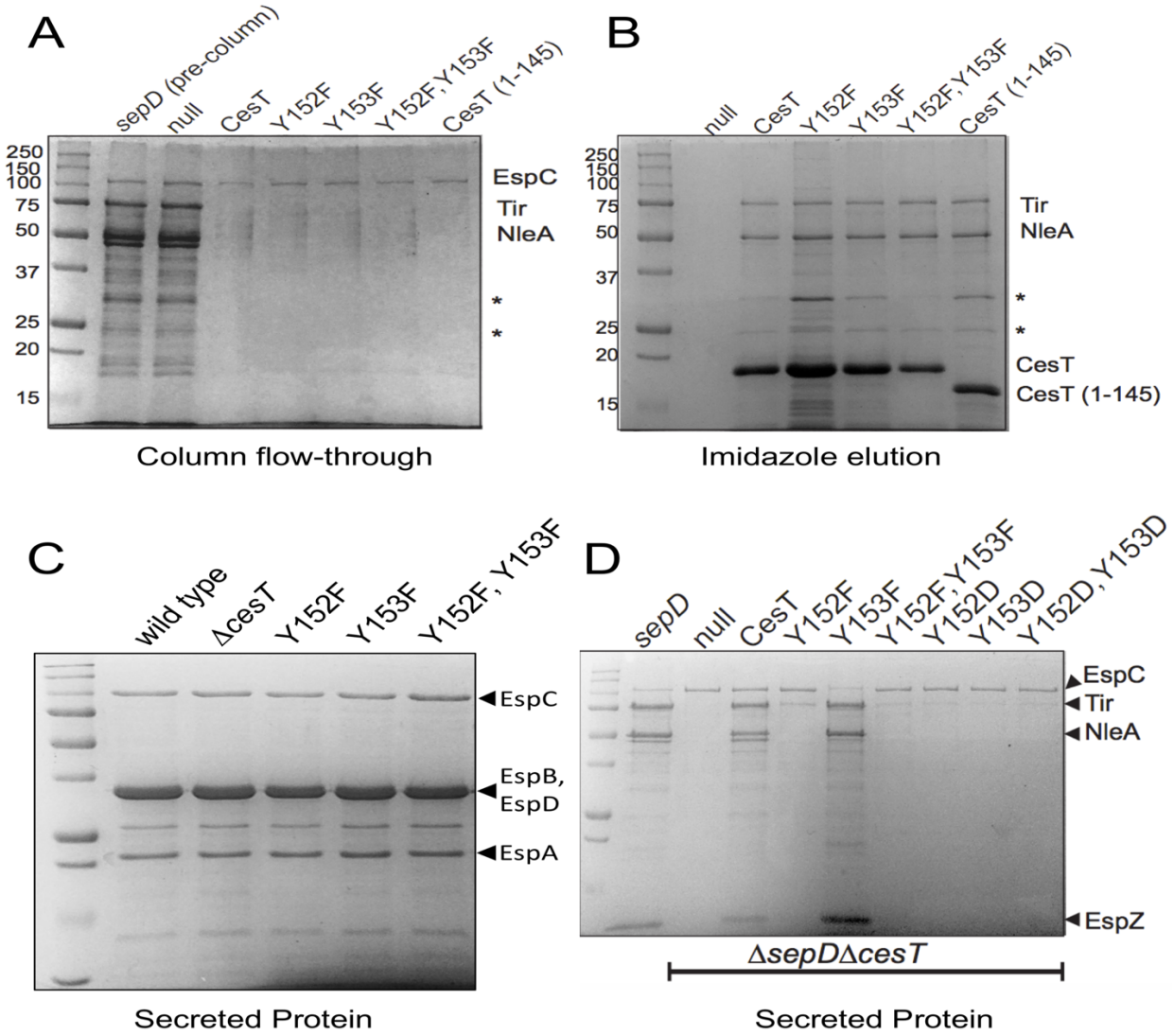

Appendix C: (A-C) CesT C-terminal phosphosite substitutions do not impact effector binding or secretion of T3SS translocator proteins. (A and B) A CesT affinity column was prepared as previously described (Thomas *et al*., 2005; 2007). Briefly, Overexpressed His-CesT from an *E. coli* BL21 lysate was purified and bound to a Ni^{2+}-nitrilotriacetic acid (NTA) resin column. EPEC Δ*sepD* culture supernatants were exposed to each column-bound His-CesT variant. (A) Unbound flow-through and (B) eluted samples were separated by SDS-PAGE and visualized by Coomassie G-250. (C) EPEC cultured in DMEM at 37 ^{o}C, 5% CO_2 for 6 h does not display altered secretion of translocator proteins EspA, EspB, or EspD. (D) CesT-dependent effector secretion is not restored by phosphomimetic Tyr to Asp substitutions at the CesT C-terminus. EHEC CesT variants are expressed from the *tir* promoter within the pSec10 low-copy vector (received from Dr. Anne Marie Hansen). EspC is a T5SS secreted protease that targets EspA and EspD to regulate translocon pore formation following cell contact (Guignot, Segura, & Tran Van Nhieu, 2015).

Appendix D: C57Bl/6 Mice Weight Measurements; *Citrobacter* Experiment 2